Université Pierre et Marie Curie
en cotutelle avec l'Université
de Santiago de Chili

THESE DE DOCTORAT DE
L'UNIVERSITE PIERRE ET MARIE CURIE

Spécialité

Sciences Mécaniques, Acoustiques et Electroniques

Présentée par

M. Victor ROMERO

Pour obtenir le grade de

DOCTEUR de l'UNIVERSITÉ PIERRE ET MARIE CURIE

Sujet de la thèse :

SPIRALING CRACKS IN THIN SHEETS

Soutenue le 9 Décembre 2010

Devant le jury composé de :

M. BICO José	Maître de Conférence
M. CERDA Enrique	Professor, Directeur de Thèse
M. CLÉMENT Eric	Professeur
M. GÉMINARD Jean-Christophe	Directeur de Recherche
M. HAMM Eugenio	Assistant Professor
M. RICA Sergio	Directeur de Recherche, Rapporteur
M. VILLERMAUX Emmanuel	Professeur, Rapporteur
M. ROMAN Benoit	Chargé de Recherche, Directeur de Thèse

Université Pierre & Marie Curie - Paris 6
Bureau d'accueil, inscription des doctorants
Esc G, 2ème étage
15 rue de l'école de médecine
75270-PARIS CEDEX 06

Tél. Secrétariat : 01 44 27 28 10
Fax : 01 44 27 23 95
Tél. pour les étudiants de A à EL : 01 44 27 28 07
Tél. pour les étudiants de EM à MON : 01 44 27 28 05
Tél. pour les étudiants de MOO à Z : 01 44 27 28 02
E-mail : scolarite.doctorat@upmc.fr

UNIVERSIDAD DE SANTIAGO DE CHILE

Facultad de Ciencias

Departamento de Física

In Cotutelle with

Université Pierre et Marie Curie

Spiraling Cracks in Thin Sheets

Víctor Manuel ROMERO GRAMEGNA

Advisor in Chile: Dr. Enrique CERDA VILLABLANCA

Advisor in France: Dr. Benoit ROMAN

Thesis submitted to the Faculty of Science of the University of Santiago and University Pierre et Marie Curie in partial fulfilment of the requirements for the degree of Doctor of Philosophy.

Santiago, Chile

December 9, 2010

Spiraling Cracks in Thin Sheets.

Víctor Manuel ROMERO GRAMEGNA

Advisor professor in Chile:	Dr. CERDA Enrique
Advisor professor in France:	Dr. ROMAN Benoit
Committee:	Dr. BICO José
	Dr. CLÉMENT Eric
	Dr. GÉMINARD Jean-Christophe
	Dr. HAMM Eugenio
	Dr. VILLERMAUX Emmanuel
	Dr. RICA Sergio

Thesis submitted for the degree of Doctor of Philosophy.

Santiago, Chile

December 9, 2010

Spiraling Cracks in Thin Sheets

Víctor Manuel ROMERO GRAMEGNA

This work has been supervised by Professors Dr. Enrique CERDA and Dr. Benoit ROMAN under a Cotutelle agreement between University of Santiago of Chile and University Pierre et Marie Curie, and has been approved by the members of the qualify committee:

.....

Dr. José Bico

.....

Dr. Eric Clément

.....

Dr. Eugenio Hamm

.....

Dr. Jean-Christophe Géminard

.....

Dr. Sergio Rica

.....

Dr. Benoit Roman, Co-advisor

.....

Dr. Enrique Cerda, Advisor

.....

Sr. Bernardo Carrasco, Director

–To my beloved parents and wife

Abstract

Opening a package made of a thin film is not always a satisfying experience. The crack is not easily controlled even though we try to guide it with our hands. This "freedom" for the crack propagation is connected with the many possibilities of thin sheets to deform. Indeed, deformation and fracture are highly related because deformation is the source of the energy required to propagate a crack. In this way, finding and explaining regular crack paths in thin sheets improve our understanding of the fracture of these objects. In previous scientific works, regular crack paths in brittle thin sheets have been reported. We can mention convergent tears obtained by peeling or tearing a flap of a thin sheet; also it is possible to find oscillatory cracks when a thin sheet is cut through by a moving blunt object. In this work we present two very robust, reproducible, divergent families of cracks paths in a brittle material (bi-oriented polypropylene, BOPP, usually used in packaging). These two final crack paths are characterized as similar logarithmic spirals although they are the outcomes of two very different set-ups. A first logarithmic spiral is the result of propagate only one crack by pushing an edge of a thin sheet, in this case the crack propagates because the material is been stretched and therefore the energy associated with the fracture propagation is "stretching energy". In the second spiral experiment, we propagate only one crack on the same material, but now we are tearing up in such a way that the energy, feeding the crack, comes from out of plane deformation. This last procedure not only results in a spiraling regular crack, but also in a beautiful and very complex out-of-plane structure of the tear.

KEYWORDS: Fracture, elasticity, thin sheet, crack, spiral, anisotropy.

Résumé

Cette thèse étudie la rupture de plaques élastiques fragiles dans deux configurations qui conduisent à une propagation en spirale : soit à la suite d'étirement provoqué par le contact avec un indenteur qui pousse toujours sur la même lèvre de la fissure, soit en tirant une languette perpendiculairement au plan de la plaque.

Dans le premier cas, on étudie expérimentalement la réponse élastique du système, et on prédit les conditions pour la propagation, ainsi que la direction, à partir du critère du maximum du taux de restitution de lénergie. En suivant ces résultats, une propagation en spirale logarithmique est alors prédite, ce qui est confirmé par les expériences.

Malgré un chargement mécanique différent, la deuxième expérience se ramène à un problème très similaire, avec cependant un taux de croissance de la spirale logarithmique plus faible. Ce processus de rupture à croissance exponentielle a fait lobjet dun dépôt de brevet pour l'ouverture facile d'emballage.

Dans les deux expériences, on observe cependant que la forme des spirales est perturbée de façon similaire par l'anisotropie des propriétés du matériau. Une extension du modèle est proposée pour tenir compte de ces effets.

MOTS-CLÉS: Rupture, élasticité, plaque mince, crack, spirale, anisotropie.

Resumen

En este trabajo de tesis presentamos dos experimentos en que trayectorias de fracturas sumamente reproducibles son obtenidas en láminas delgadas frágiles. En ambos casos, a partir de configuraciones iniciales sumamente simples y pequeñas, las trayectorias obtenidas son espirales logarítmicas de gran tamao.

Nuestro primer experimento consiste en un crack que se inicia desde un corte recto hecho en una lámina delgada y que es forzado a propagarse por medio de empujar con un objeto sólido. Este procedimiento genera una espiral de gran tamao rápidamente. Mostramos en este trabajo que la forma final no depende del movimiento del objeto con el que empujamos, siempre y cuando sea un solo borde de la lámina el que se empuja. Basándose en teoría clásica de fracturas hemos sido capaces de modelar y explicar esta trayectoria final de la fractura. Además a través de una serie de experimentos hemos validado y probado nuestras suposiciones y predicciones. Finalmente, a partir de la caracterización geométrica de la espiral obtenida, mostramos evidencia del efecto de la anisotropía del material usado en el proceso de fractura.

El segundo experimento presentado en este trabajo se inicia con una configuración inicial conveniente. Removiendo una pequea cantidad de material creamos un "convex hull", luego hacemos un pequeo corte y tiramos la "lengeta" de material que se genera. Como resultado de este proceso solamente una fractura se propaga, dando lugar nuevamente a una trayectoria final en forma de espiral logarítmica. En este caso la complejidad de la deformación hace muy difícil modelar el fenómeno, sin embargo, basándonos en simples argumentos geométricos hemos encontrado una relación que conecta la fuerza requerida para forzar el crack y la energía que se requiere para romper la lámina delgada.

Concluimos este trabajo con un análisis que explica porque, a pesar de la diferencia en la forma en que se fuerzan las fracturas a propagarse, en ambos casos el resultado final es similar. Este análisis nos entrega condiciones para que la fractura final sea divergente.

PALABRAS CLAVE: Fractura, elasticidad, láminas delgadas, crack, espirales, anisotropía.

Acknowledgements

In this process many people and institutions have been very important. My first words of gratefulness are to my advisor professors, Enrique Cerda and Benoit Roman, for their guidance in the understanding of the physics, not only as a profession but a way to observe every thing around us. Their advise and methodology have been deeply inspiring. I can not forget to mention the great patience they have had with me, and my hope is that I did not dissapoint them. Thank very much to both of you.

Because of the way in which this work has been done, I have been very fortunate to met many people all around the world, who have help me in many different ways. I can not forget to mention John Bush, Pedro Reis and his lovely wife Ines, and Pascal Raux, who receive me in Boston, where I spend three months learning and working at the applied math group in MIT.

I have to thanks many people from the academics sphere, because in them I found many help in the develop of my work. Professors Eugenio Hamm, Francisco Melo, Jos Bico, Juan Carlos Retamal, Dora Altbir, among many others, from which I learn not only formal academic contents, but also the big commitment with the develop in science.

In this process people who has always been next to me no matter what situation are my very good friend from both, Paris and Santiago. Juan Palma, Sebastian Michea, Juan Fuentealba, Fransico Santiabaez, Alejandro Pereira, Antonella Rescaglio, Daniela Briceo, Franco Tapia, David Muñoz, Gonzalo Quiroga and last but not less Miguel Piñeirua. I have counted with all this people to become the person I am, and I hope that I always will have them to my side.

My final words are to my parents, Cristina Gramegna and Victor Hugo Romero,

from whom I have recived everything and to whom I owe everything I have become. And the most special woman I have ever known, Belen Rojas, to whom I expect to be for the rest of my life, I love you very much.

This work has not been possible without the financial support of Conicyt with their national PhD Grant, CNRS, Scat-alpha Project, Smat-C, and Anillo Project (Dynamics, Singularities, and Geometry of matter out of Equilibrium).

Contents

Abstract i

Résumé ii

Resumen iii

Acknowledgements v

List of Figures xi

1 Introduction 1

1.1 Thin Sheets: Crumpling, Wrinkling, Folding and Creasing 1

1.2 Fracture of Thin Sheets 7

1.3 Convergent Versus Divergent (or Pulling versus Pushing) 10

1.4 Spirals 12

1.5 Thesis Outline 13

2 Spiral Rupture With a Blunt Object 14

2.1 Spiral Experiment 15

2.2 Tool path dependence 18

2.3 Model 21

2.3.1 Elastic Energy 21
2.3.1.1 Experimental Characterization of the Elastic Energy 22
2.3.2 Fracture Propagation 30
2.3.2.1 Geometrical Variation 32
2.3.2.2 Griffith's criterion and second Variation of the energy 34
2.3.2.3 Fracture Propagation Law 35
2.3.2.4 Model Confirmation 37
2.4 Three different stages in the Spiral 40
2.5 Spiral Results 47
2.5.1 Numerical Simulation of the Spiral Growth 47
2.5.1.1 A Local Method to Find the Spiral Pole 49
2.5.1.2 Global Method to Define a Pole of a Spiral 50
2.5.1.3 Measuring β in the experiments 51
2.5.2 Experiments 51
2.6 Anisotropy 57
2.6.1 Experiments with Highly Anisotropic Materials 57
2.6.2 Anisotropic Model 61
2.7 Conclusion 67

3 Tearing Spiral **70**

3.1 Experimental set-up 71
3.2 Geometrical characterization of the Spiral 74
3.3 Pulling forces 81
3.4 Geometrical Characterization of the Initial Seed 85
3.5 Easy Opening 88
3.6 Crumpling Structures in the Elastic Pine-Tree 91

3.7 Conclusions 93

4 Conclusions **95**

4.1 Spiraling Rupture With a Blunt Object 95

4.2 Tearing Spiral 97

4.3 General Conclusions 98

Bibliography **99**

A Résumé Français **107**

A.1 Introduction 107

A.2 Chapitier 2 110

A.3 Chapitre 3 114

B Resumen Español **116**

B.1 introducción 116

B.2 Capitulo 2 119

B.3 Capítulo 3 123

C Basics Notions in Fracture and Elasticity Theories of Thin Sheets **125**

C.1 Elasticity 125

C.1.1 Elemental Relations in Elasticity 125

C.1.2 Energy Storage in Thin Sheets 127

C.2 Fracture Mechanics 129

C.2.1 Fracture Modes 129

C.2.2 Griffith Criteria 131

C.2.3 Brittle, Quasi-static Crack Propagation, Stable 131

C.2.4 Path Selection Criterion 133

D Patent 135

List of Figures

1.1 Examples of crumpling, wrinkling, and creasing. 4

1.2 Illustration of converging tear experiment 11

2.1 Pictures of the experiment “spiral rupture with a blunt object”. 15

2.2 Illustration of the possibles places where the blunt object can push the edge of the film 16

2.3 Resulting experimental tear. 17

2.4 Tool tracking experiment 18

2.5 *Tool Trajectories and its respective resultant crack paths.* 19

2.6 *Diagram of the configuration for energy storage in the system.* . . . 21

2.7 *Experimental diagram of the energy storage when a tool pushes a lip of a thin sheet.* 22

2.8 *Data from experiments with different lengths and different thickness sheets. The penetration of the tool is given by the quantity* d/L. . . . 23

2.9 *Data from experiments with different lengths* L *and sheets with different thicknesses. The penetration angle of the tool is given by the quantity* d/L. 24

2.10 Exponent law for the energy storage process 25

2.11 *Non-symmetric experimental measure of force.* 29

2.12 *Force measurements in a non-symmetric experimental configuration.* 29

2.13 *Geometry of the system configuration.* 31

(a) *Geometry before fracture.* 31

(b) *Geometry after the crack, of length* s*, propagates a distance* δs*.* 31

2.14 *Critical value of penetration angle* α_c *as a function of the dimensionless quantity* EL/γ *plot with red dots. The black line corresponds to the linear fit of the logarithmic rectification of the collected data.* . 38

2.15 *Convex hull illustration.* 40

2.16 *Initial stage for the spiral formation* 41

2.17 *Second stage for the spiral formation* 42

2.18 Oscillatory crack path. 42

2.19 *Final stage for the spiral formation* 43

2.20 *Geometry in a logarithmic spiral.* 44

2.21 *Numerical functionality between* $\cot\phi$ *and* β*.* 46

2.22 *Illustration of the bases use to simulated the path formation.* **Top.-** *Example of the results of the simulation in the first stage of the spiral formation.* **Bottom Right.-** *Example of the results of the simulation in the second stage of the spiral formation.* **Bottom left.-** *Example of the results of the simulation in the final stage of the spiral formation.* 48

2.23 *Geometry in a logarithmic spiral.* 49

2.24 *Diagram of the procedure to find the pole.* 51

2.25 *Determination of the orientation of the Film. An illustration of the three experiments.* 52

2.26 *Experimental measurements of the radius r, normalized with the initial size r_o, from three experiments. Red and green circles are experiments with a same initial orientation to the incision. Blue circles are data from an experiment initiated with a perpendicular orientation.* 53

2.27 *Crack propagation angle β as a function of the angle of the spiral, θ.* **inset** *The angle β as a function of the orientation in the film θ_g* . . 55

2.28 *Spiral made with a very anisotropic material.* 58

2.29 *Illustration of the lines passing through the kinks intersecting in the pole.* 59

2.30 *Radius (distance to the pole) as a function of angle, for two spirals initiated with perpendicular orientations in a very anisotropic material.* 60

2.31 *Case of a very anisotropic spiral. Crack propagation angle β as a function of the angle of the spiral, θ.* **inset** *The angle β as a function of the global orientation in the film θ_g* 61

2.32 *Illustration of the geometry used to compare the fracture energy and the direction of the crack.* 63

2.33 *With red, blue and green circles, the values of $\beta - \langle\beta\rangle$, are plotted. With black circles we present $2(\gamma - \langle\gamma\rangle)/\gamma$. The inset presents the measures of $\gamma(\theta')$.* 65

3.1 *Illustration of the initial cut.* 71

3.2 *Illustration of the experimental set-up.* 72

3.3 *Initial stages of the propagation. Note the 3D "pine-tree" shape.* . . . 74

3.4 *Final tear from propagating a crack by pulling.* 75

3.5 *Normalized distance from the pole $\mathcal{O}$ to all the points in two spirals initiated with perpendicular orientations.* 77

3.6 *Measurements of β as a function of the spiral angle.* **Inset** *The same data presented as a function of the absolute orientation in the film.* 78

3.7 *Superimposed measurements of β collapsed in one period for both spiral experiments. With blue dots is plotted β from a pushing spiral, the dots in red are the measurements of β from a pulling spiral.* . . . 79

3.8 **Left**.-*The elastic pine-tree.***Right**.-*The Internal structure of the elastic pine-tree.* 81

3.9 *Measurements of the pulling force versus time. The data for experiments with films of 30μm (lower curve), 50μm (center curves) and 90μm (high curves)* 83

3.10 *Initial Configuration. Geometrical frustration of the secondary crack.* 85

3.11 *Initial Configuration. Mechanical frustration of the secondary crack.* . 86

3.12 *Illustrations of an unsuccessful initial configuration:* **Left.-** *Initial configuration made by removing a disk of material and a straight notch.* **Right.-** *Evolution of the morphology of the convex hull when the crack advances. In this case the perimeter of the convex hull contains two discontinuities, hence two cracks nucleate at points $\mathcal{T}$ and $\mathcal{B}$.* 88

3.13 *Illustration of the optimal initial configuration for the spiral creation.* . 89

3.14 *Easy opening using our method to remove the packaging for a compact disk.* 91

3.15 *The final shape of the crumpling structures in the elastic pine-tree.* . 92

3.16 *Sequence of pictures showing the formation of crumpled structures.* 93

C.1 Modes in fracture analysis 129

Chapter 1

Introduction

1.1 Thin Sheets: Crumpling, Wrinkling, Folding and Creasing

Thin sheets are defined as objects with one dimension (thickness, t) that is much smaller than the other two. Thickness usually goes from some hundreds of microns, as for example a sheet of paper, adhesive tape, normal packaging materials, etc., to a few nanometers, as in graphene sheets, lipids and nanoparticle films and polymer coatings (these systems have a very small aspect ration t/a, where a is the characteristic length for the width and length of the sheet). Mechanical properties like bending and stretching stiffness (we use B for bending stiffness and Y for the two-dimensional stretching modulus) decrease with thickness, making these objects flexible and soft; the ubiquitous examples of soft matter systems. Behaviors typical of soft system, such as wrinkling, can be observed in a macroscopic flexible rubber sheet, but also in a semiconductor silicon crystal a few nanometers thick, usually associated as a stiff material due to its high Youngs

Modulus (10^2 GPa) [1].

The same thickness reduction explains why a smaller number of material constants are needed to describe a thin sheet (two for an elastic isotropic sheet, three for an elastic isotropic body [2, 3]). Similarly, when one dimension is reduced, a strong coupling between geometry and mechanics is concomitant. Pure geometrical concepts, such as the Gaussian and mean curvature, or differential geometry theorems such as the Theorema Egregium play a significant role in describing a thin sheet [4, 5]. Isometric deformations, preserving the first fundamental form, are observed in elastic sheets when confined. Lipids are assembled into membranes of zero mean curvature to minimize surface area [6]. Thus, there are geometrical constraints that need to be fulfilled independently of the specific nature of the sheet material.

In recent years, there has been growing interest to identify the specific modes of deformations in thin sheets satisfying these geometrical requirements. Phenomena like crumpling, wrinkling, creasing and folding are some examples of these possible modes of deformation that, although previously studied in works by Wagner, Reissner [7]. Mansfield [3], Sheppard [8], Biot [9], and others, have now been analyzed with new theoretical, numerical and experimental techniques. These research efforts are not only driven by a quest for knowledge. The interest in developing technologies at smaller and smaller scales has posed new questions and challenges for engineers and scientists to understand and control the mechanical behavior of these objects.

Crumpling a paper sheet shows many of the geometrical and physical ideas that are used in the analysis of thin sheets. In [10], Professor Thomas Witten has made an extensive review and discussion of the main results in crumpling. His pioneer

work to understand the localization of energy along ridges [11] provided a first glimpse of the complexity and richness of the phenomena involved in thin sheets. This complexity can be observed in a crumpled piece of paper: when it is unfolded it is possible to observe permanent deformations distributed randomly on it and a resulting structure characterized by sharp points connected by ridges. This permanent deformation indicates concentration of stresses in those points and ridges. The stress concentration distribution is not trivial nor intuitive, underlying a focusing mechanism of the energy that is intimately connected to geometry. Since resistance to membrane stretching is linearly proportional to membrane thickness (t), and membrane bending goes with thickness cubed (t^3), the ease of bending versus stretching increases for thinner films [12]. As a result, thin films primarily respond to loads by bending rather than stretching, and approximate geometrical solutions can be obtained by studying isometric deformations of the initial flat geometry. This purely geometrical view fails in regions of high curvature that are necessary to connect the four possible isometric deformations of a flat sheet: a plane, a cylinder, a cone and a tangent developable [4, 5].

These isometric deformations and regions of high curvature have been studied by several groups [13–16]. Ridges and point singularities show beautiful scaling laws that are another characteristic feature in the study of thin sheets, for example, the mean curvature scales as $t^{-1/3}$ in a ridge [11] and a point singularity [17]. These scaling laws have been checked by numerical simulations, indirect experiments and theoretical arguments [10]. There are no analytical solutions available for these deformations due to the highly nonlinear nature of the equations describing them.

There is growing interest in studying crumpling structures at high confinement.

These structures show some degree of *randomness* that have motivated theoretical efforts to use probability distributions in the analysis of crumpling [18–20]. More modestly, but perhaps more applicable, other researchers have used the same ideas of crumpling to evaluate the collapse of packaging structures [21].

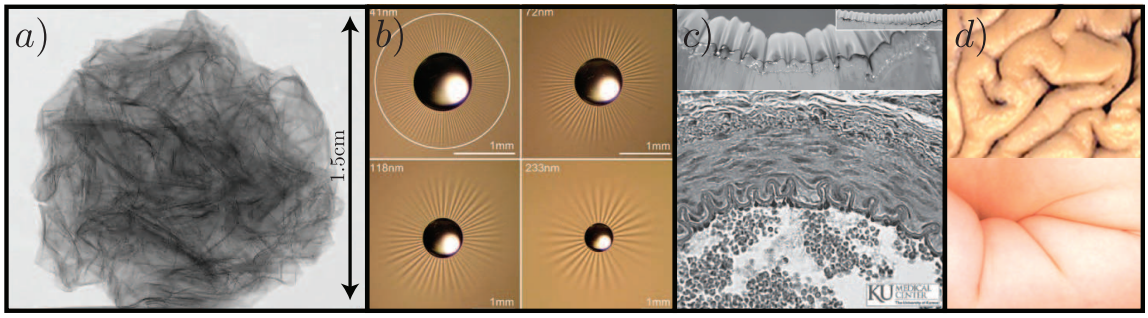

Figure 1.1: **a.-***Image extracted from a video made by D. Cambou and avaible in the internet. It is a reconstruction of X-ray computerized tomography made of a* 1.5 *cm crumpled aluminum foil.* **b.-** *Figure extracte from reference [22], in this figure the number of wrikles depends of the thickness of the polystyrene thin sheet.* **c.-** *Image extracted from reference [23], in the top image the controlled experiment is presented, the bottom image is a histological slide of a muscular artery cross-section, where it is possible to appreciate the resembles with biologycal systems.* **d.-** *Image extracted from reference [24], in the top picture the sulci in a primate brain is presented. In the bottom picture the arm of an infant. Representative sulcus structures.*

The analysis of wrinkling patterns has been also an important area of research based on the possibility of using them in metrology. Beginning with the work of Bowden et al. [25], who studied the wrinkling of a film on top of an elastic substrate, we have seen the appearance of new techniques to measure the mechanical properties of thin sheets [26]. The idea is extremely simple: the wavelength of

these patterns is defined by the relation $2\pi t(E_f/3E_s)^{1/3}$ where E_s and E_f are the Young modulus of the substrate and film respectively. Thus, measuring the wavelength, thickness and Youngs modulus of the substrate gives Youngs modulus of the film. The same ideas have been used to take advantage of wrinkling patterns generated by other mechanisms [27–29]. Wrinkling can also be observed when a sheet is floating in a fluid or stretched from two boundaries. The determination of the wavelength provides equivalent methods to measure the mechanical properties of these films. Moreover, J. Huang et al. [22] introduced the idea of also measuring the length of the wrinkles as an assessment tool for metrology in thin sheets. The wavelength and length of the wrinkles provide two independent measurements that can be used to obtain mechanical properties in thin sheets. This work has also opened new questions since there is no clear theoretical understanding of the conditions that define the length of the wrinkles in this case.

The experiments studying deformations in floating thin sheets have shown the existence of buckling cascades near the boundaries where the wavelength of the wrinkles adjusts to match the flat geometry of the fluid [30]. Similar cascades have been observed by Y. Pomeau and S. Rica [31] when a rectangular acetate sheet is clamped in one boundary and compressed in the same direction of that boundary. However, the cascade in this setup shows ridge and point singularities typical of crumpling deformations. Recently, Schroll et al. [32] have introduced the concept of smooth and focusing stresses to connect two different phenomena: crumpling and wrinkling. Geometrical parameters and boundary conditions then explain wrinkling or crumpling in a thin sheet.

More recently, there are several works showing how thin sheets on top of a fluid or an elastic substrate can localize wrinkles into folds [33–35]. This localization

is surprising since it does not require stretching of the thin sheet as in the case of crumpling [10]. Experiments have been carried out in two-dimensional configurations similar to a Langmuir-Blodgett trough (LBT) configuration. Moreover, the wrinkling to fold transition is observed in different material sheets. It has been observed in lipid monolayers, nanoparticle films, polystyrene films, microparticles ranging from a few micrometers to hundred of micrometers, when resting on top of a fluid. It has also been observed in PDMS and polyester thin sheets resting on top of an elastic substrate and the stiff crust made by heating the surface of soft foam. It has been suggested that this transition provides an effective mechanism to obtain extensibility in biological interfaces, such as lung surfactant or the endothelial and epithelial linings of tissue [23, 33].

The strong resemblance of folding observed on thin sheets to the creases observed in swelling gels gives another example of the deep connection between mechanics and geometry in thin sheets. Although creasing has been studied since the beginning of the last century [8], it has been studied more extensively in recent years [24, 36, 37]. There are some theoretical works that show the close similarity between the theoretical explanations of these two phenomena [37], however it is still early to draw clear conclusions.

1.2 Fracture of Thin Sheets

We have briefly described the importance and richness of the study of thin sheets and highlighted the fact that there is an intimate connection among these phenomena due to the strong coupling between mechanics and geometry. We now focus on one particular aspect, which is the core of this thesis work: fracture in thin sheets.

In the last century, fracture mechanics emerged and matured as an engineering discipline that is fundamental to understanding man-made structures. This has become even more important as societies increasingly rely on highly technological structures, such as tall buildings, planes or ships.

Dramatic examples of fractured systems are presented in introductory books to fracture mechanics. The most extensive and widely known examples are those that occurred in tankers and cargo ships that were built, mainly in the U.S.A., under the emergency shipbuilding programs of the Second World War [38]. Another tragic example of ship fuselage failure is the Exxon Valdez oil spill described (from the point of view of fracture) by Cotterell [39]. In 1989, the Exxon Valdez tanker struck the Bligh Reef off the coast of Alaska. Millions of gallons of oil were spilled into the ocean with consequent environmental damage. Images of the torn hull of the tanker showed divergent tears (named *concertina tearing*) that prompted several research studies [40, 41]. Many others major disasters have occurred throughout history that have forced engineers to focus on fracture. The seminal works of Griffith, and later Irwin and Orowan [42], have provided the standard tools to explain fracture in engineered structures.

Interestingly, fracture theory has mainly been applied to structures that deform in-

plane or have a small out-of-plane displacement (compared to the system size or local radius of curvature). However, there are important examples that require including a strong coupling between large out-of-plane displacements and fracture. The tearing to open a package and concertina tearing are some examples. To our knowledge, the first research works focused on these types of problems were conducted by Atkins [43]. He and coworkers studied the tearing of metal sheets under two approximations: first, the material sheet behavior is dominated by plasticity, and second, the tear is initiated by using a rectangular flap with two cracks. Using different constitutive models, Atkins was able to show that the cracks always converge, so that tears form pointed shapes.

The complex geometries observed in fracture of thin sheets, was shown in the tearing of plastic wrapping sheets in [44, 45]. In a classical traction configuration, these authors studied the wrinkles left by cracks due to different degrees of plastic deformation when moving from the edges to the interior of the sheet. These experiments opened new questions about the connection between in-plane stretched sheets and their out-of-plane, bent and stretched, counterparts.

More recently, Vermorel et al. [46] studied fracture in aluminum foil made by pushing a rigid object through a small hole. The stretching produced when moving a cone perpendicular to the plane of the sheet generates equidistant cracks that propagate in divergent radial directions. These divergent tears are similar to the concertina-tearing mode, however the direction of propagation is now dictated by symmetry.

Recent works have been focused on studying fracture in brittle sheets where fracture propagation does not leave strong signs of deformation far from the edges. The oscillating fracture paths studied by Audoly et al [47] and Mahadevan [48]

belong to this category. They studied a rectangular film clamped at two borders, where an initial notch is made. When a cylindrical blunt object is put inside the notch to push and fracture the film, a crack propagates following an oscillatory path. The same oscillatory trajectory has been studied under different geometrical and boundary conditions [49], and a theoretical model has been formulated that successfully reproduces the fracture trajectory [47].

For the same brittle thin sheets, Hamm el al. has studied [50] the tearing of a thin film adhered to a solid substrate. A rectangular flap with two cracks was pulled at 180 degrees with respect to the film plane to propagate cracks. It was shown that the cracks always converge to a point, and the final shape is a perfect triangle. In this case, the angle at the vertex of the tear is related to elastic properties of the film and the adhesion between the solid substrate and the film. The authors suggested that this angle could be used in metrology as a tool for assessment of the material properties of the film and adhesion. The same idea was used in reference [51] to study the mechanical properties of graphene.

Two other groups have reported a similar study where the same initial configuration is made but there is no adhesion [52, 53]. In this case, the two crack paths are also convergent, but they propagate along curved trajectories. The width of the tongue depends on a power law with the distance to the vertex, a result that has not yet been explained theoretically because of the complexity of deformation of the pulled flap.

1.3 Convergent Versus Divergent (or Pulling versus Pushing)

Although in most cases the tearing of a rectangular flap leaves a convergent tear, the concertina mode [40], or the radial fracture reported by Vermorel et al. [46] shows that divergent tears are also possible (although in plastic materials). These types of path are important in packaging and other applications where continual tearing is needed. Reference [50] showed that under general conditions a rectangular flap will propagate in a brittle material at an angle θ (see Figure 1.2) given by

$$\sin\theta = \frac{1}{\gamma t}\partial_W U_E(W,G) \tag{1.1}$$

Here $U_E(W,G)$ is the elastic energy of the flap, W is the length of the line connecting the flap with the film and γ is the work of fracture of the material. A displacement controlled configuration is represented by the symbol G: there are a set of geometrical parameters that need to be prescribed to store elastic energy on the surface. For example, the pulling case studied in [50] where the elastic energy is stored in a cylindrical fold of width W can be written as $U_E = 4BW/(2\ell - x)$ where B is the bending stiffness of the film and ℓ and x represent geometrical parameters defined in Figure 1.2). In the figure, we observe that $2\ell - x > 0$ has a fold connecting the flap with the film, hence the right side of equation (1.1) is always positive and the tear must converge. This is a rather intuitive result since we expect the elastic energy stored in a flap to be an increasing function of the size of the region where elastic energy is stored. How then can $\partial_W U_E(W,G)$ be negative to have divergent tears?

Figure 2.7 in section 2.3.1.1 shows a configuration inspired by the experiments made to produce an oscillating crack path. If two cracks are forced to propagate symmetrically instead of only one, the elastic energy stored when pushing the lip can be written based on dimensional grounds as $U_E = YW^2u(d/W)$ (in this case stretching energy is dominant in the fracture process, see section 2.3.1.1 for more details) where d is the distance that the lip is pushed and $u(x)$ is a dimensionless function. We expect the function $u(x)$ to be an increasing function of the in-plane displacement d, so that for small displacement, the energy can be assumed of the form $U_E = aYW^2(d/W)^n$ where n is an unknown positive exponent and a is a dimensionless constant. Thus, if $n > 2$, the elastic energy can be a decreasing function of the width of the lip switching the sign in equation (1.1). Since experiments show that $n > 2$, this explains why concertina tearing is also observed in brittle thin sheets.

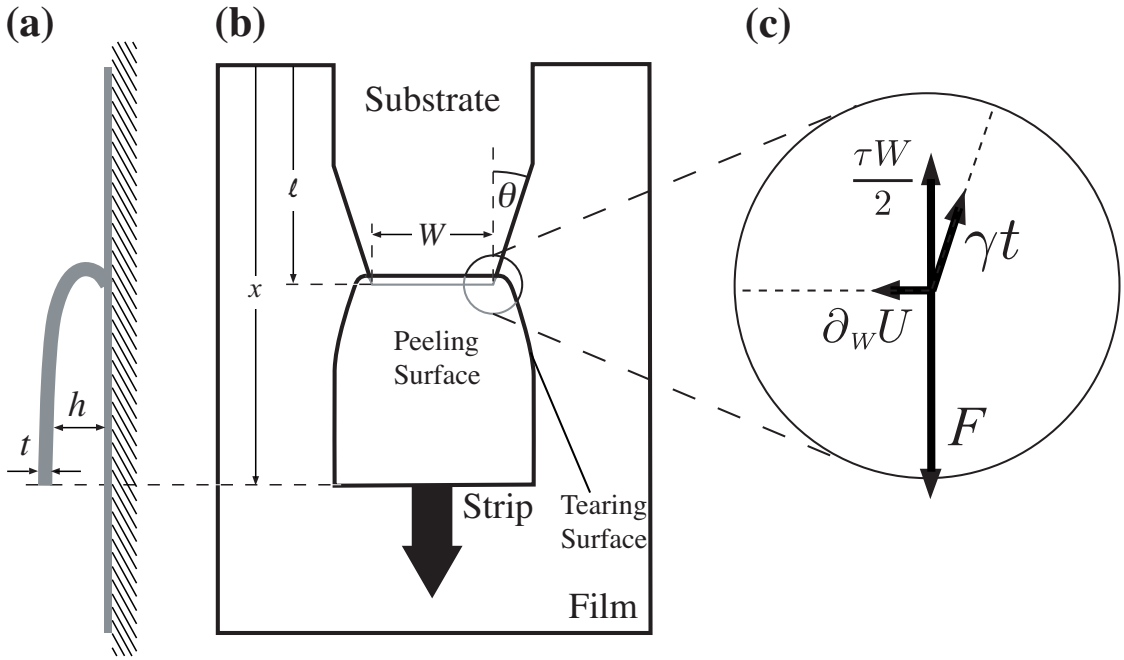

Figure 1.2: *Figure extracted from reference [50]*

1.4 Spirals

This thesis proposes a different mechanism to obtain divergent trajectories in brittle materials based on simple geometrical conditions. Under these conditions, we show that the fracture path can be forced to propagate in a spiral trajectory with a very robust and reproducible divergent path. Moreover, the crack trajectory asymptotically approximates a logarithmic spiral $r = r_0 e^{\theta \cot \phi}$ [54] (in polar coordinates r, θ) with a pole located in a position that depends on the starting seed" made to initiate the fracture, and a constant angle ϕ, the spiral angle, that is fixed by the material properties of the film.

Spiral shapes are not unknown in fracture mechanics. Shrinkage of a sol-gel layer producing a stress field that cracks the film in a complex 3D conical spiral has been reported in the literature [55]. The drying of thin layers of precipitates shows millimeter size spiral paths that move inwardly by propagation of a desiccation front [56, 57].

A first experiment presented in this work is connected to the oscillatory path experiment described in a section 1.2 and the pushing experiment described in last section. In this case, the blunt object is not forced to push in the center of the lip, so that only one crack starts to propagates. As the object follows and pushes the lip, a spiral crack trajectory is observed.

A second experiment is connected to the pulling experiment described in the last chapter 3. We pull a flap of the film, taking care that only one crack is allowed to propagate. It also generates a logarithmic spiral path.

Since most of the *"easy opening"* problems in packaging are related to the convergence of crack paths. We believe that our work could be very useful in applica-

tions based on brittle film enclosures. In fact we have deposited a patent with our findings. This patent is in appendix D.

1.5 Thesis Outline

We present this work in the following order:

1. In Chapter 2, we present a complete description of the formation of a spiral crack path with a blunt object.

2. In Chapter 3, we present a second kind of spiral crack path produced by tearing.

3. In Chapter 4, we conclude this work summarizing our findings.

Chapter 2

Spiral Rupture With a Blunt Object

In this chapter we experimentally and theoretically characterize a very smooth and reproducible spiraling crack path in a brittle thin sheet. In the experiment, a single crack is forced to propagate in a thin sheet of brittle material using a blunt object (tool). We found that the final crack shape is independent of the details of the movement of the tool, and the fracture trajectory is a spiral.

We have developed a simple model to explain the main characteristics of the process and the final shape, based on an energetic approach of fracture, and classical thin-sheet elasticity. With some help from basic geometry, we prove that the crack path obtained is a logarithmic (or equiangular) spiral.

Our model is supported by a separate quantitative experiment, which enabled us to measure the stored elastic energy in the system. It is also corroborated by measurements made of the predicted functionality for the fracture parameter. Finally, we present evidences in the geometry of the spiral path of the role of material anisotropy.

2.1 Spiral Experiment

A brittle thin sheet (Bi-Oriented polypropylene, BOPP, thickness t from 30 to 90μm) is carefully attached to a 100x80cm^2 aluminum frame, so that it is not pre-stretched, and there are no visible elastic structures, such as wrinkled zones.

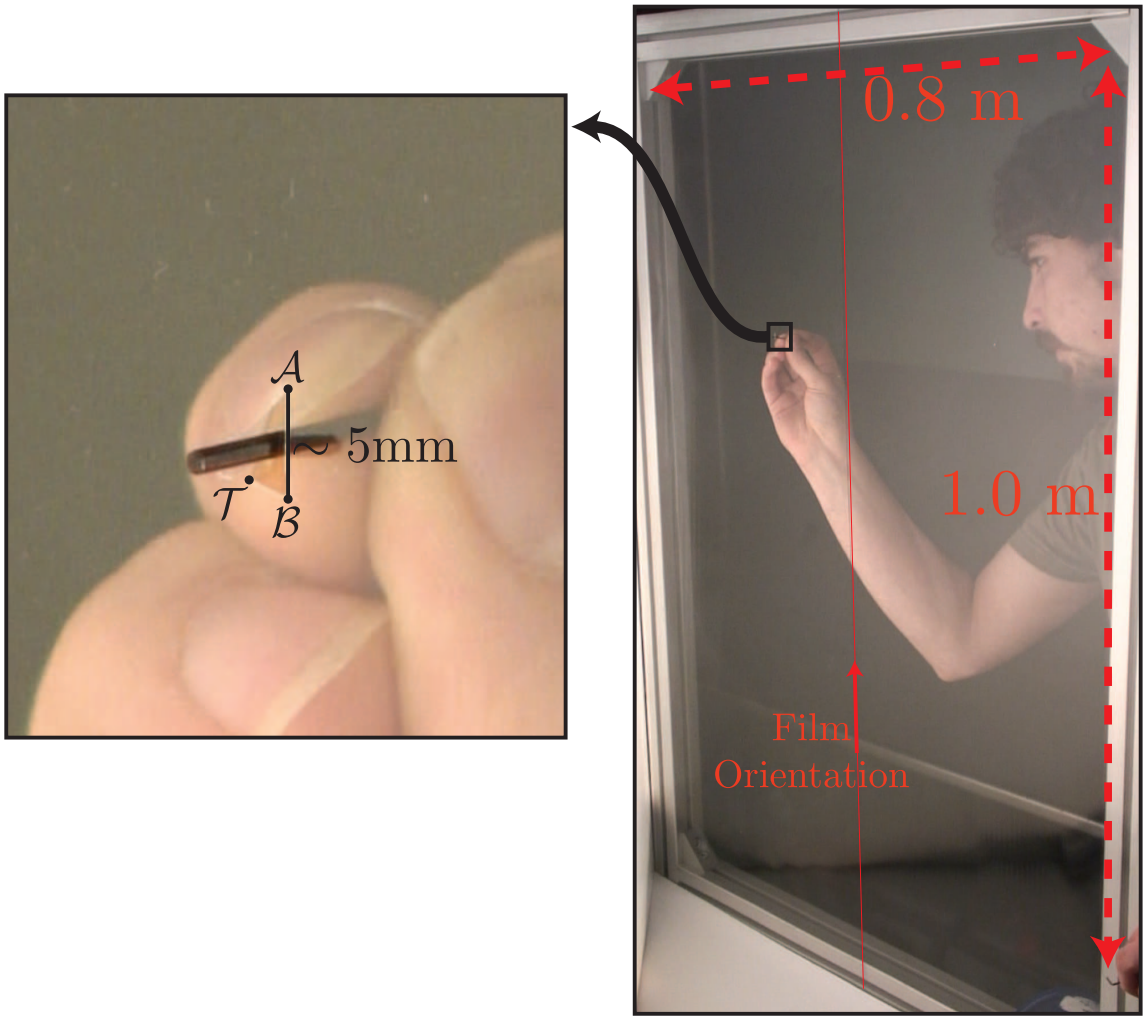

Figure 2.1: *Pictures of the spiral experiment.***Right:** *The whole experiment is presented; the red line in the center of the picture is the universal orientation of the film. In this case, the initial incision has been made parallel to the film orientation.***Left:** *Zoom centered on the initial incision, the points A, B, and T define the zone where we placed the used tool.*

Far from the edges of the thin sheet, we make a small straight cut with a knife, typically of ~ 5mm. We place a slim cylindrical[1] in the incision perpendicular to the plane of the film. Using this tool we nucleate and force to propagate a crack at point $\mathcal{B}$, by pushing one lip of the initial incision. By continually doing this, a curved path appears. At the beginning of the experiment it is important to keep the tool closer to the crack tip than to the other end of the incision because this asymmetry determines which crack will start to propagate (In Fig. 2.1 points $\mathcal{T}$ and $\mathcal{A}$ respectively), however this will be important only while there is another potential nucleation point (In this case point $\mathcal{A}$), and later in the experiment, it is not longer necessary.

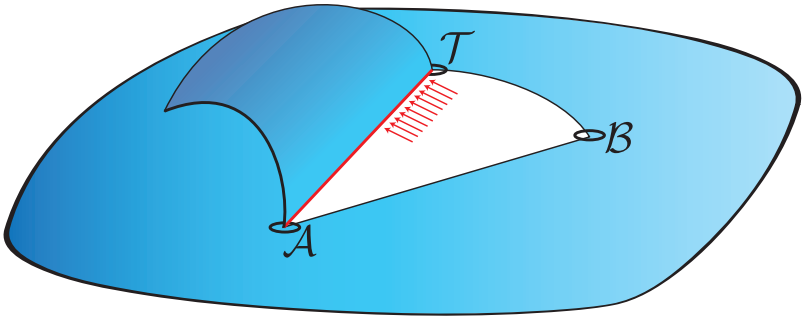

Figure 2.2: *In the figure we diagram the wide range of possibilities we have to push the lip at the beginning of the experiment (red arrows), within rule $\mathcal{R}$. In this case we only draw arrow close to point $\mathcal{T}$ to ensure that the propagation occurs at this point.*

Note that we are careful to maintain the orientation of the film (the effect of orientation will be discussed later in section 2.6), so we use pieces from a single very long rolled sheet and define a universal orientation across all the experiments.

[1] The shape of the tool is not be important in the fracture process, however it is important to use a small tool compared to the initial size of the incision

Throughout the experiment, we move the blunt tool according to only the following rule: $\mathcal{R}$:*"always push the same lip"*. This rule is rather loose, and leaves the freedom to push anywhere in the lip as we illustrate in Fig. 2.2.

However, following this process, we obtain a smooth crack path, a large spiral which grows from a ~ 10mm initial cut to a roughly ~ 1m diameter spiral in only 2.5 turns.

An example of the final tear is shown in the picture in Fig. 2.3.

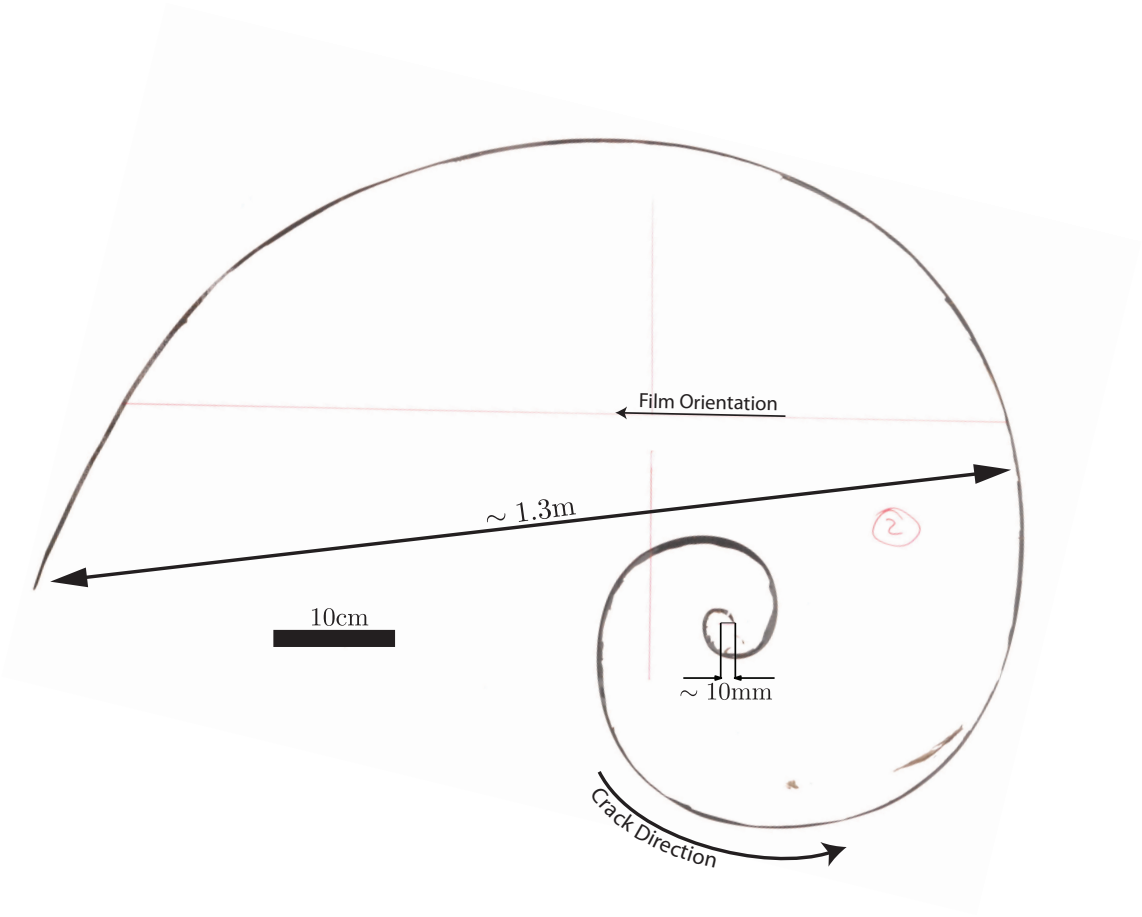

Figure 2.3: *Picture of the final tear obtained. The external edge of the darker zone is the resulting crack path. Notice the regularity of the shape.*

2.2 Tool path dependence

Although the experiment is done by hand, the regularity of the resulting spiral crack path in Fig. 2.3 is impressive because the movement of the tool has in fact not impacted on the final shape, as we show now.

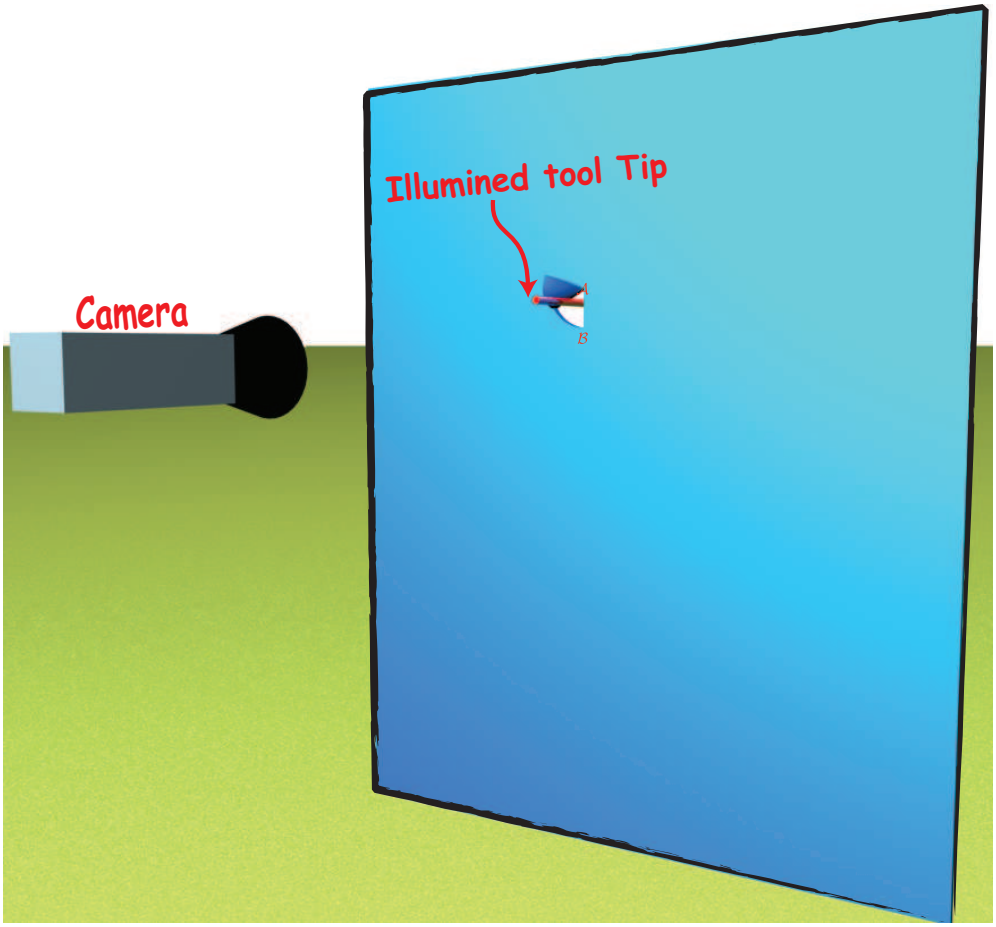

Figure 2.4: *Illustration for the tool tracking experiment*

Starting with the same initial conditions, we have deliberately chosen to impose very different tool paths and velocities in two experiments (still following rule $\mathcal{R}$). The movement of the tool is tracked in images taken by a camera (see Fig. 2.4). To help with the image processing, the tip of the tool is illuminated with a LED.

In Fig. 2.5 we present the superposition of the tool positions and the contour (post-mortem) of the crack paths. The solid and dashed outlines are the crack paths, and the circle and squares are the respective tool trajectories (tool position at equal interval of time).

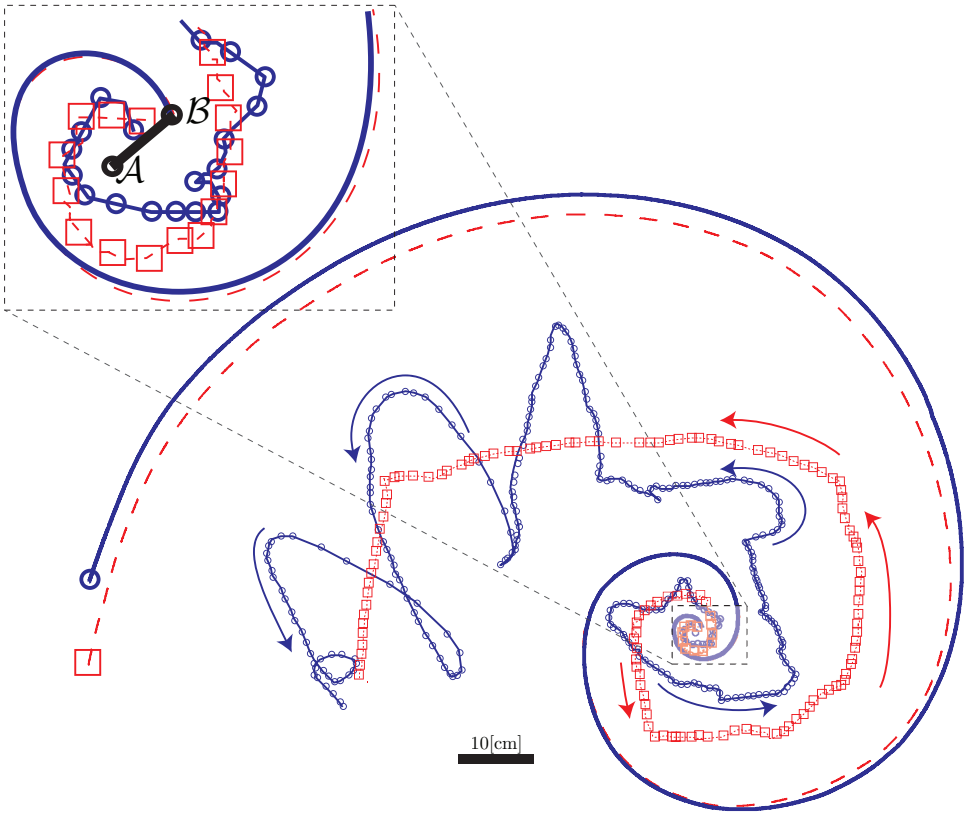

Figure 2.5: *Tool Trajectories and its respective resultant crack paths.*

Since the video gives us the position at equal intervals of time, ~ 0.5 second, the distance between two consecutive points of the tool path is a measurement of its velocity. It is obvious that the tool paths were very different. However, as can be seen in Fig. 2.5 the resulting crack paths are very similar and the small difference at the end of the spirals ($\sim$ 1cm)can be contrasted with the rapid growth of the spiral: any small difference at the beginning is quickly amplified. The difference is very small compared to the final size of the spiral, no more than 1% of the 1.3m

diameter.

This shows that the crack path is not determined by the will of the experimentalist, as one could imagine at first, but rather the system itself chooses the direction for crack propagation (as long as rule $\mathcal{R}$ is obeyed). In the rest of this chapter we try to explain this puzzling behavior.

2.3 Model

We now present a general model, for fracture propagation in a thin sheet loaded by a blunt object. Using simplifying assumptions for the mechanics of thin sheets and fracture mechanics (Griffiths criterion [58] and the criterion of maximum energy release rate, initially postulated by Erdogan [59]), we find the condition for crack propagation and predict the direction of the propagation. We will test our assumptions experimentally on a simple and more controlled configuration, and then we will compare the model and experiment in the case of spiral propagation.

2.3.1 Elastic Energy

We identify a basic configuration of energy storage and release of energy, and the Spiral propagation is based on the repetition of this basic configuration throughout the experiment. Suppose that the crack has propagated a distance s from point $\mathcal{B}$ to point $\mathcal{T}$, as illustrated in Fig. 2.6. At this point in the experiment, the unstressed lip, segment $\mathcal{AT}$, is pushed by moving the tool from point $\mathcal{O}$ to point $\mathcal{P}$ (see illustration on the right in Fig. 2.6). Consequently, the zone around the lip deforms and stores elastic energy. The elastic energy in the system plays a key role for fracture

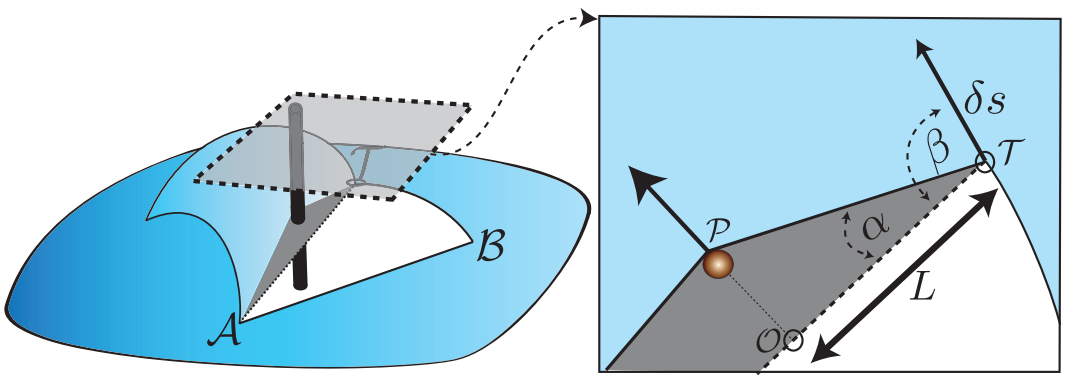

Figure 2.6: *Diagram of the configuration for energy storage in the system.*

propagation, and we now characterize it experimentally.

2.3.1.1 Experimental Characterization of the Elastic Energy

In order to explore more easily the energy storage functionality in the system, we slightly modify the configuration observed in the spiral experiment. A straight cut $2L$ long is made in a thin brittle sheet of thickness t and Youngs modulus E (see Fig. 2.7). Both ends of the incision are blunted by small perforations (diameter of $h \sim 4$mm). This procedure, if performed carefully, leaves no appreciable notches in the film, reducing the probability of initiating fracture. The size of the perforations is much smaller than that of the incision, in order to keep a constant length of the stretched lip. An illustration is presented in the inset in Fig. 2.7.

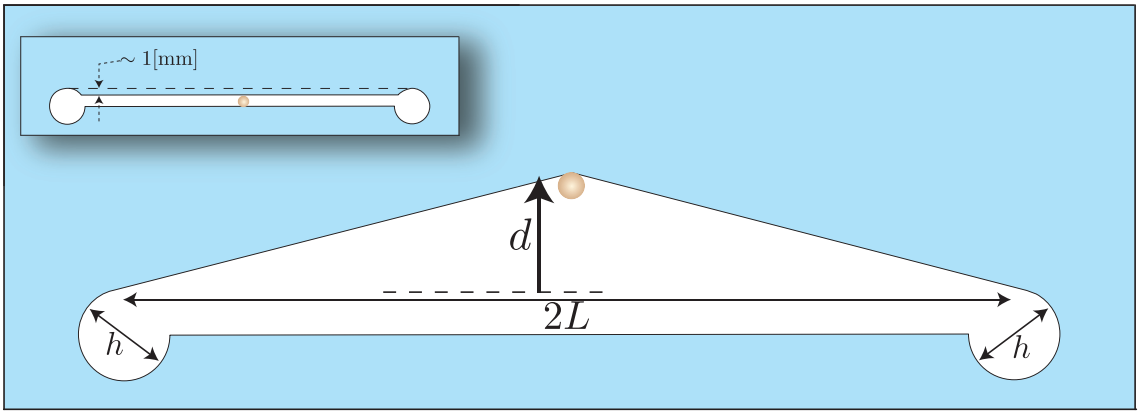

Figure 2.7: *Experimental diagram of the energy storage when a tool pushes a lip of a thin sheet.*

The force required to push the lip a distance d is measured in order to estimate the elastic energy. If the tool is placed at the midpoint of the lip, owing to symmetry, the elastic contribution of the left and right sides will be the same. Using an

Instron 5865 electromechanical testing device, we slowly (speed ~ 1mm/s) move the tool perpendicularly to the lip and record the applied force with a load cell Instron 2525-807, with a limit load of 100 N. Using this data and the size of the lip, we determine the penetration angle $\alpha \approx d/L$ at equal intervals of time.

For this experiment we used materials of thicknesses of 30, 50 and 90μm, with Youngs modulus $E = 2.9, 2.6$ and 2.7GPa, respectively. We have measured the force for initial cuts with lengths $2L$, of 6cm, 12cm, 18cm. The data, with combinations of different film thicknesses and lengths L of the lip, are presented in the plot of Fig. 2.8.

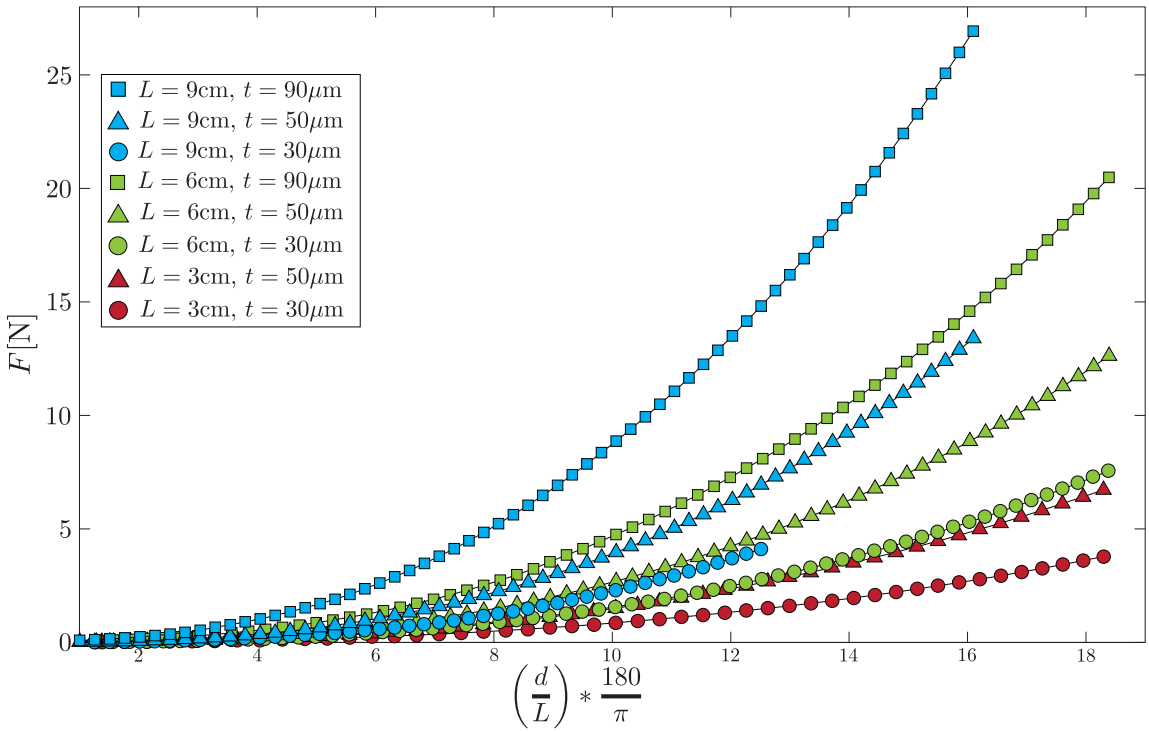

Figure 2.8: *Data from experiments with different lengths and different thickness sheets. The penetration of the tool is given by the quantity* d/L.

The curves stop for a given value of d/L, for which fracture initiates from the blunt tip and the film breaks. But the procedure captures the relevant range of values

for α observed in the spiral experiment, $[6^o, 12^o]$, presented as a yellow region in the graph in Figs. 2.9 and 2.10.

Since the sheet is very thin (compared to relevant lateral size L), we assume that bending energy is negligible compared to stretching energy (see section C.1.2). Since stretching energy is characterized by the combination Et, where E is the Youngs modulus and t is thickness, we expect from the dimensional analysis that the force obeys $F = EtL\phi(d/L)$, which can be developed for small values of d/L into $F = EtL(d/L)^n$. And indeed, all the measured force collapsed when F/EtL is presented as a function of d/L in Fig. 2.9.

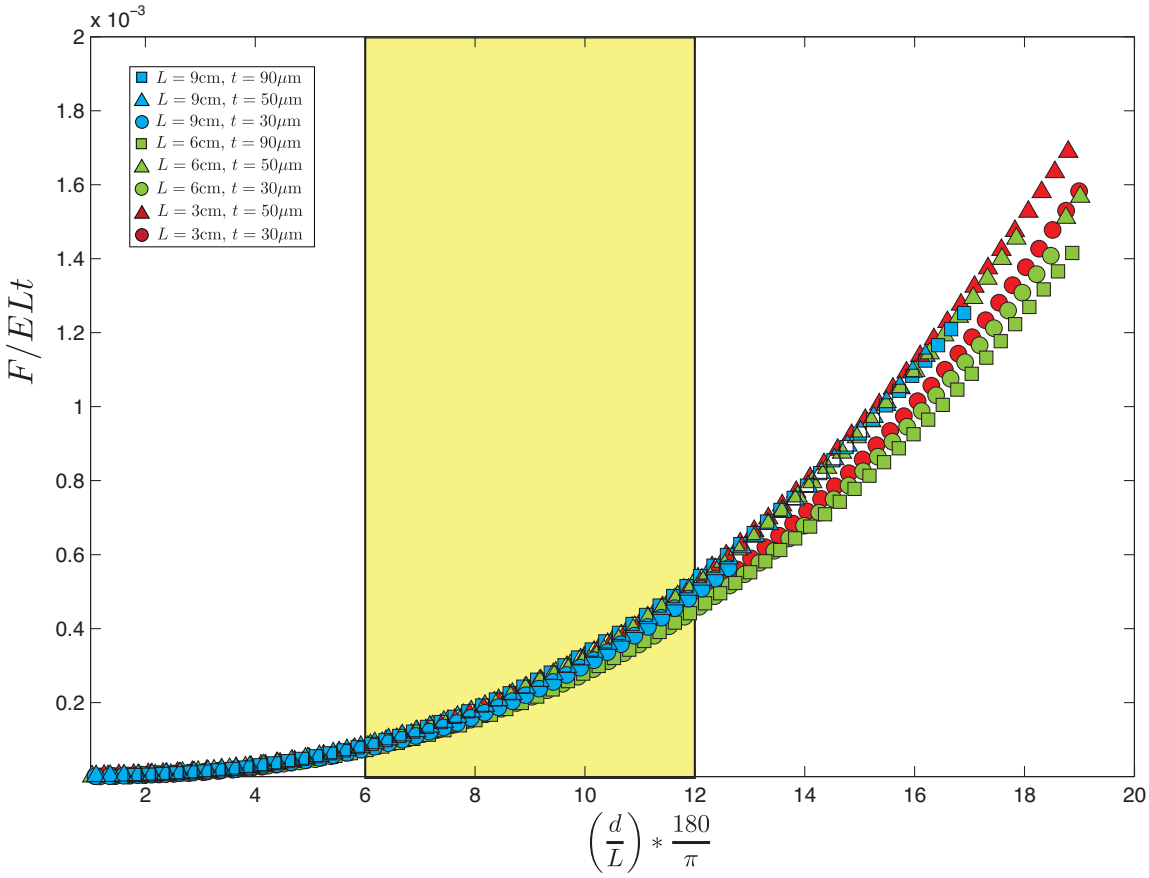

Figure 2.9: *Data from experiments with different lengths L and sheets with different thicknesses. The penetration angle of the tool is given by the quantity d/L.*

The assumption of a mechanical response dominated by stretching energy[2] in [47, 60] is therefore confirmed experimentally. An experimental measurement of function $\phi(.)$ is obtained by plotting the same data in a semi-log plot (in Fig. 2.10).

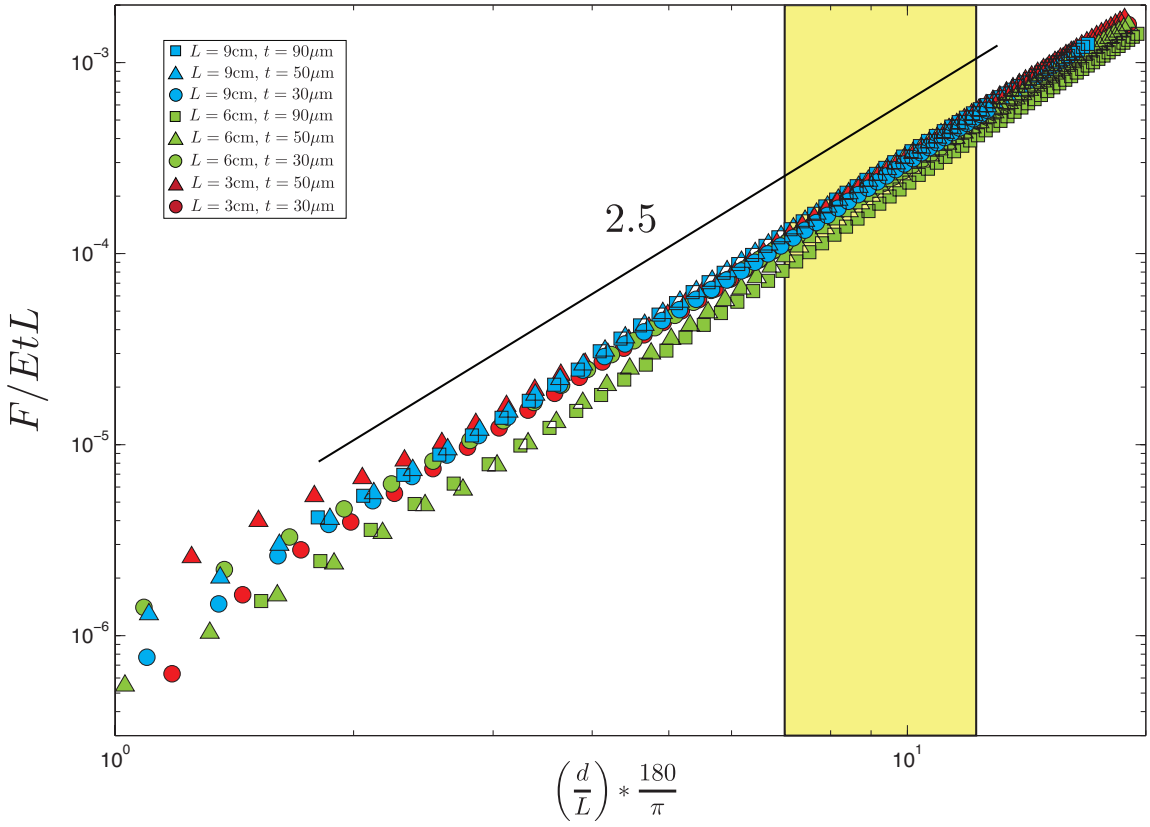

Figure 2.10: *Experimental data presented in terms of F/EtL versus the penetration d/L in a log-log plot.*

In this graph, forces measured at small values of $\alpha < 1^o$ are not represented for two reasons. First we expect that in the early stage of indentation, bending de-

[2]Note however that in thin sheets theory, one usually use the opposite argument : if stretching energy is very costly, then the system tends to avoid stretching and stays close to isometric solutions, *if possible*. But this argument, at the base of [48], cannot hold here, since the loading condition clearly inevitably imposes some stretching.

formations exceed incipient stretching deformations and are therefore outside of our theoretical description. Secondly, the experimental determination of zero in d is difficult and modifies this part of the graph. In the inset on the top left corner in Fig. 2.8,we illustrate the initial configuration. A small flap is produced when the initial cut is made. This flap has two consequences on the experimental measurements. One is that at the beginning of the experiment some bending related energy is measured, and the second effect is related to the position in which lip AB begins to be pushed. The procedure for setting the initial position is the following: we manually approach the pushing tool to the lip until it is very close to the edge. Then, after the experiment is done, omit the part of the data where the force is small, because it means that there is no contact between the tool and the film. When this data is plotted in a log-log graph, they collapse in straight lines, however for small values of d/L not all the curves are straight. We attribute this to the setting of the zero position. We have reset the zero for the curves that did not collapse completely. These curves are ($L = 3$cm $t = 50\mu$m), ($L = 6$cm, $t = 90\mu$m), ($L = 9$cm $t = 90\mu$m). The correction for these curves has been a shift in (d/L) in 0.04, which means a change of d in 1mm, 2.4mm and 3.6mm respectively. These changes are not small but are within the range of the experimental conditions. We remark that doing this only affects the curves at very small values of (d/L) (in the interval of $\frac{180}{\pi}\frac{d}{L}$ between 1 and 2) and the data is unaffected in the fracture zone (in yellow in Figs. 2.9) and 2.10 The collapse over three decades of the force measurements in Fig. 2.10, demonstrates that the constitutive relation for the force in this system can be very well approximated by:

$$F = 0.0266EtL\left(\frac{d}{L}\right)^{2.5} \tag{2.1}$$

where the factor 0.0266 and the power 2.5 are the average of the intersects and the slopes of the respective parameters obtained fitting the curves in Fig. 2.10. If we now calculate the work done by the tool movement, we obtain the stored elastic energy, U_E, in the system.

$$U_E = \int F\delta d = 0.0266EtL \int L\alpha^{2.5}\delta\alpha \tag{2.2}$$

Finally a good approximation of the constitutive relation for the energy of the system is:

$$U_E = 0.0076EtL^2\alpha^{3.5} \tag{2.3}$$

The non-linear law in Eq. 2.3 cannot be explained by the usual linear elastic response approach, which would lead to a quadratic energy dimensionally equivalent to $EtL(d/L)^2 \sim EtL\alpha^2$. It is not easy to include the non-linearities due to large out-of-plane displacement. A first approach [3] is to consider that such a thin material cannot convey compressive (negative) stresses, because they are released by infinitely easy buckling. Following this idea, Audolys [47] estimated the typical strain in the system from the change in length of the pushed lip (initially with length L and now $L/\cos\alpha$) to be proportional to $\epsilon \sim \alpha^2$. Since no compression is transmitted, only a triangular zone (with size $S \sim Ld = L^2\alpha$) is actually displaced ahead of the pushing tool. The estimated stretching energy in the system would be proportional to $EtS\epsilon^2 = EtL^2\alpha^5$. The experimental data obtained in this section disagrees with this result, the exponent being close to $\alpha^{3.5}$.

In a study of a similar problem, but in a different geometry, Vermorel et al [46] have described the propagation of radial cracks when a cone pierces a thin sheet, leading to the propagation of several radial cracks. Propagation owes to the cone pushing on the lip in between consecutive cracks, leading to orthoradial tension ϵ

similar to that in [47]. But the stored elastic energy was this time estimated from the ideal 2D situation of a circle with radius R subject to an orthoradial strain ϵ. The solution for 2D elasticity shows that strains decay like $1/r^2$, where r is the distance to the center of the disk, and that the disk radius increases by a distance $d = R\epsilon$. Finally, the energy is found $Et(1+\nu)^{-1}(\epsilon R)^2$. Although the interpretation is not perfect because of radial geometry, we take R as an equivalent of L, use $\epsilon \sim \alpha^2$, and find that this model leads to an energy scaling like $Et\alpha^4 L^2$, with an exponent 4 which is closer to 3.5.

Energy functions proposed in [47] and [46] are built on the same hypothesis : only the lateral extensional stresses balance the pushing force in such a thin film. But in [46] these extensional stresses are transmitted up to a characteristic distance L, even if material points in this area are not directly pushed by the tool. This assumption is reasonable and gives a good approximation of the experimental law. We note that the experimental exponent is slightly smaller than predicted, which suggest that the assumption of infinitely thin sheet might not be completely valid.

We now turn to non symmetric loading, as depicted in Fig. 2.11.The energy is the result of a spatial integration of the strain square, so that it is the sum of the integrals of the left and right sides respect to the tool. Nevertheless this does not necessarily mean that the energy from the left and the right have the same functionality as in Eq. (2.3), because the strains from left and right sides are coupled. We have measured the force in a non-symmetric situation, as in Fig. 2.11

Based on the results expressed in Eq. (2.1), we assume that the force has the form,

$$F = aEt\left(L\left(\frac{d}{L}\right)^{2.5} + L'\left(\frac{d}{L'}\right)^{2.5}\right) \tag{2.4}$$

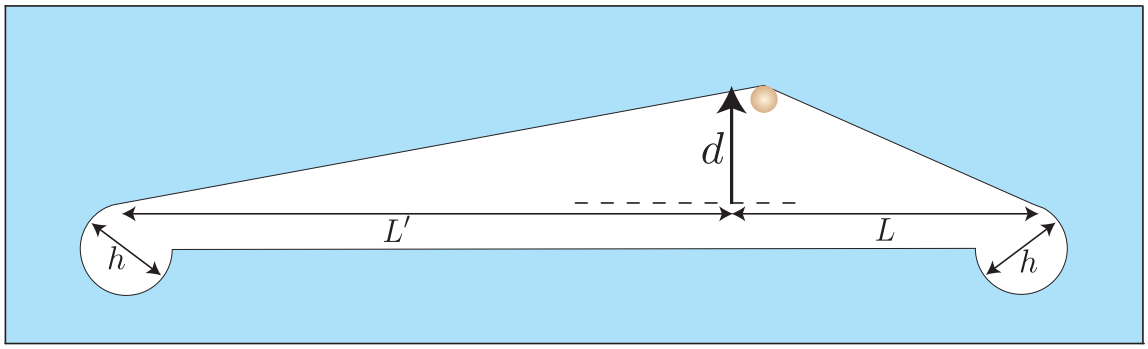

Figure 2.11: *Non-symmetric experimental measure of force.*

Where a is a factor to be obtained from the data.

The combined nonlinear dependency on the two parameters, d/L and d/L' makes it impossible to analyze this data in a dimensionless way, as we do in the symmetrical case. However, we present in the plots in Fig. 2.12, how the quantity F/Et behaves as a function of $L'(d/L')^n + L(d/L)^n$, for $n \in [1, 3]$ for 4 experiments, in a 50μm-thick sheet, made with different asymmetric positions of the tool and keeping the total length of the edge, $L + L' =$const.

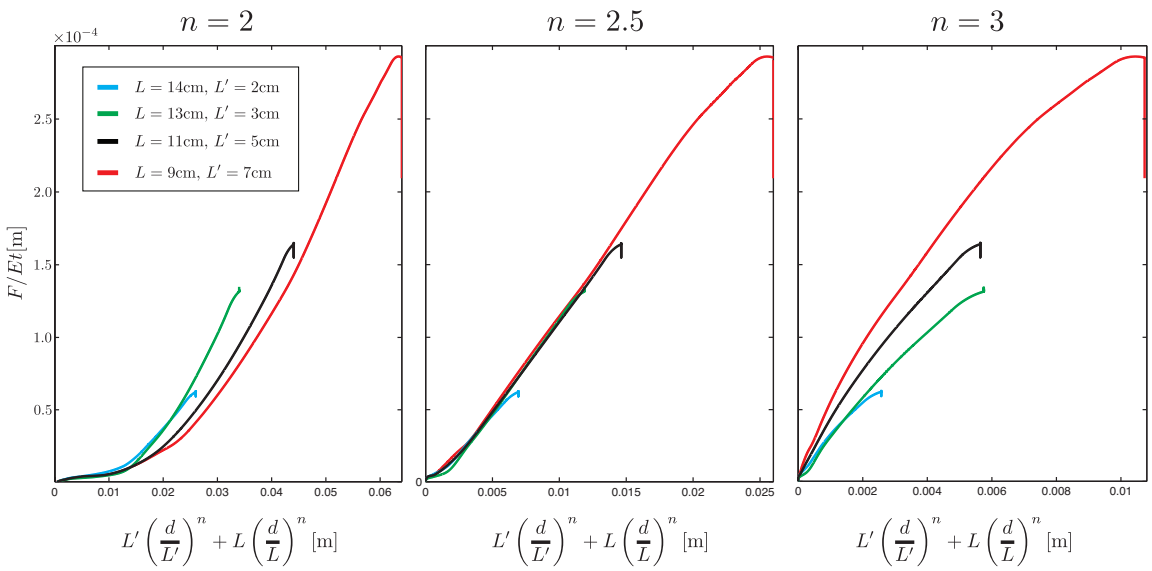

Figure 2.12: *Force measurements in a non-symmetric experimental configuration.*

The linear behavior and the collapse observed for F/Et in the central plot in

Fig. 2.12, $n = 2.5$, shows us evidence to assume that it is possible to separate the energy in the contribution of the left and right side of the lip with respect to the tool, a simple verification is possible with a linear polynomial fit. In averaging the resulting slopes for the corresponding linear behavior, we obtain the empirical mechanical response:

$$F = 0.0129Et\left(L\left(\frac{d}{L}\right)^{2.5} + L'\left(\frac{d}{L'}\right)^{2.5}\right), \tag{2.5}$$

If we compare Eqs. (2.1) and (2.5) we note that the factor in the first is twice that of the second expression. Indeed in the symmetrical case, both sides contribute in the same way, leading to a factor 2. Thus, we conclude that, at least in the regime where fracture occurs, it is possible to express the energy in the form of Eq. (2.4)

2.3.2 Fracture Propagation

Once we have an expression for the energy, we turn the discussion to model fracture propagation. We reformulate in a different way an argument equivalent to that of [47]. Consider the example where the crack is at point $\mathcal{T}$ after it has propagated a distance s (see Fig. 2.13(a)). As was done by Audoly et al. [47].,we define the convex hull of the crack path. In this case it is the interior zone demarcated by the points $\mathcal{A}$, $\mathcal{B}$ and $\mathcal{T}$. In the previous section we have shown that the system is guided by stretching energy, and not bending. This implies that the tool will not induce fracture if it is placed within the convex hull (which is in Audolys work it is called the “soft zone”), but only bending of a flap. In contrast, if we move the tool outside of the convex hull, the energy in the system will dramatically increase, as we show with the relation in Eq. (2.3. The zone occupied when the tool leaves the

soft zone is called the active zone since it is where the tool is working. At some threshold value, the system cannot store any more energy and releases it, at the cost of creating a new surface: the crack now moves from the point $\mathcal{T}$ to $\mathcal{T}'$, and we see that the elastic energy decreases in the process: the active zone transfers area to the soft zone (now defined as the area demarcated by the points $\mathcal{A}$, $\mathcal{B}$, $\mathcal{T}$, $\mathcal{T}'$, see Fig. 2.13(b)).

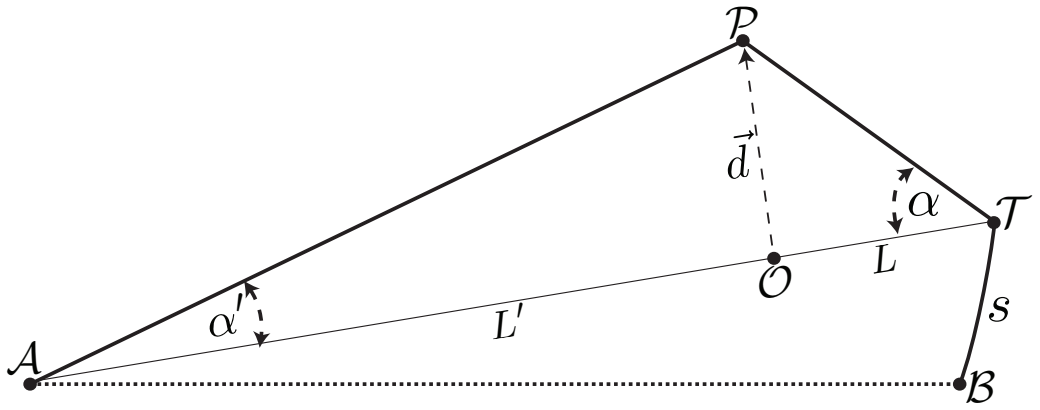

(a) *Geometry before fracture.*

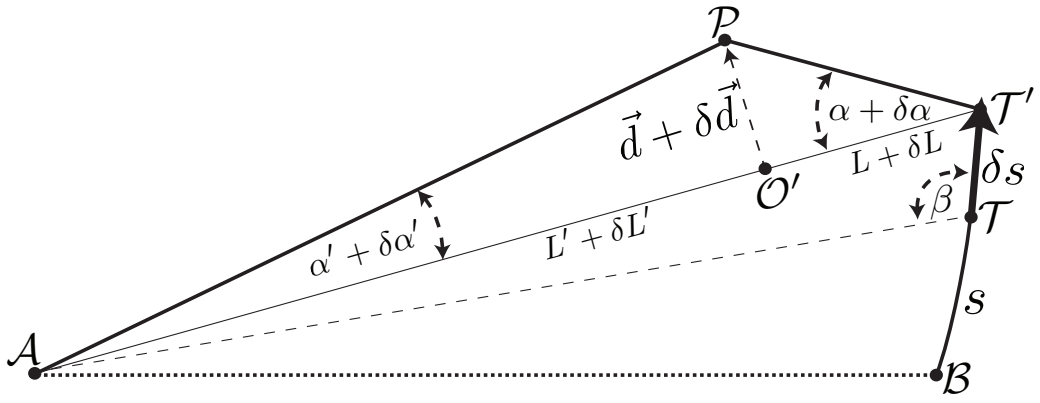

(b) *Geometry after the crack, of length s, propagates a distance δs.*

Figure 2.13: *Geometry of the system configuration.*

In order to formalize the ideas presented above, we separate the fracture process in two stages:

1. **Before rupture:** The tool performs work by pushing the edge of the film from point $\mathcal{O}$ to point $\mathcal{P}$. Energy increases because of the stretching, which is evaluated from the experimentally obtained expression in Eq. (2.3)

2. **Rupture:** Now that $\mathcal{P}$ is held fixed, we ask about crack propagation: does the crack advance and to what position? .

Griffith's approach [58, 61] was to consider that the cracks position is the one that minimizes total energy

$$U_T = U_E + \gamma t s \tag{2.6}$$

where we have noted U_E the elastic energy, and γts is the energy associated with a crack of length s, in a film of thickness t (γ is the work of fracture [61]). This minimization is done with respect to the geometrical changes due to rupture propagation of a small amount, from $\mathcal{T}$ to $\mathcal{T}'$. This modifies the values d, L, and L' (see Fig. 2.13(b)). From the geometric dependence we obtain:

$$\delta U_T = (\partial_d U_E)_{L,L'} \delta d + (\partial_L U_E)_{d,L'} \delta L + (\partial'_L U_E)_{d,L} \delta L' + \gamma t \delta s = 0 \tag{2.7}$$

Where $(\partial_x U_E)_{y,z}$ is the variation of U_E respect the variable x with y and z fixed. Note that the force applied is connected with the energy by the relation $\vec{F} = \partial_d U_E \hat{d}$, therefore the magnitude of the force is given by $F = \partial_d U_E$, so the equilibrium equation is:

$$\delta U_T = F\delta d + \partial_L U_E \delta L + \partial_{L'} U_E \delta L' + \gamma t \delta s = 0 \tag{2.8}$$

2.3.2.1 Geometrical Variation

It is possible to calculate, from Fig. 2.13(b), how much the system geometrically changes when the fracture moves forward a length δs. A first result for $\delta\alpha$ is:

$$\tan(-\delta\alpha') \sim -\delta\alpha' = \delta s \frac{\sin\beta}{W} \longrightarrow \delta\alpha' = -\frac{\delta s}{W}\sin\beta \tag{2.9}$$

where $W = L + L'$ and β is the direction of the crack with respect to the unstressed edge, segment $\overline{\mathcal{AT}}$ in Fig. 2.13(b).

Using the fact that $\tan(\alpha + \delta\alpha + \delta\alpha') = (L\tan\alpha - \delta s)/(L - \delta s\cos\beta)$, we solve for $\delta\alpha$:

$$\begin{aligned} \delta\alpha &= \frac{\delta s}{L}\cos\alpha\sin(\alpha-\beta) - \delta\alpha' \\ &= \frac{\delta s}{L}\cos\alpha\sin(\alpha-\beta) + \frac{\delta s}{W}\sin\beta \end{aligned} \tag{2.10}$$

The distance $\delta L'$ comes from:

$$\begin{aligned} L' + \delta L' &= \frac{L'}{\cos\alpha'}\cos(\alpha' + \delta\alpha') \\ \delta L' &= -\delta\alpha'\tan\alpha' \\ &= \delta s\frac{L'}{W}\tan\alpha'\sin\beta \\ &= \delta s\frac{L}{W}\tan\alpha\sin\beta \end{aligned} \tag{2.11}$$

To calculate δL we use the fact that $-\delta\alpha' \ll 1$:

$$\begin{aligned} \frac{L + L' - \delta s\cos\beta}{L + \delta L + L' + \delta L'} &= \cos(-\delta\alpha) \sim 1 \\ \delta L &= -\delta s\cos\beta - \delta s\frac{L}{W}\tan\alpha\sin\beta \end{aligned} \tag{2.12}$$

Finally, we calculate δd using $(L\tan\alpha + \delta d)/(L + \delta L) = \tan(\alpha + \delta\alpha)$. Directly we obtain:

$$\delta d = L\sec^2(\alpha)\delta\alpha + \tan(\alpha)\delta L \tag{2.13}$$

After some algebra and using results from Eq. (2.9) and (2.10), we get δd changes as a function of δs as:

$$\delta d = -\delta s\frac{L'}{W}\sin\beta \tag{2.14}$$

2.3.2.2 Griffith's criterion and second Variation of the energy

The first variational equation that represents equilibrium of the system in Eq. (2.8) is Griffiths criterion. With the geometric relations obtained above, Eqs. (2.11), (2.12) and (2.14), it may be written:

$$\left(-\frac{L'}{W}F - \frac{L}{W}\tan\alpha\left(\partial_L U_E - \partial_{L'}U_E\right)\right)\sin\beta - \partial_L U_E\cos\beta = -\gamma t. \tag{2.15}$$

where the left side of the equation is the energy release rate, which equals fracture energy when the crack propagates. We see that the energy released depends only on the direction β in which the crack propagates for a given loading condition (L, L', d and therefore F are fixed). Maximum release rate criteria establish that the crack will choose the direction in which more energy is released. This implies the second variation:

$$\frac{\partial}{\partial\beta}\frac{\delta U}{\delta s} = \left(-\frac{L'}{W}F - \frac{L}{W}\tan\alpha\left(\partial_L U_E - \partial_{L'}U_E\right)\right)\cos\beta + \partial_L U_E\sin\beta = 0 \tag{2.16}$$

These equations can be written in a more compact way. Solving for $\partial_L U_E$ in the last term on the middle expression in Eq. (2.16) and replacing this result with the corresponding term in Eq. (2.15) we obtain:

$$F = \frac{L}{L'}\tan\alpha\left(\partial_{L'}U_E - \partial_L U_E\right) + \frac{W}{L'}\gamma t\sin\beta \tag{2.17}$$

If we use this result in Eq. (2.16) a second expression is obtained:

$$\partial_L U_E = \gamma t\cos\beta \tag{2.18}$$

This set of equations is the basis in our analysis to compute the fracture parameters. For a given position of the tool (set by L and L'), in a given material (with Youngs modulus E and fracture energy γ), we need three constitutive relations to solve for the critical value of α and α and the direction of the crack β.

2.3.2.3 Fracture Propagation Law

We can now use our estimates for the force and elastic energy, to obtain the rules for the propagation of the crack in our configuration. From the results in section 2.3.1.1, we know that the dominant energy is stretching and it can be written as the sum of the contribution of the left and right sides, this is $U_E = U_l + U_r$:

$$U_E = U_l + U_r = aEt\left(L'^2\left(\frac{d}{L'}\right)^n + L^2\left(\frac{d}{L}\right)^n\right). \tag{2.19}$$

The total force is:

$$\begin{aligned} F &= \partial_d U_E \\ &= aEt\left[nL'\left(\frac{d}{L'}\right)^{n-1} + nL\left(\frac{d}{L}\right)^{n-1}\right] \\ &= anEtL\left[1+\left(\frac{L}{L'}\right)^{n-2}\right]\alpha^{n-1} \end{aligned} \tag{2.20}$$

Similarly, we obtain the other terms in Eqs. (2.17) and (2.18)

$$\begin{aligned} \partial_L U_E &= \partial_L U_r \\ &= -aEtL(n-2)\left(\frac{d}{L}\right)^n \\ &= -aEtL(n-2)\alpha^n \end{aligned} \tag{2.21}$$

$$\begin{aligned} \partial_{L_l} U_E &= \partial_{L'} U_l \\ &= -aEtL'(n-2)\left(\frac{d}{L'}\right)^n \\ &= -aEtL'(n-2)\alpha'^n \end{aligned} \tag{2.22}$$

We are interested in the critical value α_c when the crack starts to propagate, and the direction for the propagation, angle β. We begin by replacing Eqs. (2.20), (2.21) and (2.22) in (2.17). This leads to:

$$anEtL\alpha^{n-1}\left(1+\rho^{n-2}\right) = \gamma t \sin\beta\,(1+\rho) + aEt(n-2)L\alpha^{n+1}\rho\left(1-\rho^n\right), \tag{2.23}$$

where we have defined $\rho = L/L$' a geometric parameter that is small if the tool is close to the crack tip. Since we are working in the regime $\alpha \ll 1$, we neglect the last term in Eq. (2.23), because of the high order of α. Eqs. (2.17) and (2.18) take the form:

$$anEtL\alpha^{n-1}\left(1+\rho^{n-2}\right) = \gamma t \sin\beta\,(1+\rho) \tag{2.24}$$

$$-a\,(n-2)\,EtL\alpha^{n} = \gamma t\cos\beta \tag{2.25}$$

We have two equations and two unknowns α and β. We first resolve β:

$$\cot\beta = -\frac{(1+\rho)}{(1+\rho^{n-2})}\frac{(n-2)}{n}\alpha \tag{2.26}$$

We know through experiments that the solutions for β must be close to $\pi/2$ so $\cot\beta = \tan(\pi/2-\beta) \sim \pi/2-\beta$, consequently Eq. (2.26) becomes:

$$\beta = \frac{\pi}{2} + \frac{(1+\rho)}{(1+\rho^{n-2})}\frac{(n-2)}{n}\alpha \tag{2.27}$$

Using this result, we have for Eq. (2.24):

$$\alpha_c = \left(\frac{\gamma t}{anEtL}\frac{1+\rho}{1+\rho^{n-2}}\right)^{1/(n-1)} \tag{2.28}$$

We now review the assumptions made to obtain the last two relations. The main requirement in our calculations is to have small angles α, $\alpha' \ll 1$ along the fracture process. However, this cannot be true if the tool is too close to points $\mathcal{T}$ or $\mathcal{A}$ in Fig. 2.13(a). The divergence when the tool approaches point $\mathcal{T}$ is explicit from Eq. (2.27), however, it is a weak divergence due to the low exponent $1/(n-1) \approx 0.4$. The failure of our approach when the tool is close to point A is observed in Eq. (2.23), where a term of higher order in the angle α was neglected. Comparing this term to the left side of the same equation, we obtain (for the validity of this approximation) the condition,

$$n(1+\rho^{(n-2)}) \gg (n-2)\alpha^2\rho(1-\rho^n) \tag{2.29}$$

We have experimentally measured a typical value of $\alpha_c \sim 10^o$, if we plug this value in Eq. (2.29) we obtain that the assumption is satisfied for $\rho \lesssim 4$, which implies $L \lesssim 0.8W$. Thus, the tool cannot be closer than a distance $W/5$ to point $\mathcal{A}$. Now, when we are moving the tool within the region $L \lesssim 0.8W$, we observe, from Eqs. (2.28) and (2.27), that the factor $(1+\rho)/(1+\rho^{n-2})$ changes α and β no more than 2 and 0.9 degrees, respectively, due to variations in ρ. Therefore, it is a good approximation to neglect ρ in relation Eqs. (2.27) and (2.28). It yields

$$\alpha_c = \left(\frac{\gamma}{anEL}\right)^{1/(n-1)} \tag{2.30}$$

$$\beta = \frac{\pi}{2} + \frac{(n-2)}{n}\alpha \tag{2.31}$$

This result shows that α and β depends on L with a weak power. Thus, we conclude that the distance L is not important in crack growth, since, with some restrictions, α and β are fairly constant geometrical parameters.

By using the results from section 2.3.1.1, we expect a value of $n \sim 3.5$, which imply that Eqs. (2.30) and (2.31) take the form:

$$\alpha_c = \left(\frac{\gamma}{3.5aEL}\right)^{0.4} \tag{2.32}$$

$$\beta = \frac{\pi}{2} + 0.4\alpha_c \tag{2.33}$$

It is remarkable that the fracture process, despite large complex deformations, is completely characterized with these two geometrical expressions.

2.3.2.4 Model Confirmation

Eq. (2.32) establishes a threshold value for the angle α. The dependence on the distance L is rather weak, but we have designed a simple experiment to measure it precisely.

In a 50μm-thick sheet, we made a 23-cm-long incision. Because we want the crack to propagate only at one end, by making a small hole at the other end of the incision, we geometrically avoid secondary nucleation.

With a high-definition video camera, we recorded the fracture process and measured the critical value of the angle α (this is the value just before the crack propagates) and studied how α_c evolves with the distance between the tool and the crack tip, L.

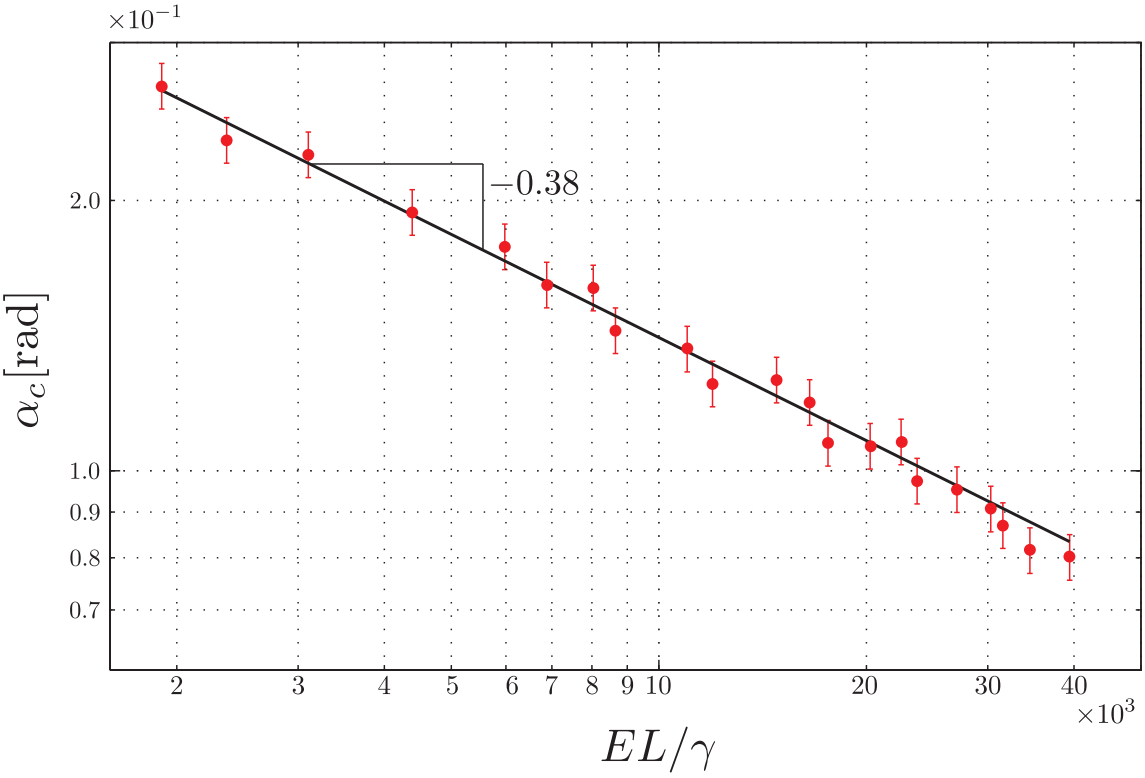

Figure 2.14: *Critical value of penetration angle α_c as a function of the dimensionless quantity EL/γ plot with red dots. The black line corresponds to the linear fit of the logarithmic rectification of the collected data.*

The measurements are presented in Fig. 2.14, where L is adimensioned by the

distance[3] $\gamma/E \sim 4\mu$m.

A reasonable power law is observed, and the best fit is given with negative exponent -0.38, and

$$\alpha_c = \left(\frac{\gamma}{3.5 \times a' \times EL}\right)^{0.38} \tag{2.34}$$

with $a' = 0.0059$. The predicted exponent in Eq. (2.30) is $1/(n-1) = 0.4$ (since $n = 3.5$ was found experimentally), which is very close to the value 0.38 found in (Eq. (2.34)

Comparing now the pre-factor in Eqs. (2.34) and (2.32) we identify a value $a' = 0.0059$. From the experimental characterization of the energy in the system, we have found a value for the factor $a = 0.0076$, see Eq. (2.3). These values show the very good agreement among them, which is impressive since these results come from very different experiments connected to derivations based on many facilitating approximations.

We conclude this section by summarizing the most important results. The energy in the system is defined by geometrical features (the soft zone is the convex hull of the crack path), and the most important contribution comes from stretching energy. By simplifying the configuration and using classical fracture mechanics, we have found two laws for the propagation of the fracture. First we found a critical value for the penetration angle α_c, at which the crack propagates. The second important result predicts the direction for the propagation (angle β). This angle is close to perpendicular to the lip.

What does this model predict in the geometrically more complex situation where we have observed a spiraling propagation?

[3] for this 50μm sheet, $\gamma t \sim 0.6 \pm 0.1$N (value obtained from reference [50]), the fracture energy is $\gamma \approx 1.2 \times 10^4$N/m, and Youngs modulus E is 2.7GPa.

2.4 Three different stages in the Spiral

Having described the way in which the crack propagates when an object pushes one lip, we are now in condition to explain spiral formation. We find that the process occurs in three stages.

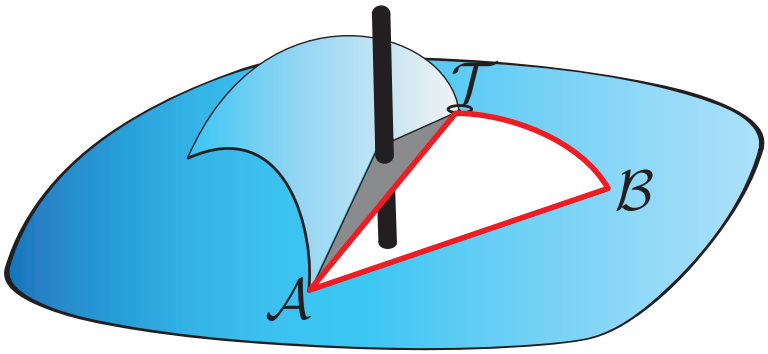

Figure 2.15: *Convex hull illustration.*

In Fig. 2.15 the zone surrounded by the red bold line is the soft zone limit (the minimum convex domain - or convex hull - that contains the crack path). If we place the tool inside this zone, the film only bends. Because bending does not affect the system, the fracture will not propagate. If the tool is moved outside this zone, the film is stretched, the energy increases and at some threshold value the fracture propagates. In particular, if we go out the convex hull pushing the segment $\overline{\mathcal{AT}}$ as is shown in Fig. 2.15, the crack ,$\mathcal{T}$,will propagate with direction β with respect to the segment $\overline{\mathcal{AT}}$. The convex hull limit remains on the new line $\overline{\mathcal{AT}}$.

It is possible to compute the exact shape of the path in these stages. Using polar coordinates, centered on $\mathcal{A}$, the differential equation for the distance of the path to the center $\mathcal{A}$ is given by $\partial_\theta r/r = -\cot\beta$, if β does not depend on θ, the solution is $r = r_o e^{-\theta\cot\beta}$, r_o is given by the initial condition, in this case it is equal to the

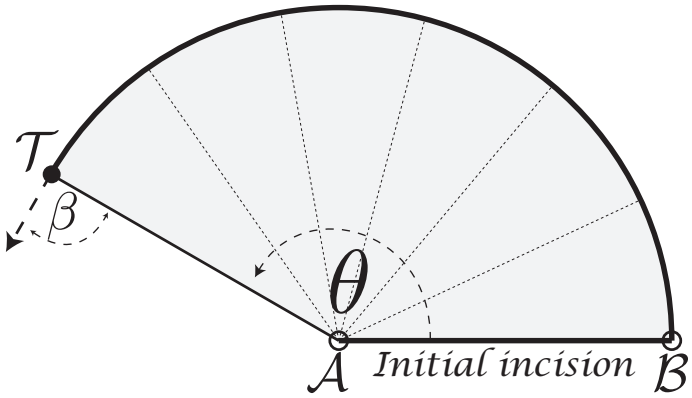

Figure 2.16: *Initial stage for the spiral formation*

length of $\overline{\mathcal{AB}}$. Since β is assumed to be constant and close to $\pi/2$, the resulting crack path is a logarithmic spiral growing very slowly around the point $\mathcal{A}$.

Throughout this stage, the convex hull has the same configuration. At all moments it is bounded by two straight lines (segments $\overline{\mathcal{AB}}$ and $\overline{\mathcal{AT}}$), the curved crack (segment $\widehat{\mathcal{BT}}$) and points $\mathcal{A}$ and $\mathcal{B}$ are always fixed, (see Fig. 2.17). When the value of angle θ reaches 180 degrees, the morphology of the system changes, because the geometry of the soft zone changes. We start a different stage with a different geometrical configuration for crack propagation.

A redefined convex hull characterizes this new stage. Now it is bounded by a straight line (segment $\overline{\mathcal{BT}}$) and the crack path (segment $\widehat{\mathcal{BT}}$), with point $\mathcal{B}$ fixed. The crack is no longer developing around point $\mathcal{A}$. Instead, the crack propagates around point $\mathcal{B}$. This new geometry is however similar to the previous stage: again β is almost constant and close to $\pi/2$, and there is a fixed center point $\mathcal{B}$. The curved path is again a spiral with the form $r = r_1 e^{-\theta \cot \beta}$, from point $\mathcal{C}$ to point $\mathcal{T}$ (see Fig. 2.17), but the initial size for $\theta = \pi$, r_1, is redefined as the length of segment $\overline{\mathcal{CB}}$. Because β is close to $\pi/2$, the quantity controlling the growth of the spiral, $\cot \beta$ is small and therefore the spiral grows slowly.

In these two first stages, the crack path has grown a little, if the initial incision is

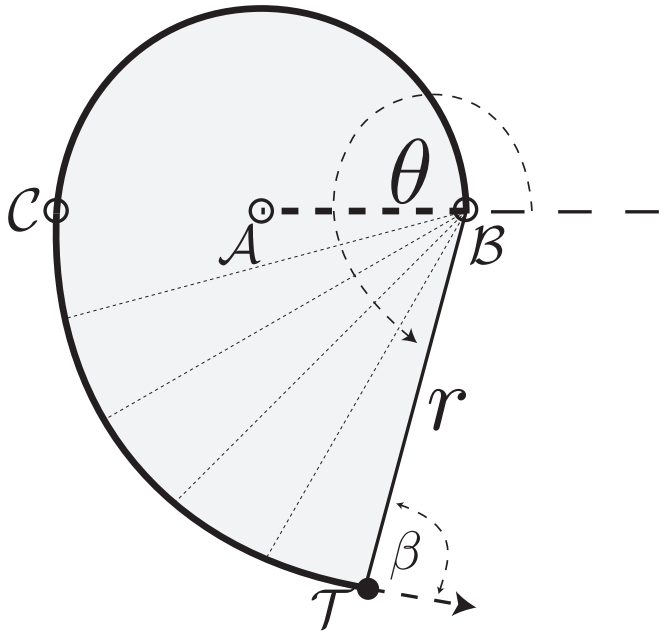

Figure 2.17: *Second stage for the spiral formation*

5mm (segment $\overline{\mathcal{AB}}$, then the diameter of the whole crack path until the second stage is at the most 1.6cm, which is a small fraction of the final spiral path.

We note that the oscillating cracks observed in [47, 48, 60] should be piecewise combination of these low-pitch spirals. Even though this has never been reported, this is a simple consequence of the model presented in [47, 60].

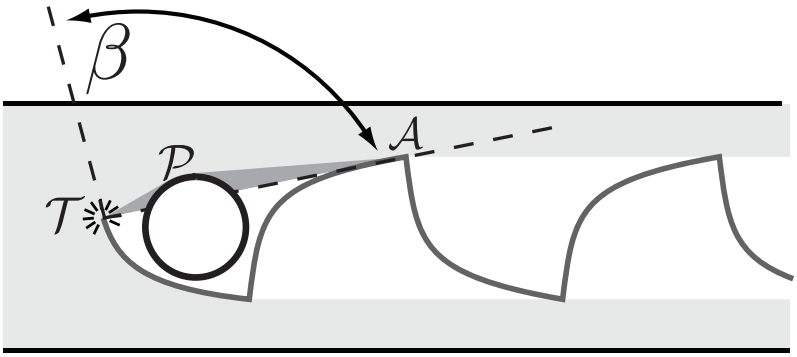

Figure 2.18: *Oscillatory crack formation. Diagram taken from reference [47]*

In fact the propagation is due to the blunt object pushing the edge of the convex hull at point $\mathcal{P}$ (see Fig. 2.18). In each half-oscillation, the crack therefore propagates around a fixed point, $\mathcal{A}$, along the same spiral as we expect in our first two stages. The shape and size of the object only defines the wavelength and amplitude of the oscillations through the size of the pieces of these universal curve.

A final stage begins after the crack has grown another quarter of a turn. The corresponding morphology of the final form of the convex hull contains one straight line ending on the crack, but the other end point is not fixed, point $\mathcal{E}$ in Fig. 2.19, which moves along the previous trajectory of the crack.

Throughout this final stage, a self-similar configuration guides the crack propagation. Points $\mathcal{E}$ and $\mathcal{T}$ define the pushed lip, the propagation now is in direction β with respect to this lip. This configuration generates a geometry guiding a very fast growth of the crack path.

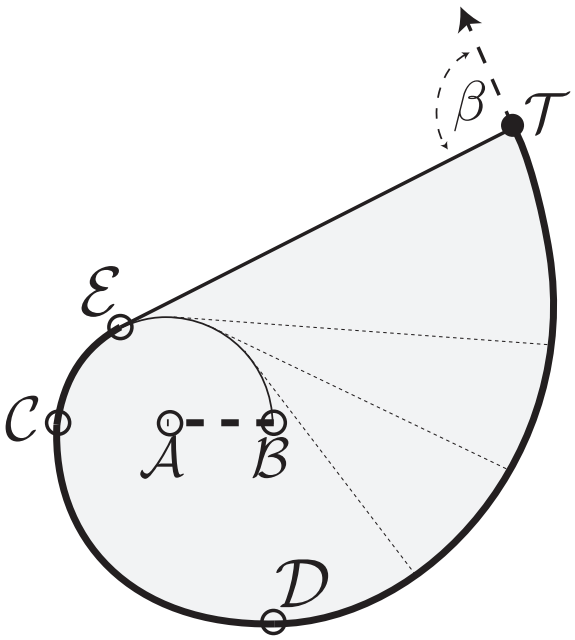

Figure 2.19: *Final stage for the spiral formation*

In contrast to the usual logarithmic spiral definition, which describes the formation of the curve from a central pole (as in the previous stages), the formation of the spiral curve is now governed by a different growth mode. Along the propagation, the system maintains a constant angle, β, between the tangent to the curve at point $\mathcal{T}$ and the tangent to the curve at point $\mathcal{E}$ (see Fig. 2.20). Of course this rule shows more complexity than in the previous stages, therefore the mathematical characterization is more complex.

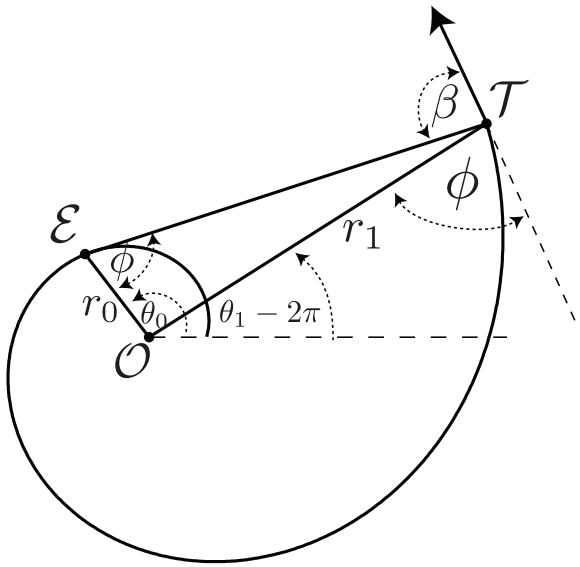

Figure 2.20: *Geometry in a logarithmic spiral.*

In fact, it has not been possible to find a differential equation containing the information of the propagation with this configuration, because it depends on the information in the past, point $\mathcal{E}$ in Fig. 2.20. Nevertheless, we probe that a mathematic logarithmic spiral with the form $r = r_o e^{\theta \cot \phi}$ centered on a given pole $\mathcal{O}$, obeys this rule for its formation. And we prove that there is a relation between β and ϕ independent of θ.

The proof comes from simple geometry. Points $\mathcal{E}$ and $\mathcal{T}$ have the polar coordi-

nates centered in $\mathcal{O}$, (r_o , θ_o) and (r_1 , θ_1), respectively (see Fig. 2.20). If we set $\theta = 0$ to coincide with the horizontal axis, line $\mathcal{OT}$ has an angle $\theta_1 - 2\pi$ with this axis. Geometry in the triangle $\mathcal{EOT}$ shows that the angle $\angle\mathcal{EOT} = \beta$, (see Fig. 2.20), hence we have the condition $\theta_0 - (\theta_1 - 2\pi) = \beta$.

From Fig. 2.20 we observe that the height of the triangle $\mathcal{EOP}$ starting from the vertex $\mathcal{O}$ can be written in the equivalent forms

$$r_0 \sin\phi = r_1 \sin(\pi - \beta - \phi) \tag{2.35}$$

The distance to the center $\mathcal{O}$ to the points $\mathcal{E}$ and $\mathcal{T}$ are respectively $r_o = e^{\theta_o \cot\phi}$ and $r_1 = e^{\theta_1 \cot\phi}$. Thus,

$$\frac{r_o}{r_1} = e^{(\theta_o - \theta_1)\cot\phi} = e^{(\beta - 2\pi)\cot\phi} \tag{2.36}$$

Comparing Eq. (2.35) and Eq. (2.36) we obtain the final transcendental relation between β and ϕ

$$\sin\phi e^{-(\beta-2\pi)\cot\phi} - \sin(\beta + \phi) = 0 \tag{2.37}$$

It is clear from Eq. (2.37), that if ϕ is constant (logarithmic spiral) then β is constant (our case).

A graphical representation of a numerical solution of Eq. (2.37) is presented in Fig. 2.21. This figure shows that the relation between $\cot\phi$ and β is univocal, which implies that the final spiral crack path is only characterized by the directional angle of the fracture propagation, β. We have marked a point in this plot to represent a value close to $\pi/2$ and its corresponding $\cot\phi$.

Note that we have only shown that the logarithmic spiral is one solution. But we conjecture that starting from any initial condition, the crack path reaches asymptotically towards that solution. A strong argument in favor of this idea is that our geometric propagation rule with a constantβ angle is essentially scaleless. If we

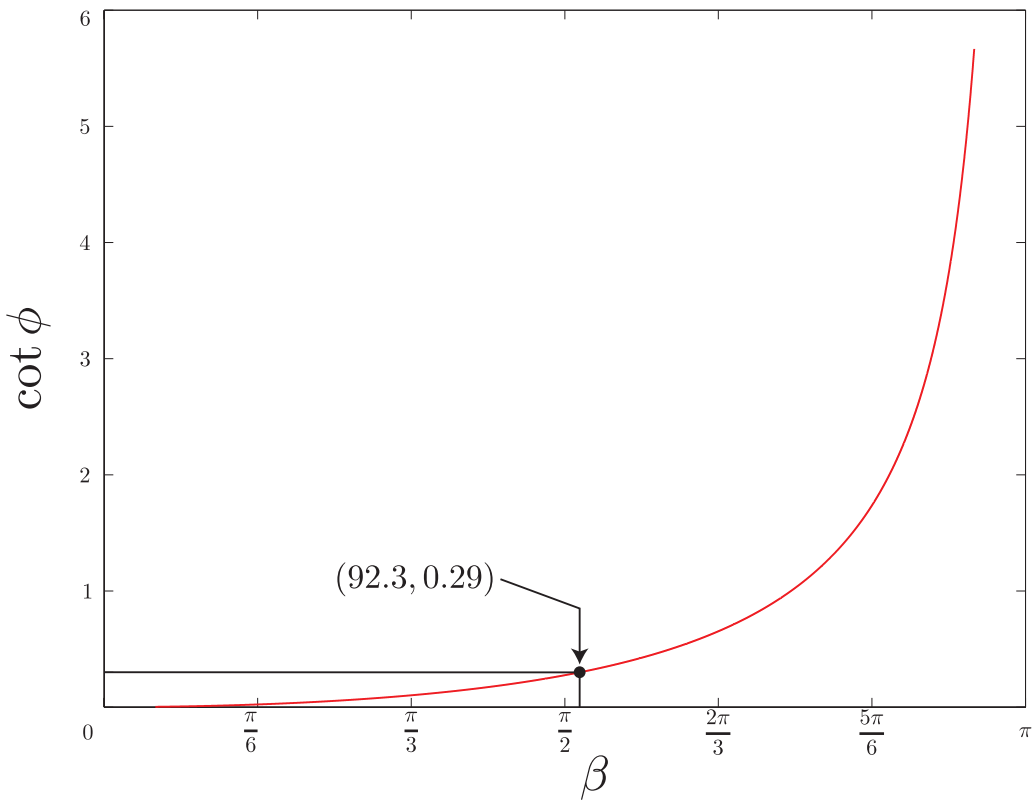

Figure 2.21: *Numerical functionality between* $\cot\phi$ *and* β*.*

observe a spiral, the spiral should be scaleless, and the logarithmic spiral is the classical scale invariant spiral. In the next section, we numerically propagate a crack with the rules given by our model, study it, and compare it to our experiments.

2.5 Spiral Results

We now turn our discussion to the geometrical measurements of the experimental spiral. To explore the consequence of our models predictions, in terms of how it generates the final spiral crack path, we have developed a numerical simulation that allow us to recreate the three stages of the spiral formation. Thus, it is possible to compare the experimental spiral to the predicted final spiral from our model.

2.5.1 Numerical Simulation of the Spiral Growth

Since the morphology of the convex hull determines the way in which the crack propagates in each stage of the spiral formation, to simulate spiral growth, it is critical to recreate the convex hull morphology in a single routine. We have developed an algorithm that allows us to quickly find the convex hull, its delimiting lines and the fixed points when it corresponds.

Our algorithm starts with two points, $\mathcal{A} = [0, 0]$ and $\mathcal{B} = [1, 0]$. The first simulated point $\mathcal{T}_1$ is generated at a distance ds in direction β respect to segment $\overline{\mathcal{AB}}$. From point $\mathcal{T}_1$ we trace lines to all the previous points in the curve. These lines make an angle δ with respect to the line of the last propagation (in this first step segment $\overline{\mathcal{T}_1\mathcal{B}}$, see top illustration in Fig. 2.22). The next simulated point on the curve, $\mathcal{T}_2$, is placed at a distance ds with an angle β with respect to the line for which the angle δ is maximum. Thus, we find that if we are at point $\mathcal{T}_n$, we trace lines to all the previous points in the simulated curve, including $\mathcal{A}$ and $\mathcal{B}$. The next point, $\mathcal{T}_{n+1}$, will be at a length ds in direction β respect the line with the first maximum of δ.

This procedure generates the three stages predicted for spiral formation. In the

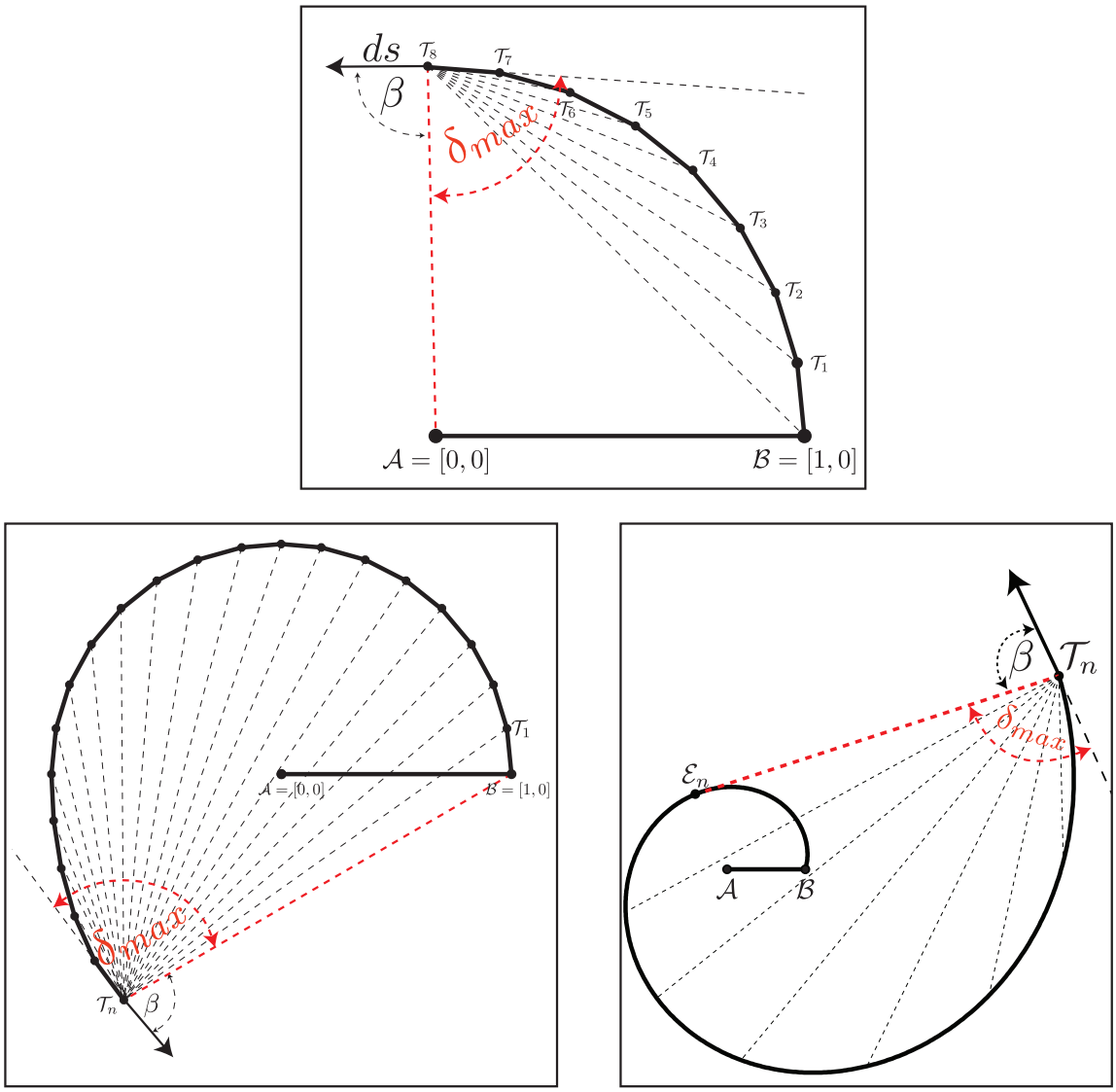

Figure 2.22: *Illustration of the bases use to simulated the path formation.* **Top.-** *Example of the results of the simulation in the first stage of the spiral formation.* **Bottom Right.-** *Example of the results of the simulation in the second stage of the spiral formation.* **Bottom left.-** *Example of the results of the simulation in the final stage of the spiral formation.*

first stage, the angle δ is always maximum at point $\mathcal{A}$ (top illustration in Fig. 2.22). When the curve passes to the second stage point $\mathcal{B}$ is the one that maximizes the angle δ (bottom left illustration in Fig. 2.22). In the last stage, the first maximum

of the angle δ is reached when the line starting in point $\mathcal{T}_n$ is tangent to the previous turn (bottom right illustration in Fig. 2.22) which agrees with the geometrical postulate in Figs. 2.19 and 2.20.

2.5.1.1 A Local Method to Find the Spiral Pole

The data obtained from the simulation is measured with a method based in an idea from the classic book of Darcy Thompson [62] which devotes a long chapter to spiral-like structures in nature. Since, commonly these structures are not complete when they are found, a method is developed in [62] where the pole is found with the use of just three near points on the curve.

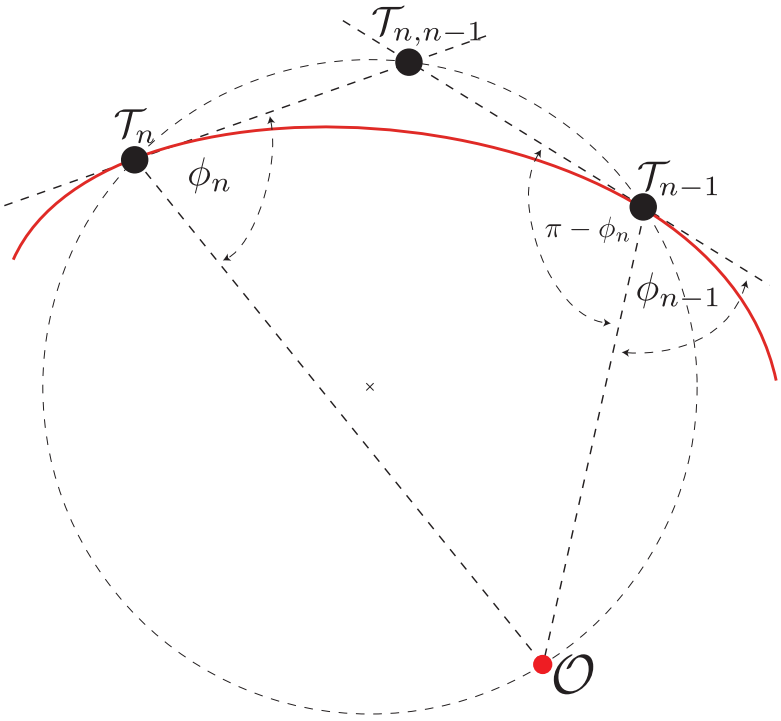

Figure 2.23: *Geometry in a logarithmic spiral.*

We start with two points on the spiral curve, $\mathcal{T}_n$ and $\mathcal{T}_{n-1}$ (see. Fig. 2.23). The tangents to the spiral curve at these two points intersect in a third point, $\mathcal{T}_{n,n-1}$.

These three points are contained by a unique circle, C_1. We demonstrate that there is a point $\mathcal{O}$ on this circle for which the angles ϕ_n and ϕ_{n+1} are equals.

The angles ϕ_n and $\angle\mathcal{O}\mathcal{T}_{n-1}\mathcal{T}_{n,n-1}$ are opposed and circumscribed in the circle in Fig. 2.23, the value of $\angle\mathcal{O}\mathcal{T}_{n-1}\mathcal{T}_{n,n-1} = \pi - \phi_n$, since $\angle\mathcal{O}\mathcal{T}_{n-1}\mathcal{T}_{n,n-1} + \phi_{n-1} = \pi$, directly we obtain $\phi_n = \phi_{n-1}$.

With a third near point $\mathcal{T}_{n+1}$ it is possible to repeat this procedure and obtain a second circle C_2. These circles will intersect in two points, one is $\mathcal{T}_n$ because of construction, and the other intersection gives us a pole $\mathcal{O}_n$. If for any n describing a set of three points in the curve we obtain the same pole, then the curve is a logarithmic spiral.

In the numerical simulation, we determine the local pole $\mathcal{O}_n$ for each point $\mathcal{T}_n$, and measure its distance $\mathcal{O}\mathcal{T}_n$ (local radius of the spiral).

2.5.1.2 Global Method to Define a Pole of a Spiral

This method is difficult to use for the experimental spiral because it induces too much noise. Since we identify poles for the first and second stage, there is no need to use any method to find the pole. A different situation is observed in the third stage, because the propagation has no distinguishable point playing the role of the pole. Hence, it is necessary to find a point from which we measure the distance to the points on the spiral. To do so, we use a global method to obtain a single pole $\mathcal{O}$ for the third stage of spiral formation, assuming that the shape is a logarithmic spiral.

From the definition of the logarithmic spirals, we know that for any given point on the curve the radius vector joining it and the pole makes a constant angle with the tangent to the curve at that point. Thus, if we find two points with parallel tangents,

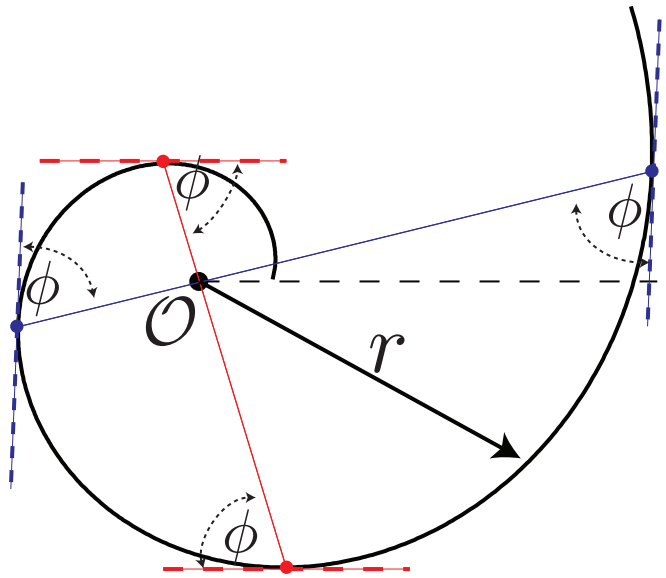

Figure 2.24: *Diagram of the procedure to find the pole.*

the line connecting both points must contain the pole. Hence, the pole is obtained from the intersection of the lines connecting two set of points (see. Fig 2.24). Of course this is only valid if the curve is a logarithmic spiral.

2.5.1.3 Measuring β in the experiments

On the post-mortem spiral shape, the direction of propagation is simply given by the tangent to the curve. But we are interested in the direction β measured with respect to the limit of the crack path convex hull (a key prediction of the model is that this value should be constant). The computation of the convex hull is easily done by treating the experimental curve with the same algorithm used in section 2.5.1.

2.5.2 Experiments

We present data from three final spirals, two of which were made with an initial incision parallel to the film orientation, the third was made with the initial incision

perpendicular to the film orientation (see Fig. 2.25). Fig. 2.26 presents our mea-

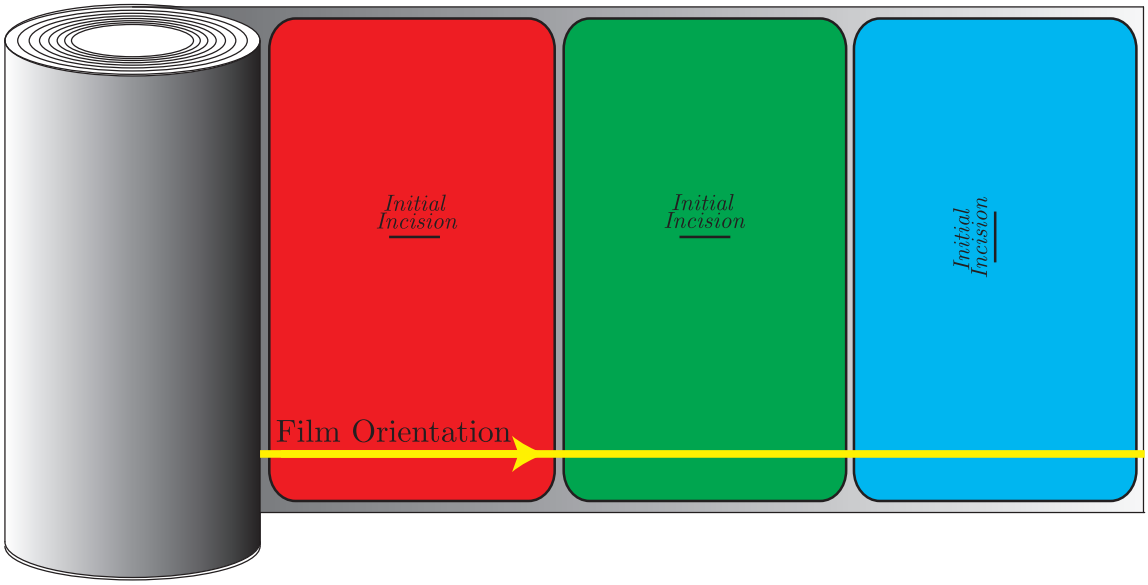

Figure 2.25: *Determination of the orientation of the Film. An illustration of the three experiments.*

surement of the distance to the local pole, normalized with the size of the initial incision, r/r_o. In the semi-log plot in figure Fig. 2.26, it is possible to distinguish the three stages. From θ equal to 0 to π, a roughly linear growth is observed. A slope for each of the experiments is obtained by fitting the data with a linear polynomial, the average of the slope over the three experiments gives a value of $\cot\phi = \cot(\pi - \beta) \approx 0.04$, which corresponds to the pitch of the spiral in this stage, and it implies very slow logarithmic growth.

When θ reaches π the curve abruptly doubles its size, which is explained by the change of the pole (now it is $\mathcal{B}$). Again the curve is roughly linear and with a small slope until θ is close to $3\pi/2$. The data is fitted and the average of the values of the three experiments at this stage gives a similar result for the pitch, $\cot\phi = \cot(\pi - \beta) \approx 0.04$, hence this stage behaves as the same logarithmic spi-

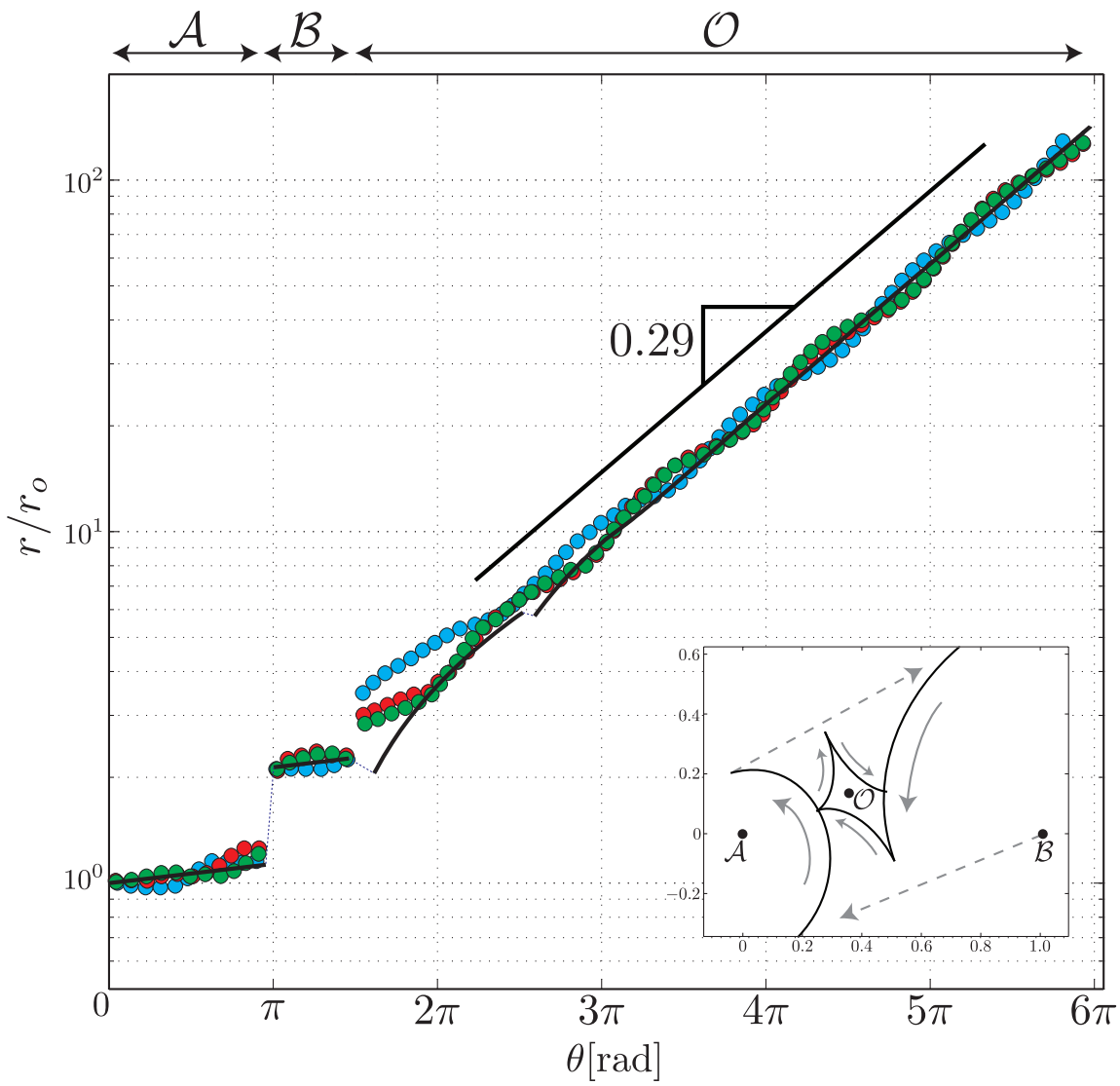

Figure 2.26: *Experimental measurements of the radius r, normalized with the initial size r_o, from three experiments. Red and green circles are experiments with a same initial orientation to the incision. Blue circles are data from an experiment initiated with a perpendicular orientation.*

ral.

When θ is bigger than $3\pi/2$ the last stage begins. This stage also shows linear behavior in the semi-log plot, however the slope is steeper, and the size of the spiral grows almost 100 times in just 2.5 turns. In this case, the result of averaging

the slopes obtained from a linear fitting gives a value $\cot\phi \approx 0,29$.

The first two stages do not cover a wide range of the angle θ, or a wide range in r/r_o so it is hard to ensure that the behavior is logarithmic, but they are compatible with our model. However, in the last stage we observe a clear behavior characterized by exponential growth. In Fig. 2.26 we present line of measurements (in a dark black line) of a simulated spiral obtained with the algorithm described in section 2.5.1 using a normalized initial incision, the experimental average of angle β (shown later in this section), and a step for the propagation of 10^{-3}. The global agreement is very good. We also show in inset in Fig. 2.26 the movement of the pole found through local measurements over the simulated spiral. We see from this data that the pole converges to the value $\mathcal{O} \approx [0.4, 0.1]$, which implies that the spiral is converging to a logarithmic one. To compare with the experimental spiral, we take the average of the coordinates of the poles found in the last stages of the three presented experiments, we obtain a value $\mathcal{O} \approx [0.36, 0.13]$, which is in good agreement with the value from the simulation.

We recall that the three spirals are made with no particular control of the movement of the tool, so the agreement between the plotted data with the red and green circles is particularly impressive.

Despite the clear logarithmic behavior, there are evident oscillations of r/r_o around the simulated curve. Note that these oscillations are in phase between the data plotted with red and green circles, and there is a $\pi/2$-shift with the spiral plotted with blue circles. If we consider that the difference between the blue experiment and the green and red is a $\pi/2$-rotation of the orientation for the initial incision. Hence, it is possible to assure that these oscillations are a consequence of material orientation properties.

We present in Fig. 2.27 the measurements of the angle β performed on the final crack path, as a function of the angle measured for each spiral. In the same figure we have plotted in the inset on the bottom corner the same data but with respect to the orientation in the film, θ_g. As we might imagine, it oscillates. The parameters

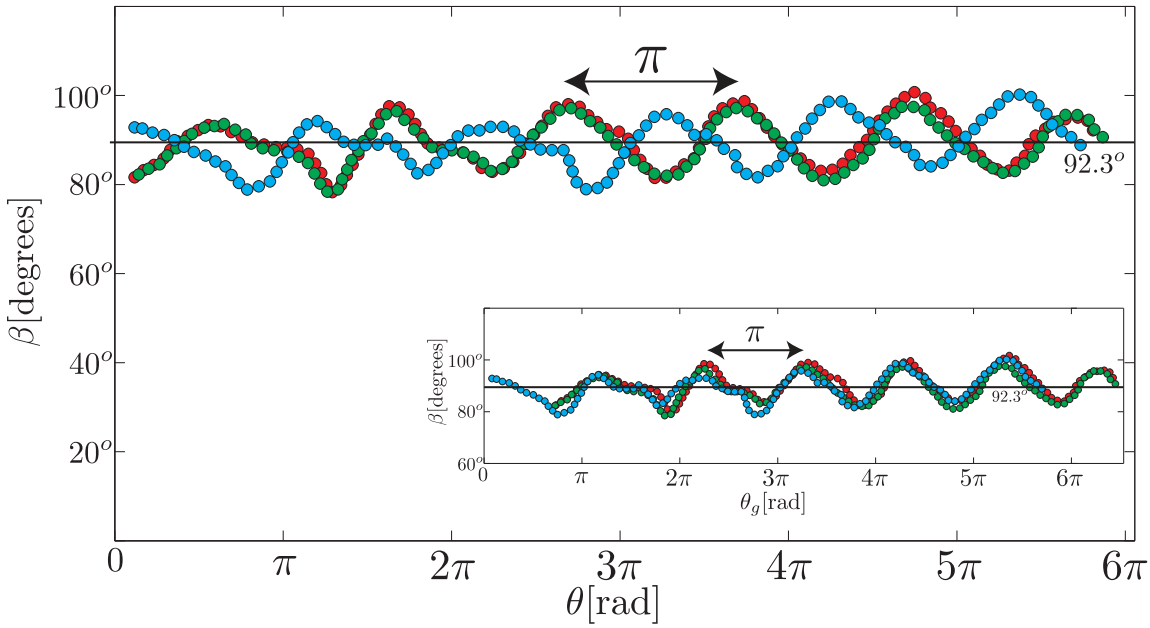

Figure 2.27: *Crack propagation angle β as a function of the angle of the spiral, θ.* **inset** *The angle β as a function of the orientation in the film θ_g*

governing this oscillation have an amplitude of $\sim 10^o$, a periodicity of π, and an average value of $\langle\beta\rangle \sim 92.3^o$. The π periodicity is consistent with the anisotropy of fracture energy, which has the same value when the direction of fracture is reversed. We also note that all the curves collapse when they are measured with respect to the orientation in the film. This shows that although the spirals are different, the propagating process is identical and only depends on the orientation of the crack.

We stress the fact that despite the exponential growth of the system, angle β con-

tinues to oscillate around a fixed value. This reinforces the idea that the process is scaleless. Indeed, with this average value, we obtain a very interesting result: if we use the average value of β in Eq. (2.37), we obtain the predicted pitch of the spiral $\cot\phi \approx 0.29$. The exact agreement with the slope of the curve in Fig. 2.26 is impressive and it gives us the certainty of the characterization of the spiral formation.

It is not possible to measure α from the post-mortem crack path. Nevertheless, we measured this quantity with different orientations in an experiment. We did not observe a strong correlation with the orientation, therefore the oscillations in β did not come from variations in α. The average value of α is $\approx 10^o \pm 1.0^o$, so that the predicted value for β is $\pi/2 + 0.4\alpha = 94^o$ (see Eq. (2.33)), in contrast to a smaller experimental value that on average is $\langle\beta\rangle \sim 92.3^o$.

2.6 Anisotropy

The oscillations observed in the plot of r/r_o and the angle β in Fig. 2.27 could offer a testing method of material properties. This was also suggested by Atkins [43, 63] when observing torn strips from metal sheet. In this section we show a spiral experiment where a very anisotropic material is used, and then develop the first step for an anisotropic model.

2.6.1 Experiments with Highly Anisotropic Materials

The anisotropic material that we are now going to use is made from the same polymer (polyproylene) as in experiments above. The difference between these materials comes from the manufacturing process.

To make the films, the polypropylene in the form of a resin is melted in an extruder. The molten polymer is fed from the extruder to the nozzle. This nozzle distributes the film evenly on a cooling roll, where the liquid polypropylene hardens. With a series of rollers, the film is stretched in the longitudinal direction (called machine direction), the material is clamped on the borders and then pulled in the transverse direction. This process results in a transparent material with a highly homogenous thickness.

It is natural to think that the manufacturing process rearranges polymer chains, producing special orientations in the material.

The material we used in the previous experiments is called bi-oriented polypropylene with balanced stretching, meaning that, when manufactured, the stretching in the aforementioned machine and transverse directions were almost equal, leading to very weak anisotropy. In contrast, the material used in the following experiments

is simply bi-oriented polypropylene commonly obtained in flower stores.

The way in which this experiment is carried out is the same as we have done with the less anisotropic material: a small initial incision, of ~ 0.7cm is made and with a cylindrical tool we follow the crack, pushing always on the same lip.

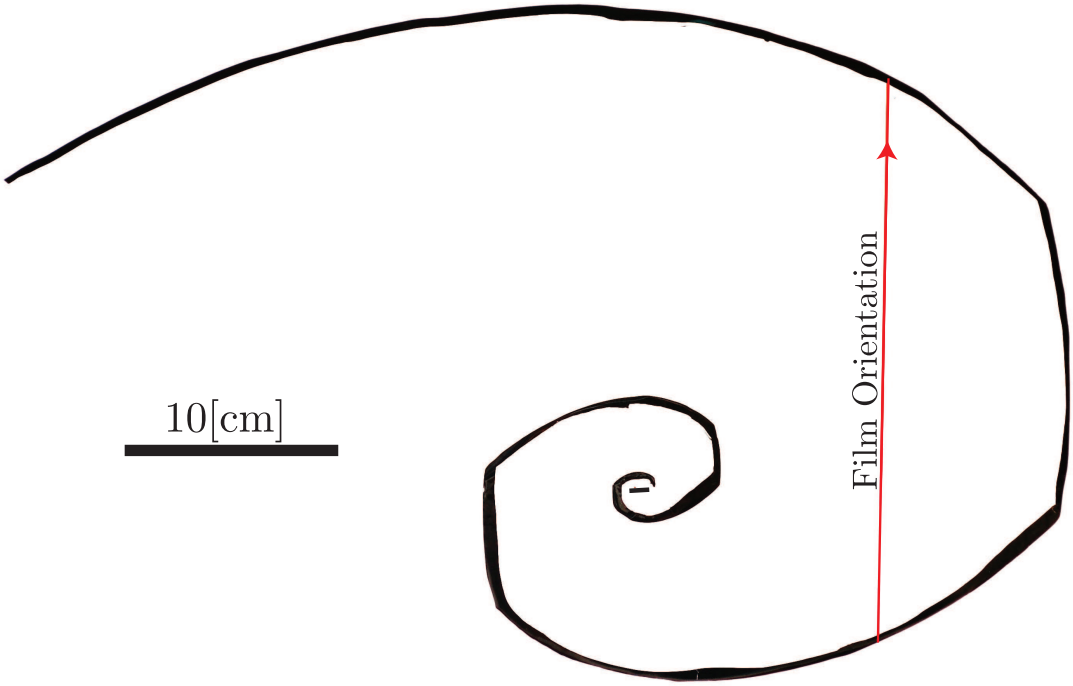

Figure 2.28: *Spiral made with a very anisotropic material.*

A simple inspection of the shape of the resulting cut presented in Fig. 2.28 shows that the crack propagates differently in different direction: we have quasi-straight sections that show preferred directions of the propagation.

The final shape is spiral-like in the sense that it grows quickly with the rotation, but now includes quasi-straight lines and kinks.

Surprisingly, as shown in figure Fig. 2.29, we observe that the lines joining points with parallel tangents do intersect at the same point $\mathcal{O}$ near the initial incision. We also see that the lines joining the kinks intersect at $\mathcal{O}$. Hence, it seems possible

to find a pole $\mathcal{O}$ with the same global method used in the less anisotropic spiral. It is tempting to measure the distance to this pole along the crack path.

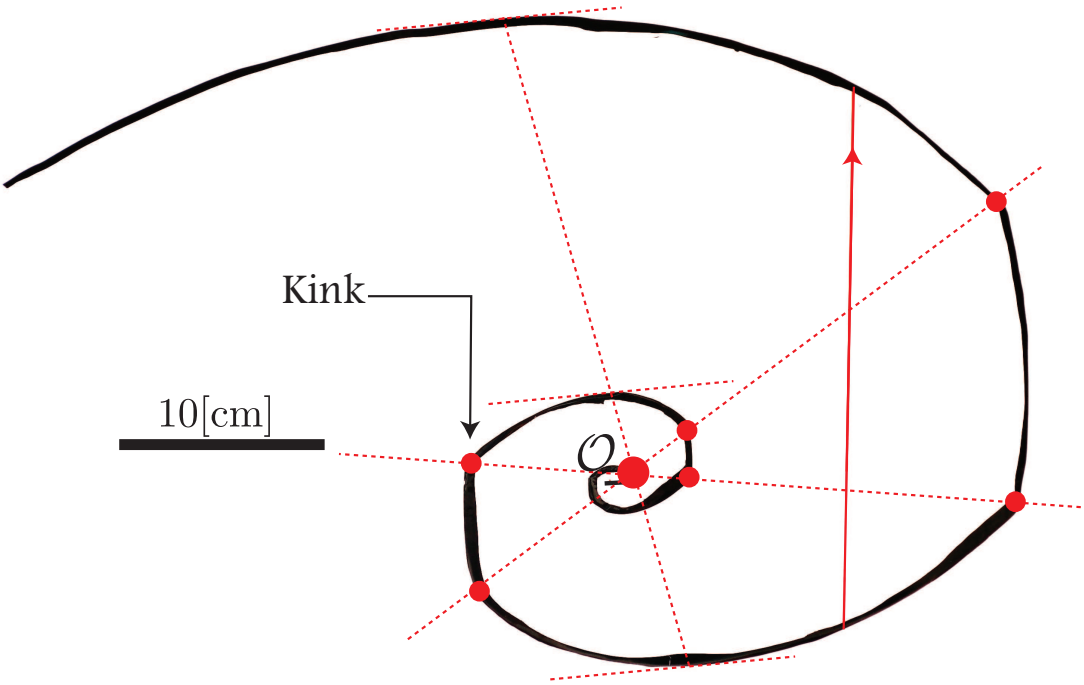

Figure 2.29: *Illustration of the lines passing through the kinks intersecting in the pole.*

In Fig. 2.30 we show data from two experiments initiated with perpendicular orientations. We only plot r/r_o for the final stage of the formation, because this part allows a test of the logarithmic behavior.

The result of this plot is remarkable because it shows on average a logarithmic behavior, but with stronger oscillations. It seems that in fact this fracture process generates anisotropic generalization of the logarithmic spiral.

To fully compare this resulting spiral to the analysis made for the less anisotropic spiral, we present in Fig. 2.31 the measurements of the angle of fracture propagation β, measured with the same algorithm.

Again oscillations of β are observed in the plot of Fig. 2.31 around an average

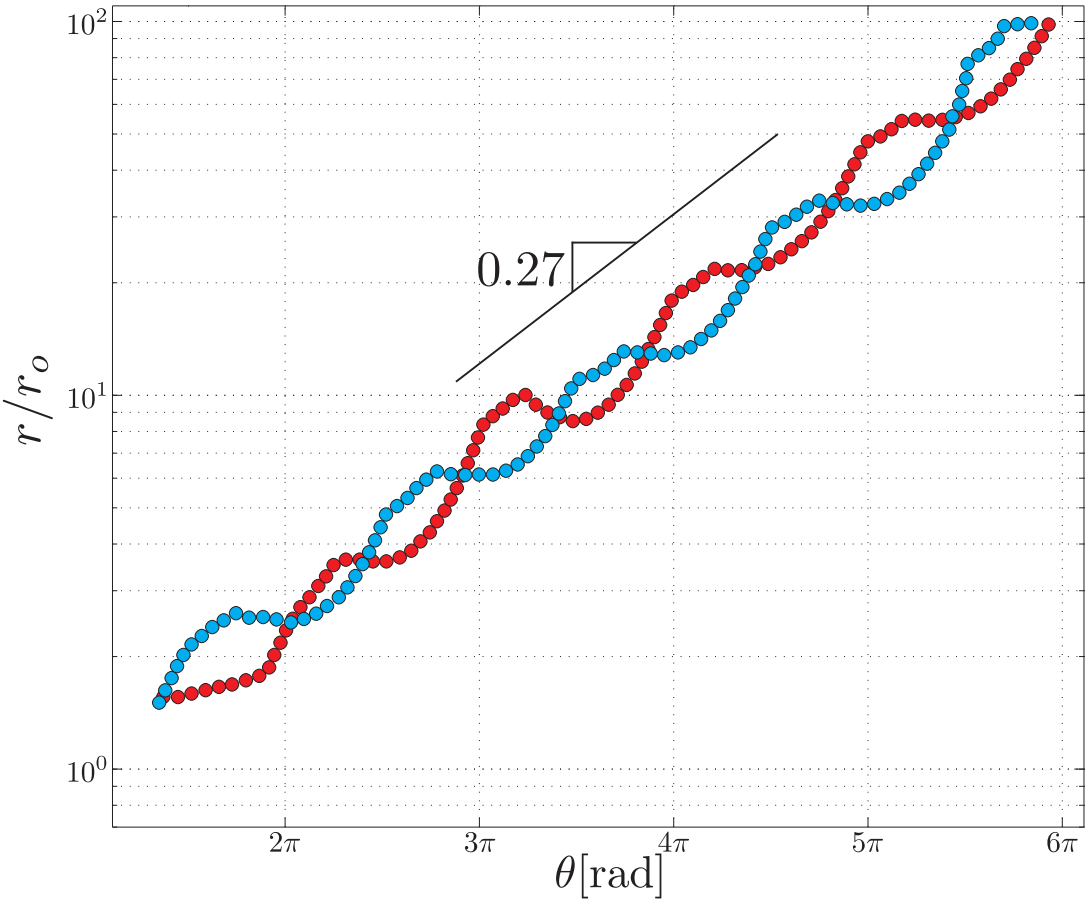

Figure 2.30: *Radius (distance to the pole) as a function of angle, for two spirals initiated with perpendicular orientations in a very anisotropic material.*

value of $\langle\beta\rangle \sim 90.5^o$, which is very close to 90^o. We can try to estimate the slope of the curve plotted in Fig. 2.30, using the averaged value of $\langle\beta\rangle \sim 90.5^o$ in Eq. (2.37). This yields $cot\phi \approx 0.28$, which again agrees well with the experimental value of the spiral pitch in (the slope in Fig. 2.30 is 0.27).

This time the amplitude of the π-periodic oscillation has increased from 10^0 (in our less anisotropic case) to 20^0. Moreover the oscillation is not quasi-sinusoidal, and includes kinks, with some plateaus. As observed in the previous experiment, the angle β for the two spirals also collapses on the same curve if measured with respect to material direction (inset of Fig. 2.31). It seems that this anisotropic

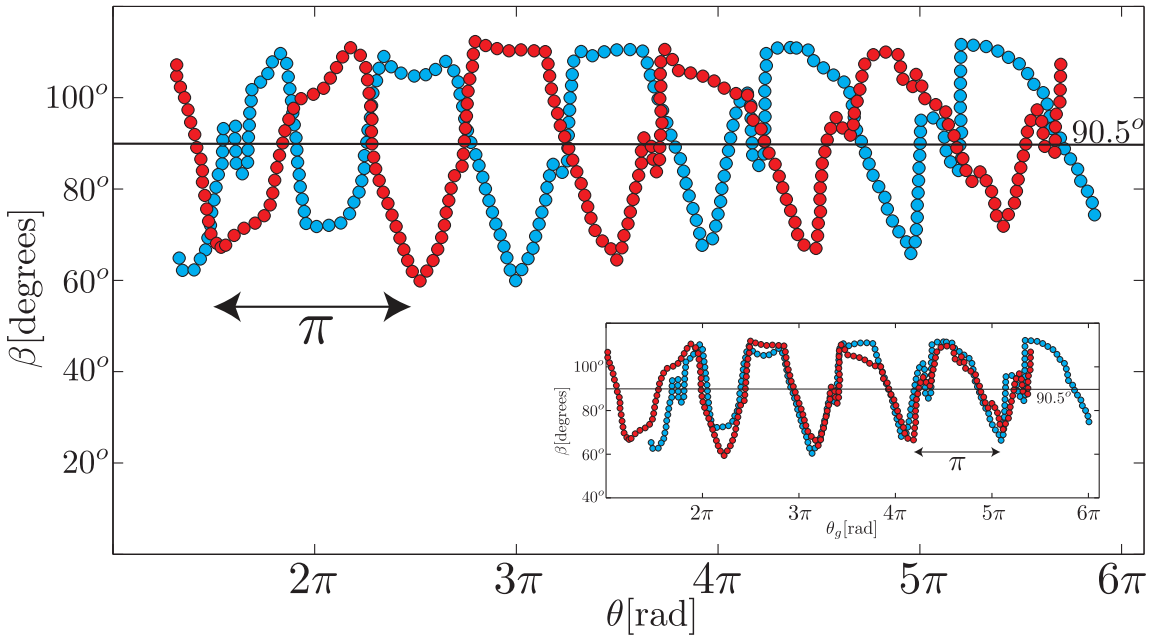

Figure 2.31: *Case of a very anisotropic spiral. Crack propagation angle β as a function of the angle of the spiral, θ.* **inset** *The angle β as a function of the global orientation in the film θ_g*

fracture process leads to an anisotropic generalization of the logarithmic spiral.

2.6.2 Anisotropic Model

Including anisotropy in fracture propagation is not easy. There is no doubt that Griffiths criterion (which can be viewed as energy conservation) still holds with anisotropic material. But finding the direction of propagation is more difficult: the most popular criterion used to predict the crack path, the principle of local symmetry (which states that cracks propagate in the direction where $K_{II} = 0$) only makes sense in the case of isotropic materials [64]. Possible generalizations of this criterion for the case where fracture energy depends on the orientation of the crack were proposed only recently [65], but are not yet widely accepted by the fracture community.

In terms of the maximum energy release rate criterion, there is a natural way to include the anisotropy of fracture energy, which is similar to that in [64]. Let us rephrase the isotropic criterion in the following way. We imagine that loading is increased from zero. We can test Griffiths criterion for propagation in all possible angles. The energy release rate dU_E/ds, a function of propagation angle[4] θ', is at first insufficient to compensate for crack energy $-dU_E/ds < \gamma$. If we assume that the crack propagates when Griffiths criterion is first satisfied, we see that this occurs at the angle in which the energy release rate is maximal (see equation 2.16). In a material where crack energy $\gamma(\theta')$ is a function of orientation θ' of the crack, the first point where the propagation condition is met also obeys a tangency condition (similarly to the correction presented in [64]):

$$\frac{\partial}{\partial\theta'}\frac{dU_E}{ds} = -\frac{\partial\gamma}{\partial\theta'} \tag{2.38}$$

which can also be written as $\partial_{\theta'}\frac{dU_T}{ds} = 0$. When applying this generalized criterion to our model, we find in the limit of small anisotropy (small amplitude of variation compared to average value) a correction to the equations (2.30) and (2.31).

If we include the dependence on the orientation $\gamma(\theta')$, in Eq. 2.15, then its derivative with respect to angle, Eq. 2.17 now includes an extra term. Following the same analysis as in section 2.3.2.3, we obtain:

$$\alpha_c = \left(\frac{\gamma(\theta')}{anEL}\right)^{1/(n-1)} \tag{2.39}$$

$$\beta = \frac{\pi}{2} + \frac{(n-2)}{n}\alpha + \frac{1}{\gamma}\frac{d\gamma}{d\theta'}, \tag{2.40}$$

[4]The propagation angle measured with respect to a fixed material direction is denoted as θ' to avoid confusion with β, the angle with the limit of the convex hull Fig 2.32 , or θ, the rotation angle along the spiral)

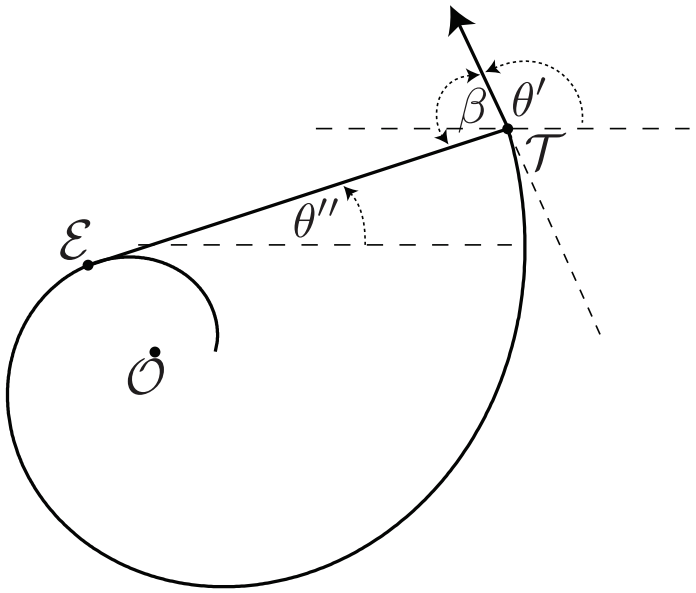

Figure 2.32: *Illustration of the geometry used to compare the fracture energy and the direction of the crack.*

(where $n = 3.5$ and $a = 0.0059$ are parameters that were measured previously in experiments). The direction of propagation β deviates from the isotropic value when it predicts a direction in which there is a non-zero gradient, $d\gamma/d\theta'$, in the fracture energy. The physical interpretation is that direction of propagation is no longer that which most efficient releases elastic energy, because crack energy (and thus the operator's work) is lowered in a different direction. The sign in $d\gamma/d\theta'$ in Eq. 2.40 indeed shows that the propagation adjusts to the direction where γ decreases (remember that $d\beta = -d\theta'$ as can be seen in Fig. 2.32): fracture avoids directions where propagation is costly.

Note that if the average value is subtracted, we find

$$\beta - \langle\beta\rangle = \frac{1}{\gamma}\frac{d\gamma}{d\theta'} \tag{2.41}$$

In order to test this prediction, we conducted preliminary experiments where the fracture energy $\gamma(\theta')$ was measured in several directions, using the tearing method

proposed by Hamm [50]. Starting from two parallel initial notches, we tear the flaps by pulling at 180^o, as in Fig. 1.2. If the notches are sufficiently far apart, the initial propagation of he cracks are almost parallel in the initial moments of the propagation. If it were exactly so, the width of the fold would be constant, and we would therefore observe the same fold throughout the experiment, with a constant elastic energy stored in the system. The energy balance shows that the operator's work $2\gamma t dx = F dx = 2F dl$ with the notations of Fig. 1.2. The measured force is indeed quite constant, and we take the fracture energy as $\gamma t = F$.

We want to compare these results to the direction β chosen by the crack and we need to use the same coordinates.From the final crack path, it is possible to obtain the behavior of β with respect to the orientation of the segment $\mathcal{ET}$ given by the angle θ''. From simple geometry, we have that $\theta' = \pi - \beta + \theta''$. Finally, we plot on the same graph $2(\gamma - \langle\gamma\rangle)/\gamma$ with black dots connected by a black line and $\beta(\theta') - \langle\beta\rangle$ for the three spirals of section 2.5.2 with the same coordinates as Fig. 2.33. We have superimposed all the values of β in one period.

If Eq. (2.40) is correct, then the color curves ($\beta - \langle\beta\rangle$) should exhibit the properties of the derivative of the black curve. We first observe that the geometrical deviations $\beta - \langle\beta\rangle$ seems well described by a a simple π-periodic sinusoidal shape.As a result, we expect the fracture energy to follow $\gamma(\theta') = \langle\gamma\rangle(1 + g\sin(2\theta'))$, with an amplitude g half of that of the geometrical deviations. Fig. 2.33 shows that the amplitude of anisotropy is compatible with this estimate (note that the variation in fracture energy are amplified by a factor 2 in the figure). But several features of these preliminary measurements seem incompatible with Eq. (2.40).The extrema of fracture energy γ in $\theta" = 90^o$ and 0^o do correspond to a zero of the $\beta - \langle\beta\rangle$: In a direction where crack energy is extremal, we expect a locally isotropic be-

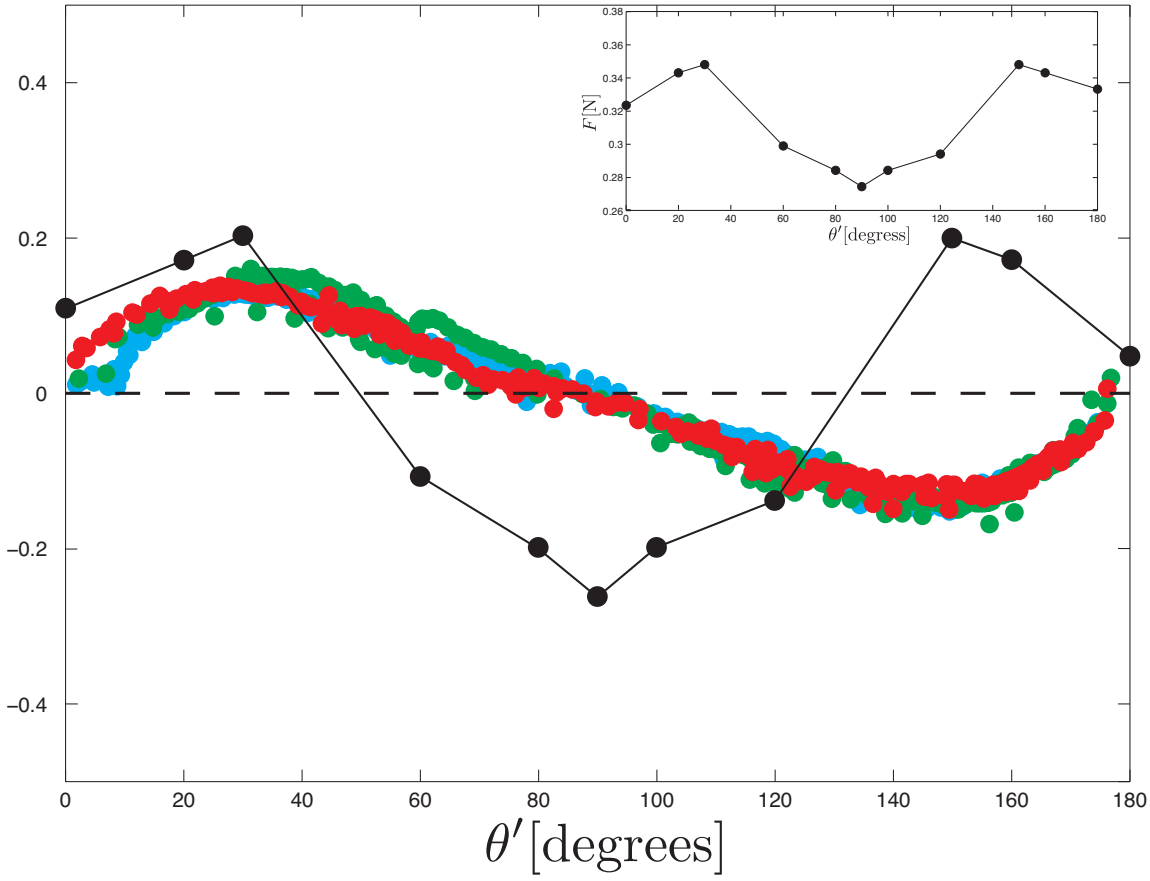

Figure 2.33: *With red, blue and green circles, the values of* $\beta - \langle\beta\rangle$*, are plotted. With black circles we present* $2(\gamma - \langle\gamma\rangle)/\gamma$*. The inset presents the measures of* $\gamma(\theta')$*.*

havior. But this seems to fail in the most costliest direction: the maximum in γ for $\theta = 30^o$ and 150^o does not correspond to a zero of the colored curves. Even if we forget about the unexpected dip in fracture energy in the values close to $\theta = 0^o$, we also observe a problem in the sign of β : positive value on $[0, 90^o]$ should lead to an increasing fracture energy γ, which on average decreases in the interval $0 < \theta' < \pi/2$. This sign issue could be cured by a simple shift of 90^o in the fracture energy, suggesting an experimental error in angle references between the two types experiments (spiral and fracture energy), that we could not evidence in our experimental procedure. At this stage of our work, we cannot conclude on the

validity of Eq. (2.40). This experiment should be repeated with a better sampling in fracture energy, and extra care in the definition of orientation.

2.7 Conclusion

In this chapter we have studied the propagation of a crack in a brittle thin sheet with a blunt object. In the experiment, we start with a slit, and a blunt tool is pushed continually on one side the slit (rule $\mathcal{R}$). A smooth reproducible diverging spiral rupture results. Since the crack continually turns, the tool movement has to adjust and also describes a rough spiral to continually obey rule $\mathcal{R}$.

The experimental rule still leaves much freedom to the tool path, but we have shown that very different tool movements lead to exactly the same smooth spiraling cut. This striking reproducibility is not very common in rupture experiments known to be very sensitive to defects, loading conditions, or residual stresses. Its origin is to be found in the fact that we are using very thin sheets.

We have shown with a simplified geometry that because thin sheets are bend so easily, the distribution of forces has to follow geometry. Indeed, negligible forces are transmitted if the tool stays in a soft zone (which consists of bendable flaps) geometrically defined as the convex hull of the crack path. This argument was first formulated for the study of oscillating crack path when a blunt object is moved along a straight line [47, 60], and later a similar approach was followed in the case of perforation [46] by a cone.

This model for fracture propagation in [47] is based on estimates of the elastic energy generated when the tool is moved out of this soft zone, leading to in-plane strains. We have experimentally characterized the elastic energy in the system in this geometrically simple configuration with an experiment where fracture could not propagate. The result are not compatible to the estimates used in previous works [47, 60] or [46] and we could not give a convincing description, but we ac-

cepted them as empirical laws that we used in the rest of our study.

The model predicts the critical condition for loading, and shows that propagation takes place in a direction almost independent of the loading, perpendicularly to the limit of the convex hull.

The prediction of this model (now including our empirical law for the mechanical response of the system) are in quantitative agreement with our measurements of the critical loading condition. A numerical implementation of the model predicts spiral propagation in three stages. The first two are logarithmic spiral with a low pitches (close to being circles).

Incidentally, we find that the oscillating cracks observed in [47, 48, 60] are a piecewise combination of these spirals.

In the third stage, a self-developing mode [5] grows at a much faster rate. We show that this last phase leads asymptotically to another logarithmic spiral with a larger pitch. These findings are also observed in the post-mortem experimental shapes. The pitch of each stage is accurately predicted by analytic (transcendental) equation.

However in the experiments, we also observed regular oscillation superimposed on the exponential growth, which we demonstrated are due to the weak anisotropy of the material used. We show that the propagation angle oscillates very regularly around a value compatible with the prediction of the model. This is also true for highly anisotropic materials, and we suggest that the simple observation of the spiral shapes allows for a qualitative image of anisotropy.

We derive an extension of the model, which includes a fracture energy depending

[5] We believe that the multiple spirals sometimes observed by Vermorel [46] when a cone perforates a thin sheet propagate in a similar self-developing mode.

on the propagation direction. In the case of weak anisotropy, this model quantitatively links the post-mortem geometry of the spiral to the relative variation of fracture energy in different directions. Although the regularity in the behavior of the fracture angle β is encouraging (in terms of test anisotropy), the preliminary experiments performed were not precise enough to confirm this result.

Chapter 3

Tearing Spiral

In this chapter we study another family of spiraling cracks in a brittle thin plate, which are not cut with a blunt object, but rather produced by simply pulling on a flap perpendicularly to the plane of the sheet. The process is initiated by artificially creating a convenient initial convex cut, creating a bendable flap that can be pulled away from the plane of the sheet to propagate a diverging spiral crack.

Although the experiment can be done by hand, we designed a more controlled set-up for measuring the forces. We studied the process experimentally and offer some preliminary explanations. We will see some analogies in the geometries with those of the previous chapter, and at the same time, many differences in the fracture mechanisms.

The resulting divergent crack path presented in this chapter and the required initial configuration, could represent an improvement in the way in which package are opened. Therefore, we have patented this system. The corresponding patent is annexed to this thesis in D

3.1 Experimental set-up

A large brittle sheet (BOPP 80x50cm, thickness 50 μm) was laid on a horizontal acrylic plate, and its borders fixed to the plate.

We began with the following initial cut: a disk (diameter ~ 6mm) was cut out far from the borders of the sheet. Through the perimeter of this disk, we made a straight cut, which generated an easily bendable triangular flap, see Fig. 3.1.

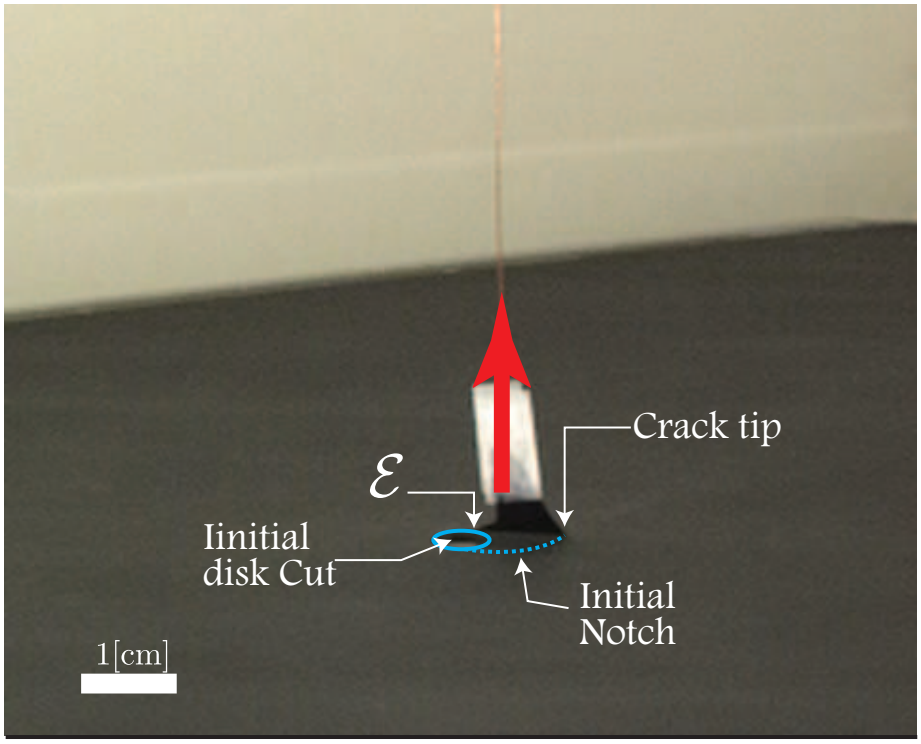

Figure 3.1: *Illustration of the initial cut.*

A wire was attached to the tip of the flap (through a hole), which was pulled vertically. In order to avoid rupture of the flap because of the wire hole, we wrapped this zone with adhesive tape.

The other edge of the wire was fixed to a device that moved upwardly with controlled velocity. The set-up, illustrated in Fig. 3.2, consisted of a motor that spun

a threaded rod, generating the vertical movement of the central piece (a moving car), two lateral rods prevented the rotation of this piece. A long lever was fixed to the moving car to pull above the initial cut. A Futek load cell LRF400 (with a load safe limit of 4.5N) was fixed to the lever to measure the pulling force.

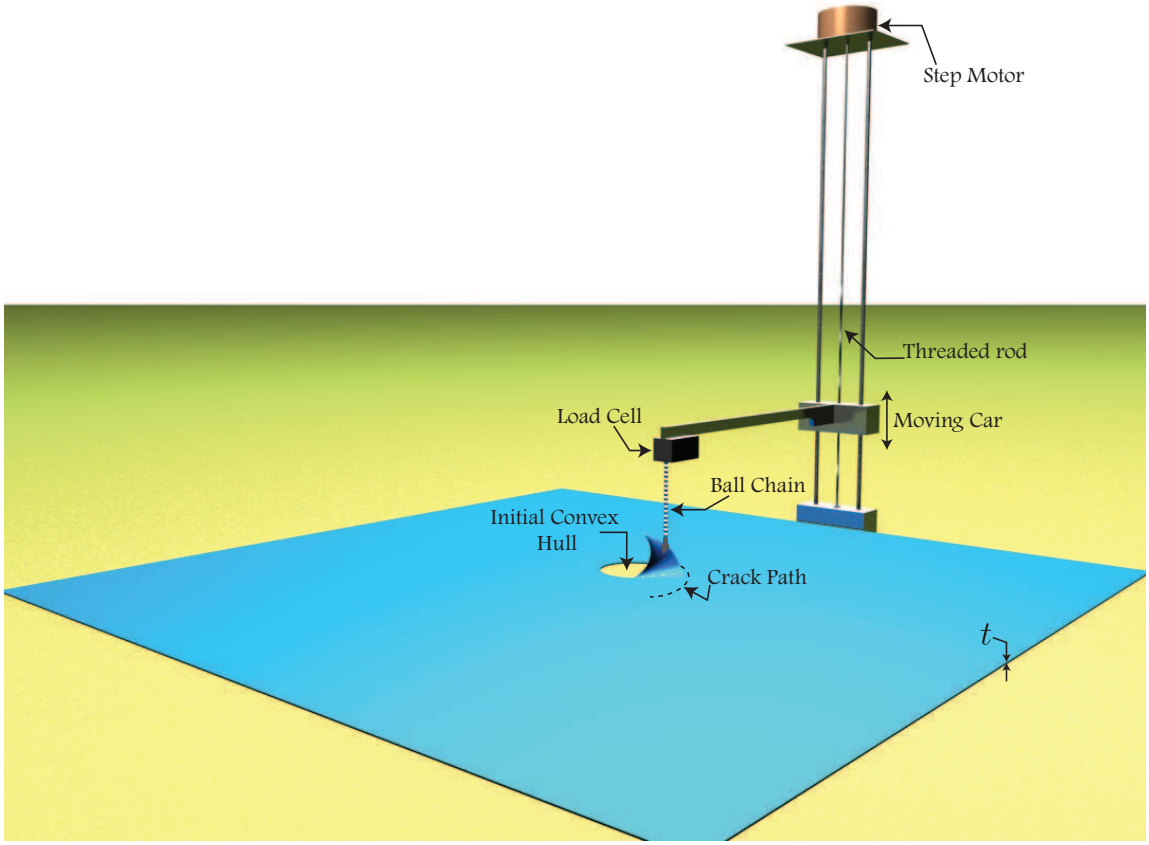

Figure 3.2: *Illustration of the experimental set-up.*

Since the material used is transparent, we apply a thin layer of black paint to help the visualization of the process (this does not affect the fracture process).

At the beginning of the experiment we carefully aligned the tear with the load cell. However, as the crack propagated this alignment was lost. The effects of this on measuring the force could have reduced by placing the load cell far from the tear but that would involve using a longer wire, which could have induced undesirable

elastic effects. Another issue to be taking into account is that in order to have a fracture process in a quasi-static regime, it was necessary to avoid torsion effects in the wire. To satisfy these requirements, we used a connecting cable consisting of a 40 cm copper wire, a 10cm ball chain, and another 20 cm wire of copper. During the experiment it was important that the pulling action was very slow. If the pulling speed is too high, the fracture would go into a stick-slip regime induced by the elastic structure of the out-of-plane flap, and probably by inertial effects of the set-up. Consequently, the pulling velocity was 0.1mm/s.

3.2 Geometrical characterization of the Spiral

When the pulling process began, the initial flap started to bend upwards, generating a fold. As the cable continues to pull up, the curvature of the fold increased and therefore more elastic energy was stored. One end of the fold lay in the perimeter of the convex hull, while the other end was at the edge of the notch, where stresses concentrated (because of the sharpness of the cut), and a crack eventually nucleated. We observe that this crack propagated as a spiral, keeping a similar geometry: a fold was pulled up, one end attached to the previous crack path and the other end being the crack tip that propagates.

A key feature is that here, as in the previous example, only one crack propagates. To ensure this, care in the preparation of the initial convex hull is necessary.

The flap grows and bends out-of-plane. This results in a three-dimensional “pine tree structure. We present three pictures of the initial moments of the pine-tree formation in Fig. 3.3.

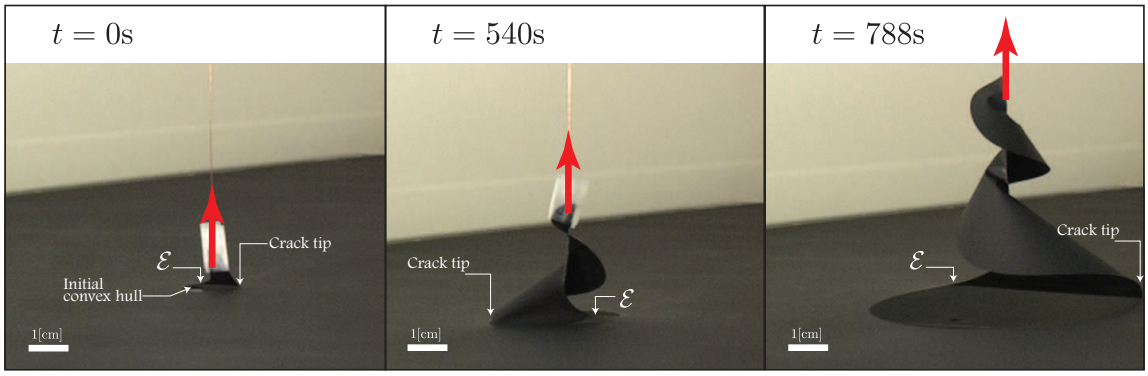

Figure 3.3: *Initial stages of the propagation. Note the 3D ”pine-tree” shape.*

This pine-tree like structure contains many interesting and complex features, briefly discussed later in this chapter. The sizes that this system reaches are remarkable

(pine-trees" up to 1m high in our experiments). Indeed, because the growth of the spiral path is very rapid, the pine-tree also grows very rapidly.

Fig. 3.4 shows a final spiral obtained with this procedure. We can observe that the spiral is very smooth. As we noted in the previous chapter, this is remarkable fracture propagation that requires some explanation.

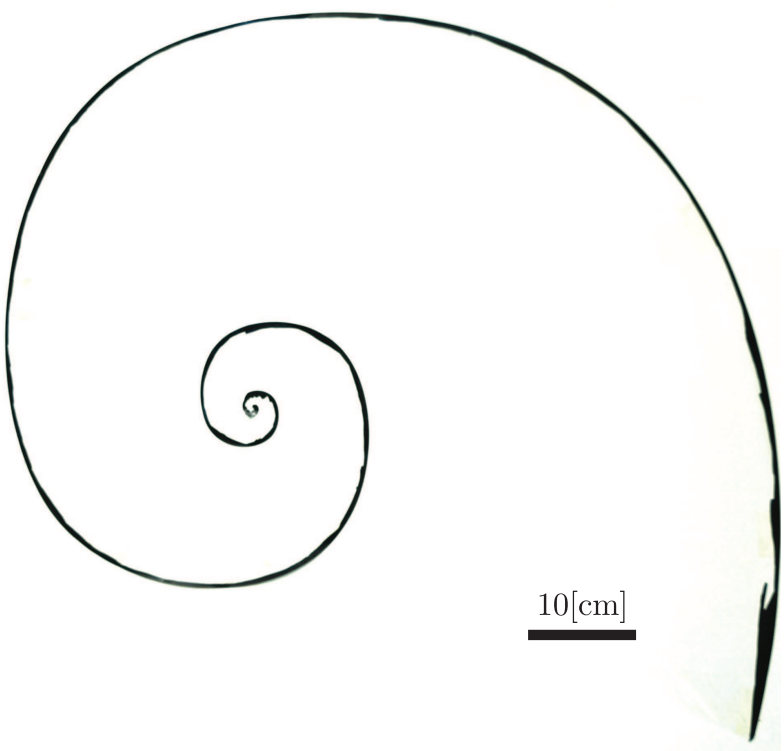

Figure 3.4: *Final tear from propagating a crack by pulling.*

We will see that some of the geometrical arguments used in chapter 2 are relevant here, but for different reasons.

We first note that the convex hull of the crack path also plays an important role here (as it did in chapter 2). Indeed, the convex hull is the part of the sheet that is not directly attached to the fixed boundary conditions, and generates the flap that has the freedom to be pulled up. We also define the limit of this convex hull, and observe that on this limit lies the strongly curved fold.

In fact the configuration of the fold is similar to that in the tearing experiment in [41, 50, 52]: a cracks propagate because a flap is pulled, and the propagation is observed to be very reproducible, and very smooth.

However, we note two differences. First, instead of pulling at 180 degrees, the pulling direction in this case is perpendicular to the plane of the sheet. Secondly, only one crack propagates, whereas in the other case both edges of the folded flap rested on converging cracks. We suggest that these important differences do not change the qualitative behavior of the system reported in [41, 50, 52]: the crack propagates in a direction almost perpendicular to the fold, but always slightly inward. Using the same notation for the propagation direction, we find that β is close to $\pi/2$, but slightly less. Note that apart from the case of strong adhesion to a substrate [50], no quantitative prediction of the value of β is available: in these system, the elastic energy is due to the dominant contribution of concentrated bending in the fold, which is not easy to describe. We will however assume that β can be taken as constant in a first approach.

It is clear that most of the geometrical results obtained in the previous chapter should hold again: we expect to observe a similar logarithmic spiral, even though the applied loading in the systems are very different (in particular, here bending energy is expected to be dominant).

In contrast with the spiral presented in the previous chapter, the resulting crack path only displays one stage of propagation. Since pulling produces a fold, the only way to frustrate a secondary crack is by initiating the system with a proper convex hull, similar to the third stage in the previous spiral.

The geometrical characterization of the final spiral is made in the same way done previously. We have digitalized the final spiral tear, defined a pole at the intersec-

tion of two lines connecting two sets of points with parallel tangents, and finally measured the distance from the pole $\mathcal{O}$ to all the points on the curve. The results from two spirals initiated with perpendicular orientations in a 50μm thick film, are shown in Fig. 3.5.

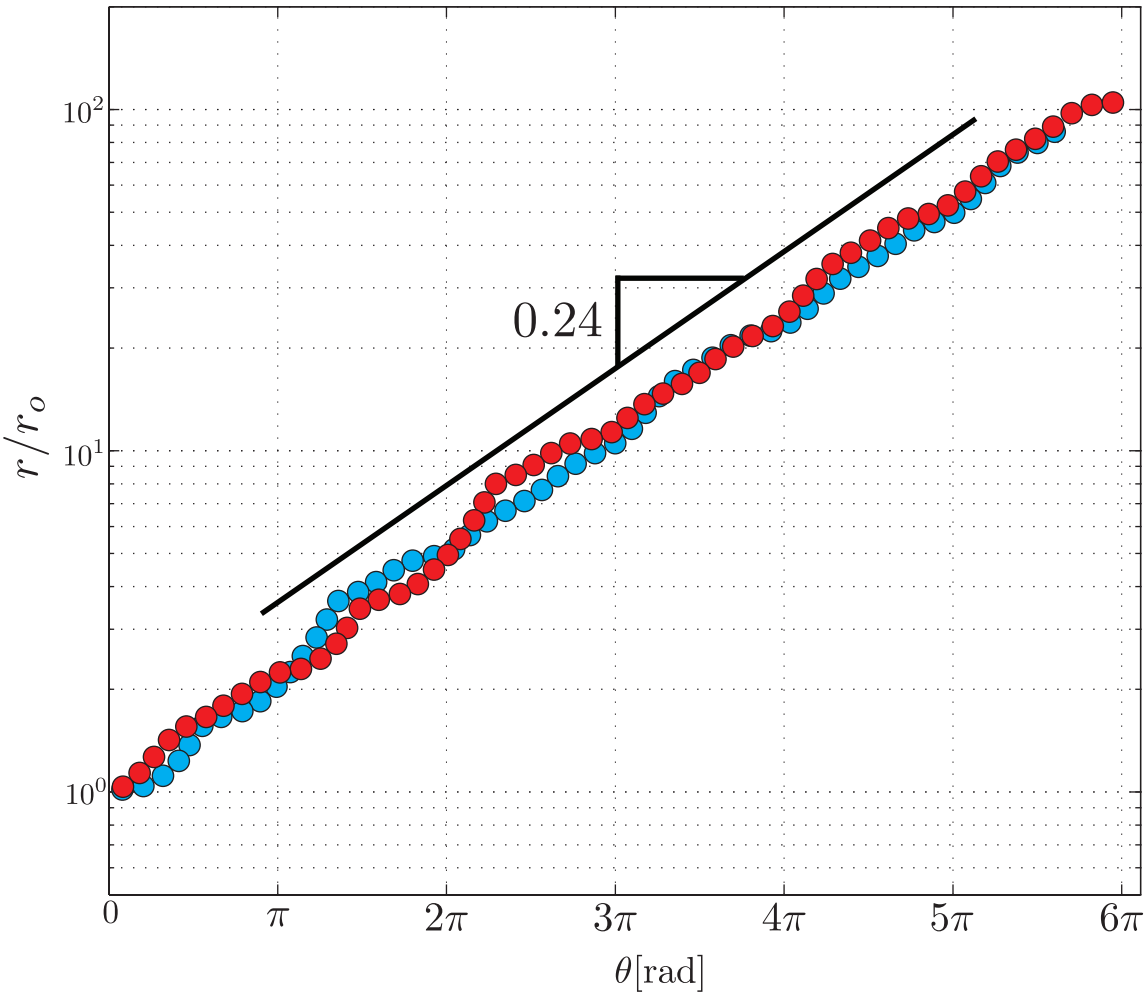

Figure 3.5: *Normalized distance from the pole $\mathcal{O}$ to all the points in two spirals initiated with perpendicular orientations.*

These data show that the spirals are logarithmic (or equiangular), as expected by our analogy. But we see that the growth is slower since the pitch of the spiral is 0.24 (obtained by the best exponential fit), in contrast to the 0.27 of the previous

spiral.

From the final crack path it is also possible to measure the propagation angle β in relation to the orientation, and we present the corresponding measurements in Fig. 3.6.

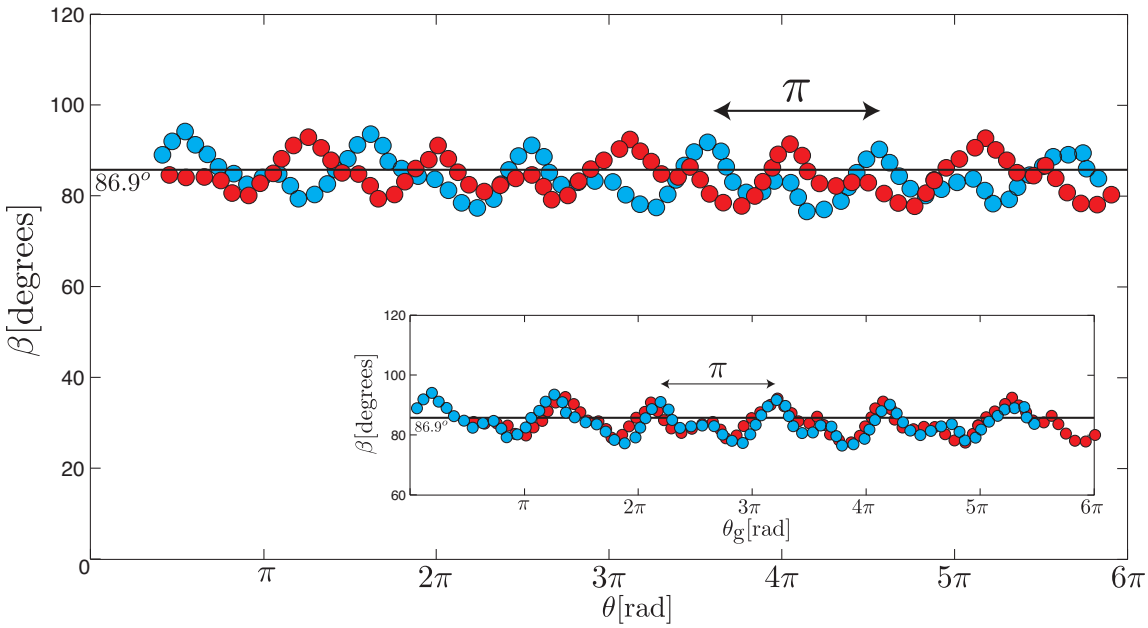

Figure 3.6: *Measurements of β as a function of the spiral angle.* **Inset** *The same data presented as a function of the absolute orientation in the film.*

As in the previous chapter, we observe clear oscillations in β, and again, although the system increases rapidly, it remains with fixed amplitude, 10^o. We observe however that the shape of the oscillation is not exactly the same as that shown for the previous spiral. However there is still periodic π, but the curve have other smaller peaks.

We have compute an average value of β equal to 86.9 ± 9^o. Not surprising, the average values is lower in the pulling experiment ($\beta < \pi/2$) than in the pushing one described earlier ($\beta > \pi/2$), and this is why the spiral pitch is different.

Using Eq. 2.37 ($\sin\phi e^{-(\beta-2\pi)\cot\phi} - \sin(\beta+\phi) = 0$) we obtain an expected value for the pitch of $\cot\phi = 0.25$. Again there is a good agreement with the experimental value (0.24) obtained by fitting the curve in the plot of Fig. 3.5.

In the inset in Fig. 3.6, we present the measured angles β but respect the global orientation in the film given by the angle θ_g, which shows that here again these oscillations are due to material anisotropy.

At this point it is natural to wonder how these geometrical deviations in the spiral compare with that reported in previous chapter (in the pushing case). In Fig. 3.7 we have plotted both measurements collapsed in one period.

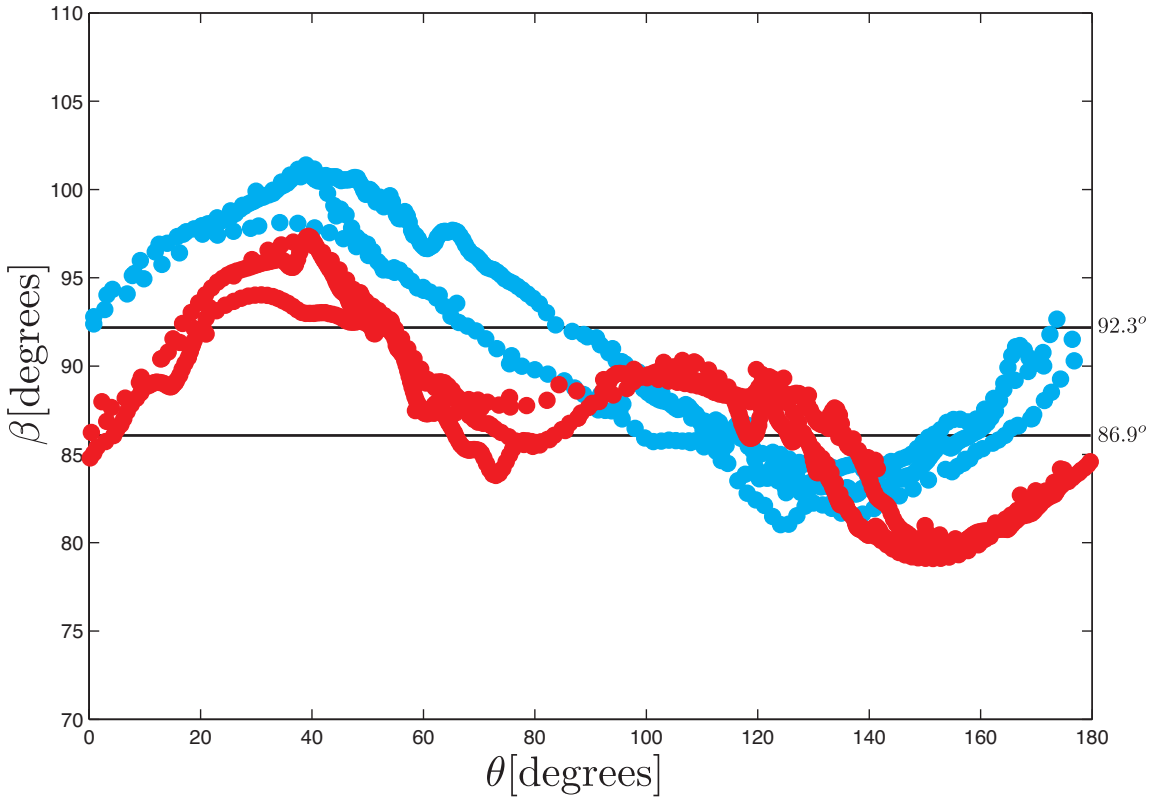

Figure 3.7: *Superimposed measurements of β collapsed in one period for both spiral experiments. With blue dots is plotted β from a pushing spiral, the dots in red are the measurements of β from a pulling spiral.*

The global shift in the curves (difference in average value of β) is related with the way in which the system releases elastic energy : pulling on a fold leads to average propagation inwards $\beta < 90^o$ (reducing the fold size as shown in [50]), whereas the pushing experiment favors outward propagation $\beta > 90^o$ (see [40]). However the amplitude of the variation in propagation angle is greater than the difference in the average values in the two cases (pushing or pulling spiral).This suggests that anisotropy may be more important to understand than the actual details of the pulling/pushing loading. The agreement between the curves, in amplitude and roughly in functionality, is natural since both oscillations are guided by the anisotropy of the same material.We also note secondary smaller peaks appears around 110^o in the pulling case. We have no explanation yet for this straking behavior.

3.3 Pulling forces

We present a simple energetic argument to estimate the necessary pulling force and compare it to the experiments.

The three-dimensional pine-tree structure has a very complex geometry and includes crumpled structures. In fact, the fold has no symmetry at all since it ends on one side at the convex hull and on the other one at the crack tip. The elastic characterization of whole system is a really difficult endeavor. In order to have some approximation, we present a very simplified model to connect the work performed by the pulling force and the energy used to increase the crack surface.

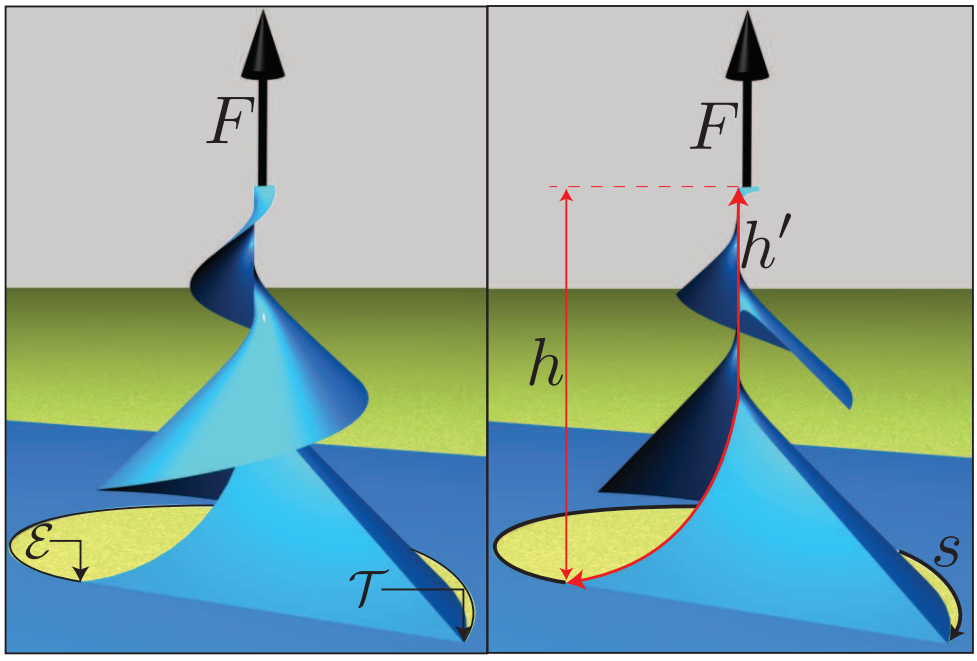

Figure 3.8: **Left**.-*The elastic pine-tree*.**Right**.-*The Internal structure of the elastic pine-tree.*

The first approximation we assume is that the work is converted into new crack

surface, or in other words, we neglect the change in elastic energy of the structures as the crack propagates. This leads to

$$Fdh = \gamma t ds \tag{3.1}$$

This relation connects the change of vertical movement made by the pulling system, dh, and the in plane rate of growing of the crack, ds.

As a second approximation, we calculate h', rather than high h (see the illustration on the right in Fig. 3.8).The reason can understood from observing figure Fig. 3.8. On the left we have drawn a schematic of the elastic pine-tree and on the right, the interior of this structure. After a careful examination of this figure, we conclude that the distance h' is equal to the distance along the crack, from the start to point $\mathcal{E}$ (as defined in the previous chapter).

We now compute s and h' as the integrals of the arc length of the spiral.

$$s = \int_{\theta_o}^{\theta_\mathcal{T}} \left(1+\cot^2\phi\right)^{1/2} a e^{\theta\cot\phi} d\theta \tag{3.2}$$

$$h' = \int_{\theta_o}^{\theta_\mathcal{E}} \left(1+\cot^2\phi\right)^{1/2} a e^{\theta\cot\phi} d\theta \tag{3.3}$$

Where a is the initial size of the sprial. The variations are given directly by:

$$ds = \frac{a}{\sin^2\phi} e^{\theta_\mathcal{T}\cot\phi} \tag{3.4}$$

$$dh' = \frac{a}{\sin^2\phi} e^{\theta_\mathcal{E}\cot\phi} \tag{3.5}$$

If we plug this in Eq. (3.1) we obtain:

$$F\frac{e^{\theta_\mathcal{E}\cot\phi}}{e^{\theta_\mathcal{T}\cot\phi}} = \gamma t \tag{3.6}$$

But we have already demonstrated that $\theta_\mathcal{T} - 2\pi = \theta_\mathcal{E} - \beta$, so the relation between the pulling force and the fracture energy is given by:

$$F = e^{(2\pi-\beta)\cot\phi}\gamma t \tag{3.7}$$

From experimental spiral we have typical values of $\beta \sim 86.9^o$, from Eq. (2.37) we compute a corresponding value of $\cot\phi \sim 0.25$. Using these values in Eq. (3.7) we obtain:

$$F = 3.29\gamma t \tag{3.8}$$

The force required to propagate the crack is greater than γt. This relation predicts that the pulling force will be constant no matter how much the spiral grows, so the same amount of force is always needed to keep the crack propagating.

We now turn to the experimental results of force measurement. We tested three films with different thickness, (30μm, 50μm and 90μm). The initial configuration was a circular convex hull with a notch on the perimeter.

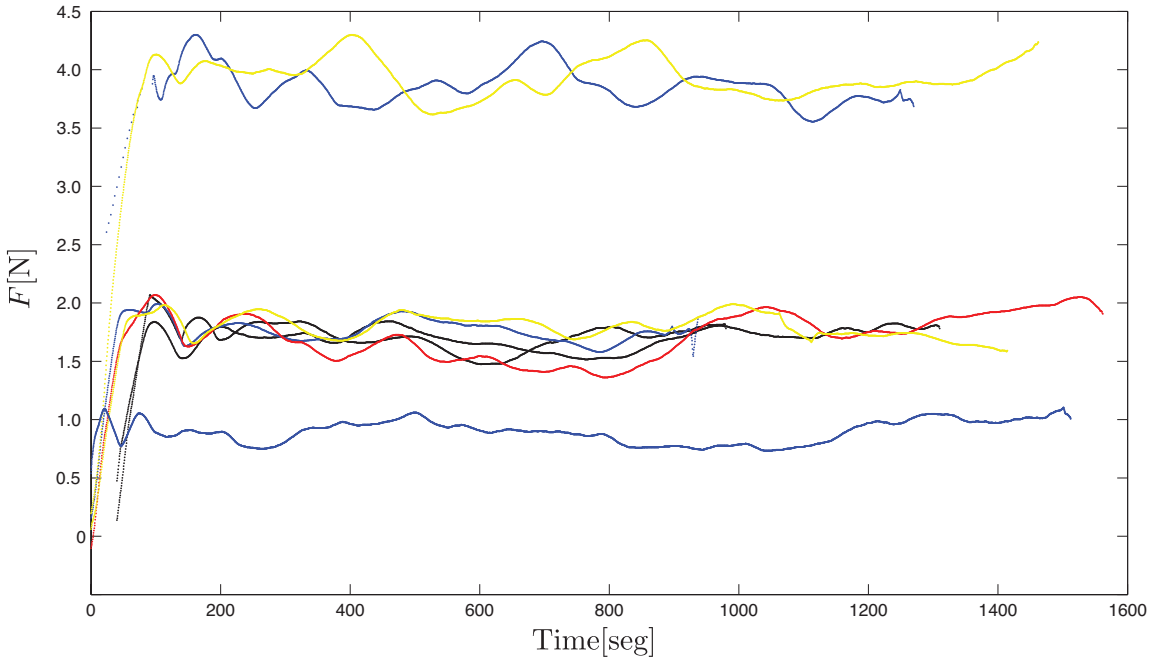

Figure 3.9: *Measurements of the pulling force versus time. The data for experiments with films of 30μm (lower curve), 50μm (center curves) and 90μm (high curves)*

With these experiments we were particularly interested in testing the validity of

Eq. B.5. Fig. 3.9 presents the data from experiments without incidents, such as breaking, tearing, secondary crack nucleation or rupture where the tear is perforated. Note that on average, an experiment that generates an 80cm diameter spiral, takes around 28 minutes. In this long period of time the spiral grows by a large factor, and there are many possibilities for the experiment to fail. For example an unexpected secondary crack may initiate along the tear or in the fold.

An initial observation from Fig. 3.9 is that the force does not diverge in any of the experiments, despite the exponential change in the size of the systems.

The top curves in Fig. 3.9 show the results of experiments with 90μm thick sheets. The average force during fracture propagation was $F_{90} \approx (3.73 \pm 0.9)$N. The center curves correspond to experiments using 50μm thick sheets, in which the average value of the force was $F_{50} = (1.73 \pm 0.5)$N. Finally the bottom curve is a single experiment with a 30μm thick sheet where the average value was $F_{30} = (0.89 \pm 0.2)$N. The corresponding fracture energies for each material are $(\gamma t)_{90} = (1.9 \pm 0.1)$N, $(\gamma t)_{50} = (0.6 \pm 0.1)$N and $(\gamma t)_{30}$ not measured yet. If we use Eq. B.5 with these values, the predicted forces are $F'_{90} = 6.25$N, $F'_{50} = 1.97$N. The agreement with the average values is only good for the experiment with 50μm. For the experiment with 90μm, the prediction is overvalued.

Although the predictions and the experimental values are not in complete agreement, given the geometry of the system, we can ensure that the force required to propagate the crack is greater than γt.

3.4 Geometrical Characterization of the Initial Seed

To initiate this experiment, it is necessary to artificially generate a tear in the film. It is possible to cut several tear shapes with a knife. However, not all the possible shapes generate a spiraling crack when pulled. For example, with a straight incision, the fold generated by pulling concentrates the stress on both ends of the incision, hence two cracks are nucleated. Consequently, this is not the proper manner to obtain a final spiral crack path.

The fundamental idea in the construction of the initial configuration is *"Just one crack must propagate"*. Therefore, we need to analyze the conditions for crack nucleation. A fold will always be generated in the process of pulling a tear. The experimental crack trajectory results in a spiral if at any moment in the experiment, one extreme of the fold concentrate much more stress than the other.

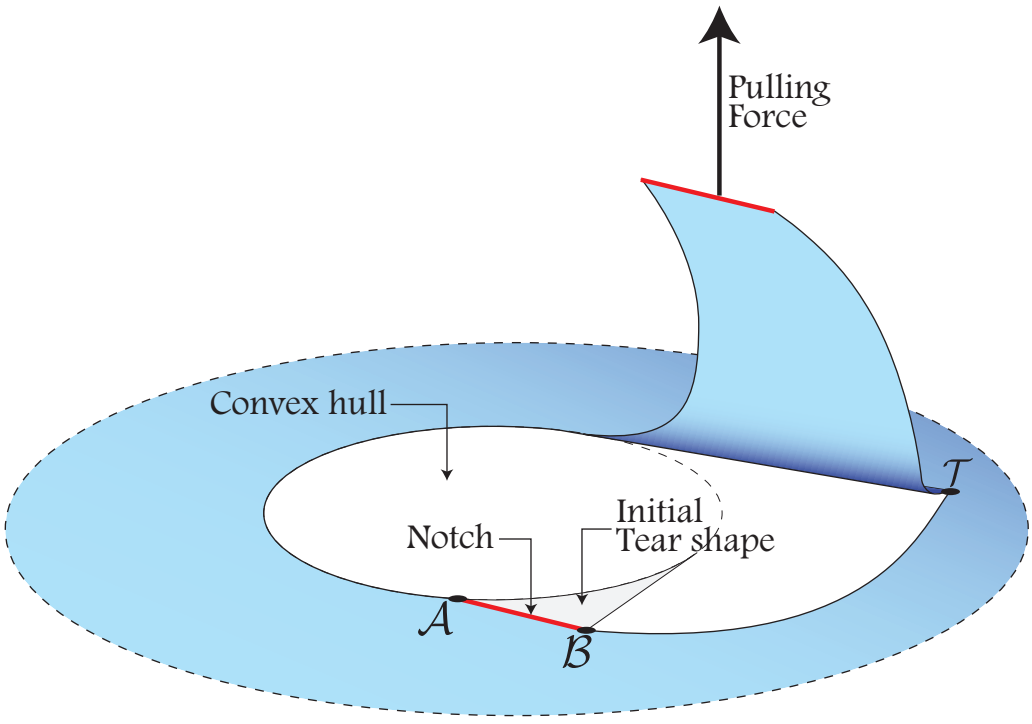

Figure 3.10: *Initial Configuration. Geometrical frustration of the secondary crack.*

One solution consists of generating a convex hull by making a hole in the film, the tear is formed by making a notch at the perimeter of the hole, see Fig. 3.10. If the tear is pulled, the crack initiates at the end of the fold within the film. A curved path grows, and the fold always moves tangentially to the convex hull. Since one end of this fold lies on the perimeter of the convex hull, we have a first constrain for the geometry of the initial hole, that is, the contour around point $\mathcal{B}$ must be sharper than the contour around the crack tip.

When the fold has surrounded the convex hull, the extreme of the fold, which is not the crack, will reach point $\mathcal{B}$ (Fig. 3.10). Not making the notch properly at the beginning of the experiment could produce fracture nucleation, so it is important not to damage the film when making the notch. A simple solution is to make a smooth curved notch, instead of a straight one.

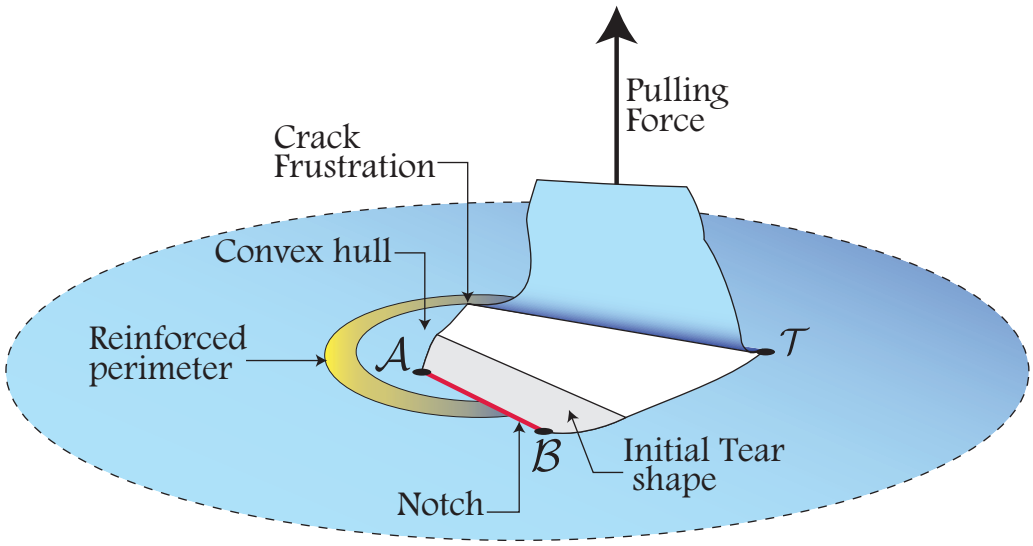

Figure 3.11: *Initial Configuration. Mechanical frustration of the secondary crack.*

A second solution that leads to a spiral trajectory is found. Now, instead of geometrically avoiding crack nucleation, we reinforce the material in such a way that

the initial convex hull is no longer a hole, but a zone surrounded by harder material, see Fig. 3.11. In this case, the tear is formed by an incision made from the inside of the convex hull to the outside through the reinforced perimeter. When the tear is pulled up at both ends of the incision, there is crack nucleation. However, when the inner crack reaches the reinforced perimeter, it stops and only the outer crack continues becoming the final spiral. In this case, the geometry of the convex hull has fewer constraints since the reinforced perimeter avoids crack nucleation. On other hand, it remains important to be careful making the initial notch because again the fold will reach point $\mathcal{B}$.

Note that both these solutions are in fact one, the creation of a convex hull plus a notch, in the first case by removing material and in the second case by reinforcing a selected contour.

3.5 Easy Opening

The divergent crack procedure described in this chapter is very simple and efficient. Therefore, it could be very useful for *"easy open"* packages made of thin brittle sheets. To be useful, however, we need to establish the conditions in which the spiral formation will be successful.

One source of failure could be that the pulling flap along the axis of the elastic pine-tree breaks due to the high concentration of stress. However, if there is failure in this zone, there will remain always a flap and the pulling process can continue. Thus, we focus in a different possibility of failure due to the nucleation of a second crack in the perimeter of the convex hull.

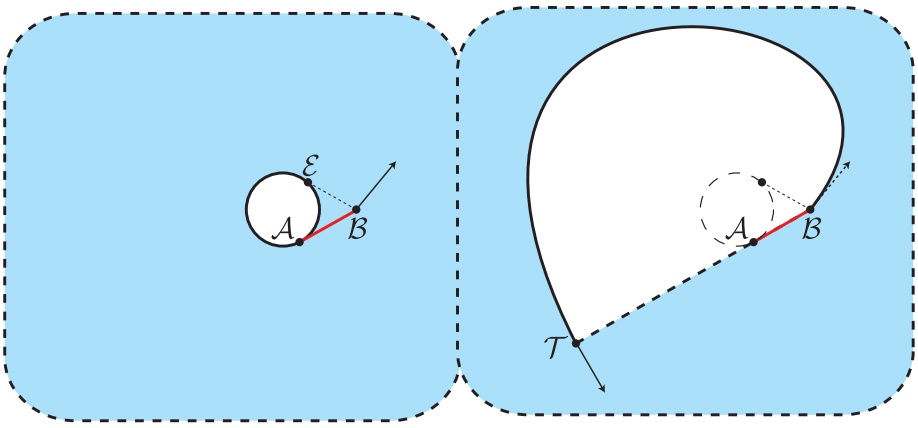

Figure 3.12: *Illustrations of an unsuccessful initial configuration:* **Left.-** *Initial configuration made by removing a disk of material and a straight notch.* **Right.-** *Evolution of the morphology of the convex hull when the crack advances. In this case the perimeter of the convex hull contains two discontinuities, hence two cracks nucleate at points* $\mathcal{T}$ *and* $\mathcal{B}$*.*

In general, the deformation associated with the fold generates two competing cracks in the film at both ends of the fold. By modifying the geometry around

one of these problematic points we can avoid the nucleation of one of the two cracks. This is what we obtain when a flap is pulled from a spiral-shaped convex hull.

It is widely known that smooth contours do not concentrate as much stress as sharp ones. Hence, the solution lies in the geometry of the perimeter of the imposed initial convex hull. We need to create a convex hull with only one discontinuity in the perimeter which will be the nucleated crack. A circular convex hull with a notch satisfies this condition (discontinuity at point $\mathcal{B}$, see Fig. 3.12 **Left**), however as the crack advances the morphology of the convex hull evolves and the perimeter is redefined. If the initial notch is any straight line the convex hull, the crack propagation will shed a second discontinuity in the convex hull (see Fig. 3.12 **Right**).

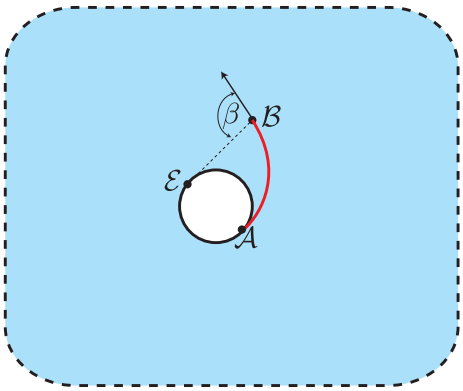

Figure 3.13: *Illustration of the optimal initial configuration for the spiral creation.*

The best solution to this problem is to soften the curvature generated at the end of the initial notch. This could be done by making the initial cut in such a way that it starts tangent to the perimeter of the removed disk of material.Then it should go smoothly until it finishes with an angle, respect to the initial fold, close to the value of the fracture angle β of the material. This configuration is illustrated in Fig. 3.13.

Note that this is in fact the best solution because it ensures that there will be only one discontinuity around the ends of the fold at any moment in the process.

Fig. 3.14 shows a possible application for this procedure in an everyday object wrapped in a brittle thin sheet, a compact disk. Note that to perform this experiment in a common object we have not change the default package material, but we only make the initial proposed configuration in the product as we bought it.

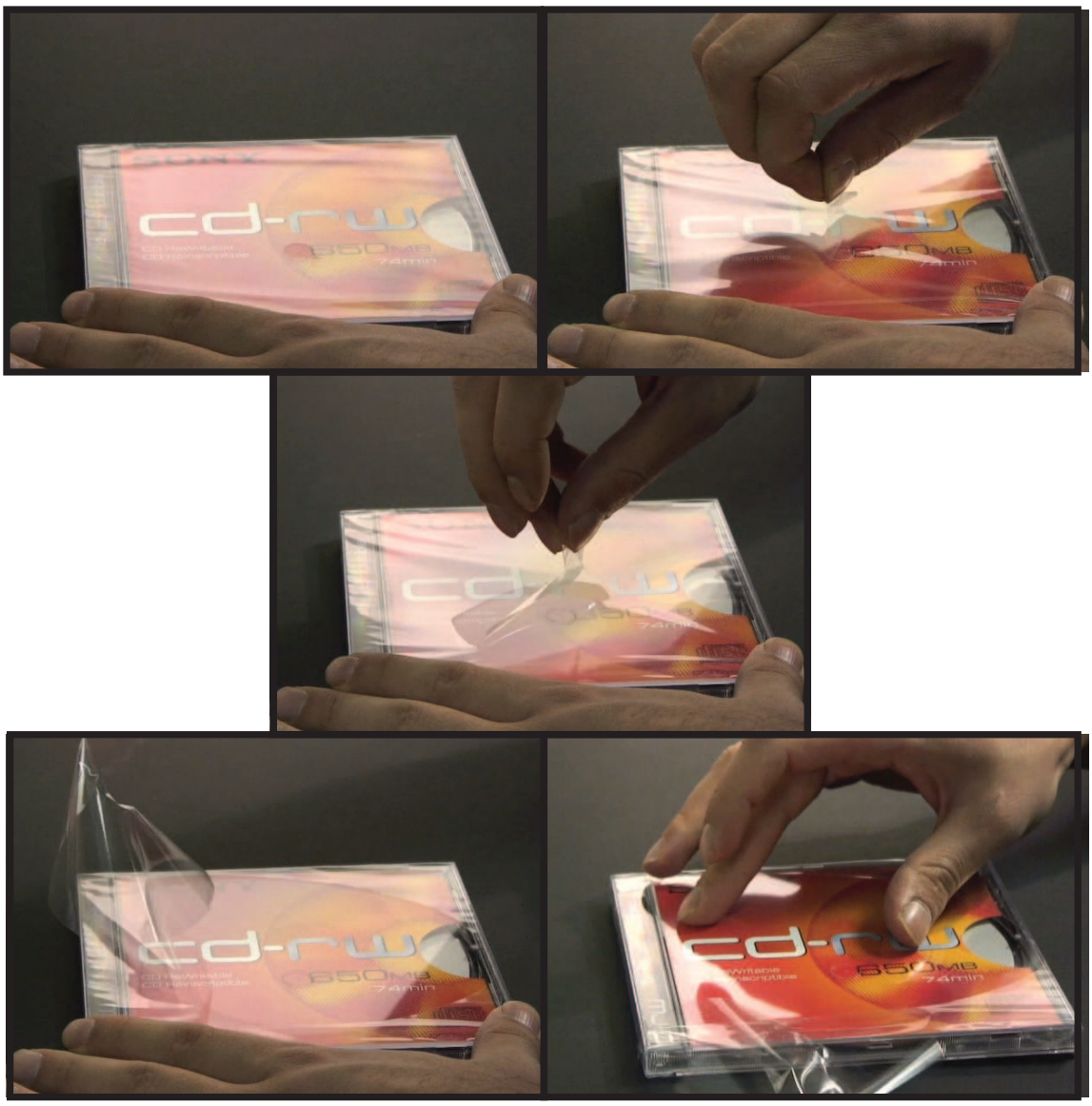

Figure 3.14: *Easy opening using our method to remove the packaging for a compact disk.*

3.6 Crumpling Structures in the Elastic Pine-Tree

The elastic pine-tree is the out-of-plane deformation of the resulting tear. The formation process of this pine-tree generated very interesting shapes on its vertical axis, shown in Fig. 3.15. In this section we do not try to characterize this phenomena but only make some qualitative descriptions.

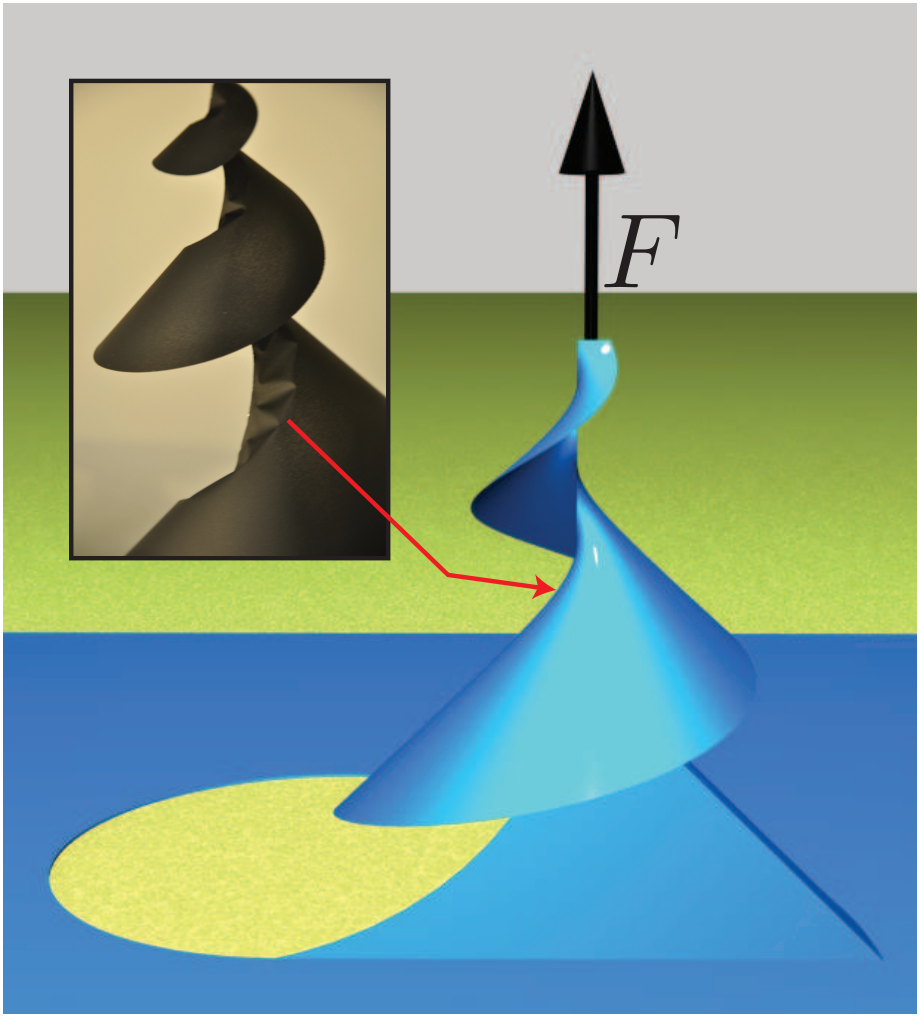

Figure 3.15: *The final shape of the crumpling structures in the elastic pine-tree.*

It is possible to observe from the Fig. 3.15 that these structures are very regular, and the lower they are, the larger they are. Once the fracture has stopped, if the tear is released, sharp points can be observed. These structures do not appear by pulling the tear again. Thus, this crumpling-like process is intrinsic to the growth of the pine-tree.

In the set of pictures shown in Fig. 3.16, we present how one of these crumpling-like structures is formed during pine-tree growth.

Note in the sequence shown in Fig. 3.16 that while the crack rotates counter-clockwise, the upper part of the tear rotates clockwise. We attribute the formation

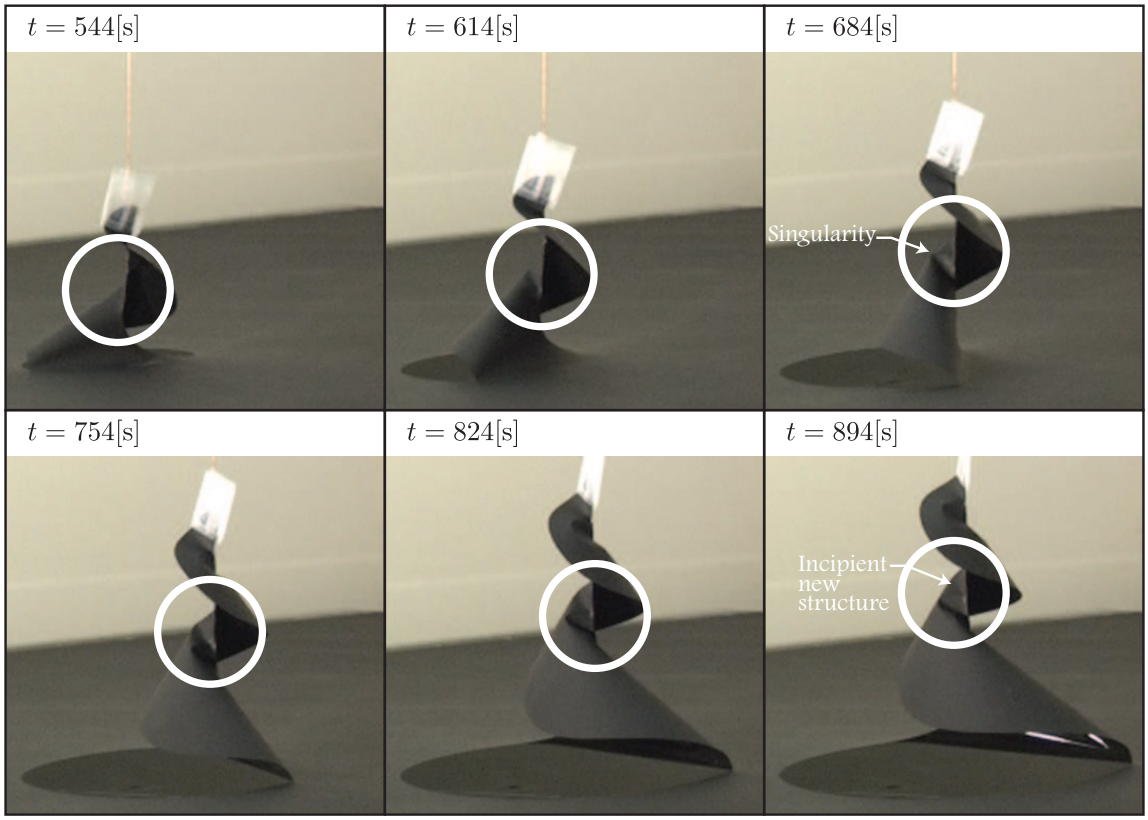

Figure 3.16: *Sequence of pictures showing the formation of crumpled structures.*

of these structures to this counter-rotation. These structures generates singular points in the curvature, as presented for $t = 684$s in Fig. 3.16. These singularities are responsible for the marks observed in the final tear. In the final picture of the sequence, a second crumpled structure is starting to grow.

3.7 Conclusions

Another spiral propagation was observed with very different loading, which does not involve a blunt object, but is rather similar to the converging tears of [41,43,50]. The final spiraling crack was treated in the same way as in the other spiral experiment, unveiling again a very reproducible logarithmic (or equiangular) geometry. We have measured and studied the pulling force, which is rather constant through-

out the experiment, even though the radius of the spiral grows exponentially. This is well explained by a geometric argument.

As in the much simpler case of the converging tears, we could not give a quantitative model for crack propagation. Indeed, this time, and in contrast to other spiraling cracks, the dominant energy is from bending the film. A good description of the bent folds is therefore required here, which is not an easy task: The part of the sheet that is bent out-of-plane takes an elegant, but very complex shape, displaying regular crumpling-like patterns.

Thin sheets of brittle materials are commonly used in the industry of packaging. We believe that the fracture process described in this chapter could be adopted as a very efficient mechanism to open enclosures. Hence, we present an analysis regarding the requirements for the initial configuration in order to obtain a divergent spiraling crack path.

Chapter 4

Conclusions

4.1 Spiraling Rupture With a Blunt Object

In chapter 2, we presented a simple experiment leading to a divergent tear that grows exponentially. It has been shown that the crack path and final tear shape are independent of the direction and speed of the pushing tool, confirming the robustness of the fracture mechanism.

Using the Griffith criterion, we have provided a theoretical model to explain our results. However, the model rests on a basic assumption that has not been explained yet: the elastic energy scales with the indentation angle α as $U \sim \alpha^{3.5}$, which does not agree with previous theoretical predictions [47]. This assumption is corroborated by, first, a direct experimental measurement of the elastic force and, second, the measurement of the predicted critical value for the indentation angle α_c.

Our results expand the conclusions reached by Audoly et al. [47]. from the analysis of the oscillatory fracture path since our spiral is obtained by carefully avoiding the nucleation of a second crack. We have found that, to this aim, the concept

of *convex hull* introduced by Audoly et al is critical. We studied the geometrical conditions allowing for the convex hull to have only one crack, or discontinuity of the tangent vector along its perimeter, in order to force the appearance of a spiral tear.

With the laws of propagation obtained from our model, we have also predicted the three stages of spiral growth when the initial convex hull has more than one crack, specifically, when the starting notch is a straight line. Each of these stages corresponds to a particular kind of logarithmic spiral. These predictions have been tested by using the geometrical measurements of the final crack path.

More detailed measurements of the fracture direction angle, β, have shown an oscillatory behavior around a constant value. Because of the periodicity, we attribute the oscillations to the anisotropy of the material. In fact, more anisotropic materials have more oscillations of β. We have included the effect of anisotropy on the maximum energy release rate criterion and obtained an expression for the oscillations of β. Although, our model correctly describes the isotropic behavior of β in our experiments, it is not completely satisfactory to explain the anisotropic behavior.

Finally, we conjecture that the simplicity of our results implies that they are not only applicable to brittle materials. In fact, Vermorel et al. [46] reported spiral crack propagation in aluminum foils. A logical step forward in our work would be to repeat our experiments with thin metal sheets.

4.2 Tearing Spiral

The experiment presented in this chapter is very simple to do, but very complex to model. Indeed the out-of-plane deformation of the tear generates many of the structures studied in thin sheets, such as d-cones, folding, ridges, and, of course, fracture. The complexity is obvious because the fracture is not being driven locally, and the applied work has to be transmitted through the whole elastic out-of-plane structure to propagate the crack. A satisfactory model should include the energy of a non-symmetric fold, the stretching of the central axis of the elastic structure, and the formations of singularities, such as d-cones observed on the elastic pine-tree structure.

In chapter 3, we have proved that this system is not very efficient in terms of the amount of force required to drive the fracture process, and by comparing the vertical movement and crack displacement. We have estimated the force $F = 3.29\gamma t$, where γt is the fracture work. This means that only a fraction of the force is used to propagate the fracture. Our experimental results, however, show that this is an overestimate since the value of the force driving the process is less than predicted. Nevertheless, overall our measurements confirm the *"amplification of the fracture work"*, so that the pulling force is always greater than the fracture work.

Despite this *"amplification of the fracture work"* we have shown that the required force is always delimited within a range. Thus, independent of the size of the tear, the same amount of force is required to continue propagating the crack.

To conclude, we remark that the experiment described here is a very efficient and simple way to open wrapping that could be used in packaging as a new *"easy opening"* mechanism.

4.3 General Conclusions

The two fracture experiments presented in this thesis show similar final tear shapes outlined by different but reproducible logarithmic spirals. This is not trivial since the deformations guiding the corresponding processes are completely different. In the case of rupture with a blunt object, the system transforms stretching energy into surface energy, while in the case of tearing, the fracture transforms mainly bending energy into surface energy. To explain the similarity, we point out that geometry is the main element in both cases: there is an almost constant angle of propagation β that is explained by the specific mechanism of fracture.

Perhaps the main problem for the applicability of our results is the need to avoid nucleation of a second crack. We have found simple rules to construct an initial configuration leading to spiral formation, but the problem of determining an optimal initial seed has not been overcome. We expect these rules to be fully applicable for the two different mechanisms discussed in chapters 2 and 3 .

There are still other unanswered questions, so that a more detailed experiment is required to connect anisotropy with our theoretical predictions based on the maximum energy release rate criterion, or a complete description of the out-of-plane structure generated in the tearing spiral. However, we think that the results presented in this thesis will contribute to a better understanding of fracture in thin sheets, and the patent presented will be helpful in practical applications for packaging.

Bibliography

[1] F. Cavallo and M. Lagally. Semiconductors turn soft: inorganic nanomembranes. *Soft Matter*, 6:439–455, 2010.

[2] L. D. Landau and E. M. Lifshitz. *Theory of Elasticity, Courses of theoretical Physics, Volume 7*. Pergamon Press, , second edition, 1975.

[3] E. H. Mansfield. *The Bending & Stretching of Plates*. Cambridge University Press, second edition, 1989.

[4] D. J. Struik. *Lectures on Classical Differential Geometry*. Dover, second edition, 1988.

[5] E. Kreyszig. *Differential Geometry*. Dover, 1991.

[6] D. Boal. *Mechanics of the Cell*. Cambridge University Press, 2002.

[7] E. Reissner. *Selected Works in Applied Mechanics and Mathematics*. Jones and Bartlet Publishers, 1996.

[8] S. E. Sheppard and F. A. Elliot. The reticulation of gelatine. *The Journal of Industrial and Engineering*, 12:727–732, 1918.

[9] M. Biot. Surface instability of rubber in compression. *Applied Scientific Research A*, 12:168–182, 1963.

[10] Thomas A Witten. Stress focusing in elastic sheets. *Review of Modern Physics*, 2007.

[11] T. A. Witten and H. Li. Asymptotic shape of a fullerene ball. *Europhysics Letters*, 23:51–55, 1993.

[12] S. Timoshenko and S.Woinowsky-Kreiger. *Theory of Plates and Shells*. McGraw Hill Higher Education; 2nd edition, 1964.

[13] M. Ben-Amar and Y. Pomeau. Crumpled paper. *Proceedings: Mathematical*, 453, 1997.

[14] E. Cerda and L. Mahadevan. Conical surfaces and crescent singularities in crumpled sheets. *Physics Review Letters*, 1998.

[15] A. Boudaoud, P. Patricio, Y. Couder, and M. Ben Amar. Dynamics of singularities in a constrained elastic plate. *Nature*, 2000.

[16] E. Hamm, B. Roman, and F. Melo. Dynamics of developable cones under shear. *Physics Review E*, 70, 2004.

[17] E. Cerda, S. Chaieb, F. Melo, and L. Mahadevan. Conical dislocations in crumpling. *Nature*, 401:46–49, 1999.

[18] L. Boué, M. Adda-Bedia, A. Boudaoud, D. Cassani, Y. Couder, A. Eddi, and M. Trejo. Spiral patterns in the packing of flexible structures. *Physical Review Letters*, 97:166104, 2006.

[19] L. Boué and E. Katzav. Folding of flexible rods confined in 2d space. *Europhysics Letters*, 80:54002, 2007.

[20] J. A. Aström T. Tallinen and J. Timonen. The effect of plasticity in crumpling of thin sheets. *Nat. Materials*, 8:25–29, 2009.

[21] J. A. Aström T. Tallinen, J. Ojajärvi and J. Timonen. Scaling behavior in non-hookean compression of thin-walled structures. *Physical Review Letters*, 105:066102, 2010.

[22] J. Huang, M. Juszkiewicz, W. H. de Jeu, E. Cerda, T. Emrick, N. Menon, and T. P. Russell. Capillary wrinkling of floating thin polymer films. *Science*, 317:650–653, 2007.

[23] L. Pocivavsek, B. Leahy, N. Holten-Andersen, B. Lin, K. Y. Lee, and E. Cerda. Geometric tools for complex interfaces: from lung surfactant to the mussel byssus. *Science*, 5:1963–1968, 2009.

[24] E. Hohlfeld and L. Mahadevan. Unfolding the sulcus (arxiv:1008.0694). *To be published*, 2010.

[25] N. Bowden, S. Brittain, A. G. Evans, J. W. Hutchinson, and G. M. Whitesides. Spontaneous formation of ordered structures in thin films of metals supported on an elastomeric polymer. *Nature*, 393:146–149, 1998.

[26] C.M. Stafford, C. Harrison, K. L. Beers, A. Karim, E. J. Amis, M. R. Vanlandingham, H. Kim, W. Volksen, R. D. Miller, and E. E. Simonyi. A buckling-based metrology for measuring the elastic moduli of polymeric thin films. *Nat. Materials*, 3:545–550, 2004.

[27] E. Cerda and L. Mahadevan. Geometry and physics of wrinkling. *Physical Review Letters*, 90:074302, 2003.

[28] Enrique Cerda. Mechanics of scars. *Journal of Biomechanics*, 38, 2005.

[29] R. Bernal J. C. Géminard and F. Melo. Wrinkle formations in axi-symmetrically stretched membranes. *The European Physical Journal E*, 15:117–126, 2004.

[30] J. Huang, B. Davidovitch, C. D. Santangelo, T. P. Russell, and N. Menon. Smooth cascade of wrinkles at the edge of a floating elastic film. *Physical Review Letters*, 105:038302, 2010.

[31] Y. Pomeau and S. Rica. Plaques très comprimées. *C.R. Acad. Sci. Paris*, 325:181–187, 1997.

[32] R. Schroll, E. Katifori, and B. Davidovitch. A curtain-type problem: pattern formation on uniaxially confined sheet with deformed edge. *(to be published)*, 2010.

[33] L. Pocivavsek, R. Dellsy, A. Kern, S. Johnson, B. Lin, K. Y. Lee, and E. Cerda. Stress and fold localization in thin elastic membranes. *Science*, 320:912–916, 2008.

[34] P. M. Reis, F. Corson, A. Boudaoud, and B. Roman. Localization through surface folding in solid foams under compression. *Physical Review Letters*, 103:045501, 2009.

[35] D. P. Holmes and A. J. Crosby. Draping films: A wrinkle to fold transition. *Physical Review Letters*, 105:038303, 2010.

[36] J. Yoon, J. Kim, and R. C. Hayward. Nucleation, growth, and hysteresis of surface creases on swelled polymer gels. *Soft Matter*, 2010.

[37] J. Yoon J. Kim and R. Hayward. Dynamic display of biomolecular patterns through an elastic creasing instability of stimuli-responsive hydrogels. *Nature Materials*, 9:159–164, 2010.

[38] E. E. Gdoutos. *Fracture Mechanics: an Introduction*. Kluwer Academy Publishers, 2005.

[39] B. Cotterell. *Fracture and Life*. Imperial College Press, 2003.

[40] T. Wierzbicki, K.A. Trauth, and A. G. Atkins. On diverging concertina tearing. *Journal of Applied Mechanics*, 65, 1998.

[41] A. G. Atkins. Opposite paths in the tearing of sheet materials. *Endeavour*, 18:2–7, 1995.

[42] B. R. Lawn and T. R. Wilshaw. *Fracture of Brittle Solids*. Cambridge University Press, 1995.

[43] A. G. Atkins. The tear length test as an indicator of anisotropy in sheet materials. *Proc. 10th Congr. on Material Testing (Scientific Society of Mech. Engineers, Budapest)*, pages 595–600, 1991.

[44] E. Sharon and H. Swinney. Geometrically driven wrinkling observed in free plastic sheets and leaves. *Phys. Rev. E*, 75, 2007.

[45] E. Sharon, B. Roman, M. Marder, G. Shin, and H. Swinney. Buckling cascades in free sheets. *Nature*, 2002.

[46] R. Vermorel, N. Vandenberghe, and E. Villermaux. Radial cracks in perforated thin sheets. *Physics Review Letters*, 104, 2010.

[47] B. Audoly, P. Reis, and B. Roman. Cracks in thin sheets: When geometry rules the fracture path. *Physics Review Letters*, 95, 2005.

[48] A. Ghatak and L. Mahadevan. Crack street: The cycloidal wake of a cylinder tearing through a thin sheet. *Physics Review Letters*, 91, 2003.

[49] P. Reis, A. N Kumar, M. D Shattuck, and B. Roman. Unzip instabilities: Straight to oscillatory transitions in the cutting of thin polymer sheets. *Europhys. Lett.*, 82, 2008.

[50] E. Hamm, P. Reis, M. Leblanc, B.Roman, and E. Cerda. Tearing as a test for mechanical characterization of thin adhesive films. *Nat Mater*, page 5, Mar 2008.

[51] D. Sen, K. S. Novoselov, P. M. Reis, and M. J. Buehler. Tearing graphene sheets from adhesive substrates produces tapered nanoribbons. *Small*, 6, 2010.

[52] C. M. Muscat-Fenech and A. G. Atkins. Elastoplastic convergent and divergent crack paths in tear testing of sheet materials. *Fatigue and Fracture of Engineering Materials and Structures*, 17, 1994.

[53] E Bayart, Arezki Boudaoud, and M Adda-Bedia. On the tearing of thin sheets. *Engineering Fracture Mechanics*, 77(11):1849–1856, Jul 2010.

[54] H. Wa. Guggenheimer. *Differential Geometry*. ASTM, 1963.

[55] M. Sendova and K. Willis. Spiral and curved periodic crack patterns in sol-gel films. *Applied Physics A: Materials Science and Processing*, 76, 2003.

[56] K. t. Leung, L. Jzsa, M. Ravasz, and Z. Nda. Spiral cracks without twisting. *Nat Mater*, 410, 2001.

[57] Z. Néda, K. t. Leung, L. Józsa, and M. Ravasz. Spiral cracks in drying precipitates. *Phys. Rev. Lett.*, 88, 2002.

[58] A. A. Griffith. The phenomena of rupture and flow in solids. *Philosophical Transactions of the Royal Society of London*, Dec 1921.

[59] F Erdogan and GC Sih. On the crack extension in plates under plane loading and transverse shear. *ASME, TRANSACTIONS, J. of Basic Engng*, 85:519–527, 1962.

[60] B. Roman, P. M. Reis, B. Audoly, S De Villiers, V Vigui, and D Vallet. Fissure oscillantes dans les feuilles minces / oscillatory fracture paths in thin elastic sheets. *C.R. Mcanique*, 331, 2003.

[61] L. B. Freund. *Dynamic Fracture Mechanics*. Cambridge University Press; 1st PAPERBACK edition, 1998.

[62] D'Arcy W. Thompson. *On growth and form. Vol. 1*. Cambridge : University Press ; New York : Macmillan, 1945.

[63] C.M. Muscat-Fenech and A. G. Atkins. The effect of anisotropy in fracture toughness and yield strength in the tearing of ductile sheet materials. *International Journal of Mechanical Sciences*, 36, 1994.

[64] A. Chambolle, G. A. Francfort b, and J. J. Marigo. When and how do cracks propagate? *J. Mech. Phys. Solids*, 57, 2009.

[65] V. Hakim and A. Karma. Crack path prediction in anisotropic brittle materials. *Physics Review Letters*, 2005.

[66] C. Gurney and Y. W. Mai. Stability of cracking. *Engineering Fracture Mechanics*, 4:853–863, 1972.

[67] J. Leblond. *Mécanique de la rupture fragile et ductile*. Hermes Science publicatons, 2003.

[68] R. V. Goldstein and R. L. Salganik. Brittle fracture of solids with arbitrary cracks. *Int. J. Fract.*, 10:507–523, 1974.

[69] K. J. Miller and D. L. McDowell. *Mixed-Mode Crack Behavior*. Mc Graw-Hill, New York, 1999.

[70] M. Marder. Craks cleave crystals. *Europhysics Letters*, 2004.

Appendix A

Résumé Français

A.1 Introduction

En accomplissement avec ce qui est requis par la convention signée par l'Université Pierre et Marie Curie et l'Université Santiago du Chili, dans le présent chapitre nous présentons un résumé en français de ce travail de thèse.

Cette thèse se focalise en examiner deux expériences de ruptures des plaques élastiques minces. Les plaques minces sont des objets tridimensionnels avec une de leurs dimensions (épaisseur t) beaucoup plus petite qui les autres deux. Ces objets montrent une grande variété de phénomènes d'intérêt suprême associés à la manière par laquelle ils peuvent être déformés, ainsi il ya des exemples comme "wrinkling", "crumpling", "folding", ou "creasing". L'entendement de ces phénomènes a pris de longues années et seulement dans les dernières décennies ont été obtenu consolider les bases mathématiques et conceptuelles pour son étude.

En particulier, la rupture de ces objets est encore un problème en développement permanent à auquel ne lui a pas pu être donnée une solution formelle complète. Il

existe une grande variété d'études faites dans ce sujet, dont, dans l'introduction du notre texte central, on décrit certains ([41, 46, 47, 50]) où il attire particulièrement l'attention la recherche de règles qui permettent de comprendre la direction que la rupture suit quand elle est forcé à propager. Dans ce cadre est que ce travail de thèse est développé et prétend être un apport à l'entendement du processus de rupture des plaques minces.

Les expériences présentées dans ce travail sont des expériences faites dans matériaux fragiles et développe en une configuration de charge quasi statique. Suite à deux configurations de charge différant nous obtenons deux familles de spirales logarithmiques suprêmement régulières et reproductibles.

La première expérience consiste en une rupture qui croît depuis une petite incision initiale. Dans ce cas la rupture est forcée à propager au moyen de pousser toujours le même bord de la plaque mince. Suite à cette procédure une trajectoire sous forme de grande spirale est rapidement obtenue. Le chapitre 2 nous décrit diverses expériences qu'ils nous permettent de caractériser et de modeler la trajectoire obtenue. La caractérisation de la trajectoire finale de la rupture résulte dans que la forme finale est en effet une spirale logarithmique, ce résultat est expliqué à partir d'un modèle qu'elle se base en la théorie classique de rupture et le critère du "Maximum du taux de restitution de lénergie". De la forme finale du crack il est possible d'extraire information qui concerne au processus de rupture, et nous avons trouvé qui il est possible d'observer une relation entre la direction de la rupture dans chaque moment et l'anisotropie du matériel. Bien que nous n'ayons pas pu le valider, nous présentons un modèle qui permettrait d'étendre le critère du"Maximum du taux de restitution de lénergie" à des situations où le matériel est anisotrope.

Dans une deuxième expérience nous présentons une autre façon de produire une spirale logarithmique, dans le chapitre il est présenté une procédure qui est commencé depuis une simple configuration qui consiste à couper, loin des bords, un petit secteur circulaire de la plaque et à travers du périmètre de cette zone circulaire nous faisons une petite entaille. Comme résulté, à l'intérieur de la plaque et loin des ses bords, on produit une languette qui est tirez perpendiculairement au plan qui contient au film. Dans ce cas la déformation qui guide la rupture est compliquée de caractériser et par conséquent n'a pas été possible à établir un modèle, depuis des premiers principes, mais il est possible de trouver une relation géométrique que nous a permis toutefois d'estimer comme il se comporte la force requise pour tirez la plaque par rapport à l'énergie requise pour propager la rupture. Cette expérience montre un système de grande complexité, être tiré la lame celle-ci est déformée hors du plan en produisant des structures suprêmement intéressantes, puisque ce travail se focalise à l'étude de ruptures, ces structures hors du plan sont seulement analysé qualitativement et on laisse ouverte l'étude quantitative de ce phénomène.

A.2 Chapitier 2

Dans le chapitre 2 on décrit les conditions dans lesquelles sont menées à bien les expériences qui produisent des ruptures sous forme de spirales logarithmiques de grande taille. Au moyen du suivi de l'outil utilisé pour pousser le bord de la plaque mince et la comparaison des spirales résultantes de cette expériences, nous avons démontré que les spirales produites sont indépendantes de la vitesse et le mouvement de l'outil, ceci pourvu qu'on respecte une seule règle dans la procédure, toujours pousser le même bord".

Pour comprendre cette régularité, nous avons isolé la manière dans laquelle on nourrit d'énergie la rupture. Une simple expérience dans laquelle un bord est poussé au centre, nous a permis de démontrer que l'énergie dans le système a la forme:

$$U_E = 0.0076 E t L^2 \alpha^{3.5} \tag{A.1}$$

Où E c'est le module de Young, t est l'épaisseur et α est l'angle d'indentacin décrit dans la Fig. 2.7. Une seconde expérience nous a permis d'étendre ce résultat pour le cas où l'outil ne pousse pas dans le centre, avec cette expérience nous avons confirmé que la forme de la énergie élastique est:

$$U_E = a E t L^2 \alpha^{3.5} \tag{A.2}$$

Il est important de souligner que cette expression, étant linéaire avec E et t, rend compte que le processus de rupture est déterminé par lénergie de stretching", ce résultat est important puisqu'il nous permet d'avoir une idée de quel est la déformation qui souffre la plaque.

Une fois que nous avons trouvé cette expression pour l'énergie dans le système, nous avons développé un modèle qui nous permet, à partir des caractéristiques

géométriques du système, trouver les paramètres de la rupture, le seuil de rupture et la direction de la rupture. Pour ceci nous avons utilisé le critère de Griffith et le critère de Maximum du taux de restitution de lénergie". Comme résultat notre modèle prédit que la rupture est caractérisée par :

$$\alpha_c = \left(\frac{\gamma}{3.5aEL}\right)^{0.4} \tag{A.3}$$

$$\beta = \frac{\pi}{2} + 0.4\alpha_c \tag{A.4}$$

Où α_c c'est la valeur critique de l'angle indentation et β définit la direction de propagation du crack.

En faisant des mesures de l'angle dans un système dans lequel on pousse le bord pour différentes distances L (voir Fig .2.13(a)) nous avons trouvé quil est compatible avec notre loi de puissance pour l'énergie élastique dans le système.

Ayant trouvé ces expressions pour les paramètres du processus de rupture, nous renversons notre effort en comprendre comme à partir d'ici nous pouvons expliquer la trajectoire finale de la rupture sous forme de spirale.

On observe trois étapes pour l'évolution de la spirale. Les deux premières étapes correspondent à des spirales centrées des points fixes qui concident avec les deux extrémités de l'incision initiale. Une troisième étape se caractérise par une spirale qui croît de manière auto semblable. Puisque c'est celle qui contrle la plus grande partie de la propagation de la trajectoire de la rupture, cette troisième étape est suprêmement importante, est par ceci que nous avons calculé comme on comporte la spirale résultante en ce qui concerne le paramètre de propagation β. Nous avons obtenu une relation qui nous dit que montre que ce processus produit une spirale logarithmique.

Pour garantir ces affirmations nous avons produit un simple algorithme qui recrée

la croissance de la spirale et comparer avec la trajectoire de la rupture obtenue dans notre expérience. On montre, à partir de mesures faites sur les spirales expérimentales et la simulation, une compatibilité complète dans des termes des caractéristiques géométriques de la forme finale de la rupture. Pour effectuer ces mesures on a utilisé deux méthodes différentes entre les spirales expérimentales et celle obtenue au moyen de la simulation, les deux méthodes sont détaillées et on explique la raison d'utiliser chacun dans chaque cas.

Un résultat suprêmement intéressant est que si bien en moyenne le comportement de la forme finale de la rupture soit celui d'une spirale logarithmique, ils existent oscillations locales dans la valeur de l'angle de rupture β. Ces oscillations ont été caractérisées et en particulier sa périodicité π, cette résultat nous indique qui les oscillation sont mis en rapport avec l'anisotropie du matériel.

Pour renforcer cette supposition nous présentons une expérience faite avec un matériel beaucoup plus anisotrope que celui utilisé le long des expériences précédentes. Nous avons reproduit la même procédure dans ce matériel, et on obtient une manière semblable à une spirale mais où on peut clairement remarquer l'incidence de l'orientation dans la direction de la rupture. Bien que la forme de la spirale ne soit pas lisse, il est possible de répéter les mesures géométriques sur le forme résultant, et nous avons trouvé qu'en moyenne il est comporté aussi comme une spirale logarithmique. Plus encore en mesurant l'angle de propagation de la rupture nous avons récemment trouvé une oscillation avec la même périodicité π, mais maintenant avec une ampleur deux fois plus grande que dans le cas avec le matériel moins anisotrope.

En utilisant des arguments qui nous paraissent naturels, nous présentons une relation qui rend compte de comment l'angle β se devrait comporter quand le

matériel est anisotrope. Cette relation dit simplement qu'il existe une concurrence entre libérer tant d'énergie élastique comme elle est possible au moyen de propager de la rupture et la fragilité du matériel dans une direction déterminée. Comme résultat une simple expression est présentée.

Bien que nous soyons suprêmement confiants de qui cette relation caractérise le processus de rupture pour un matériel anisotrope, les expériences que nous avons effectuées pour la démontrer n'ont pas été concluantes, plus encore les résultats obtenus sont contradictoires avec la physique derrière la relation proposée. Il est par ceci que nous ne pouvons pas conclure rien à ce sujet d'une relation quantitative entre l'oscillation de l'angle β et l'anisotropie du matériel.

Toutefois, nous sommes confiants de que avec des expériences plus détaillées avec un meilleur échantillonnage et précision nous pourrons vérifier la relation proposée.

A.3 Chapitre 3

Inspirés pour la spirale obtenue dans le chapitre 2 et des résultats obtenus dans le travail de Hamm et al. [50], nous avons développé une expérience dans laquelle nous tirons perpendiculairement une languette formée dans un plaque mince et qui produit une spirale logarithmique. Pour pouvoir mener à bien cette expérience il est nécessaire de créer une configuration initiale spéciale dans le sens que produit de que nous tirons la languette le système permet que seulement un crack puisse propager. La plus simple configuration consiste en décaler une petite zone circulaire de matériel et faire une petite entaille à travers son périmètre, avec ceci on obtient que le stress, produit de tirer la languette résultante, soit focalisé jus quen un point.

En tirant cette languette rapidement une rupture sous forme de spirale est formée. Cette spirale croît de manière très semblable à la manière auto-semblable laquelle croît la spirale du chapitre 2 dans se troisième étape de formation. Récemment comme il faut être attendu nous voyons que la caractérisation géométrique de la forme finale de la spirale est celle d'une spirale logarithmique, mais maintenant elle croît un peu plus lent. L'angle de propagation de la rupture est en moyenne plus petit que celui de la spirale obtenue dans le chapitre 2. En comparant les deux ruptures finales nous voyons qu'il existe une similitude claire, mais un peak secondaire étrange est observé, toutefois que nous nayons pas une explication claire pour ceci.

Pour pouvoir comprendre le processus de rupture nous avons construit un assemblage qui nous permet d'accéder à l'information de la force requise pour propager la rupture. Nous avons trouvé que bien qu'étant strictement constant, elle est

délimitée malgré la croissance du système.

Au moyen de simples rapprochements, nous avons pu trouver une expression qui nous permet de voir que la force requise pour propager la rupture est nécessairement plus grande que la quantité γt quil caractérise le propagation de la rupture. Ceci est exprimé dans la relation :

$$F = 3.29\gamma t \tag{A.5}$$

Où F est la force pour tirer, γ est l'énergie de rupture et t est l'épaisseur de la plaque. Cette expression nous donne à comprendre que le système n'est pas efficace puisqu'on requiert davantage de force pour casser de cette manière que celle qui serait simplement requise par exemple en propageant le crack de la manière présentée dans le travail de Hamm et al. [50]. Toutefois, bien que ce soit une trajectoire divergente qui croît exponentiellement, le fait que la force soit maintenue délimitée, donne beaucoup de potentiel pour son utilisation dans l'industrie d'empaquetage de produits. Il est par ceci que nous avons décidé de breveter les conditions initiales qui produit une trajectoire de ces caractéristiques. Le brevet correspondant est présenté dans l'appendice D.

Dans la partie finale du chapitre 3 nous présentons une discussion sur les conditions géométriques initiales qui doivent être satisfaites pour que la trajectoire finale de la rupture se développe à succèsment comme spirale divergente et ne soient pas produite ruptures secondaires qui font que la trajectoire converge comme elle arrive dans le travail de Hamm et al. [50]. Nous montrons finalement le type de structures, semblables à celles observées dans “crumpling”, qui se pendant le processus de on tirer.

Appendix B

Resumen Español

B.1 introducción

En cumplimiento con lo requerido por el convenio firmado por l'Université Pierre et Marie Curie y la Universidad de Santiago de Chile, en el presente capítulo presentamos un resumen en castellano de este trabajo de tesis.

La tesis se enfoca en discutir dos experimentos de fracturas en láminas delgadas. Las láminas delgadas son objetos tridimensionales con una de sus dimensiones (espesor t) mucho mas pequeñna que las otras dos. Estos objetos muestran una gran variedad de fenómenos de sumo interés asociados a la manera en que se pueden deformar, así tenemos ejemplos como "wrinkling, "crumpling, "folding, o "creasing. El entendimiento de estos fenómenos ha tomado largos años y solamente en las últimas décadas se han logrado consolidar las bases matemáticas y conceptuales para su estudio.

En particular la fractura de estos objetos es aún un problema en permanente desarrollo al que no se le ha podido dar una solución formal completa. Existe una gran variedad de estudios hechos en este tema, de los cuales, en la introducción

del texto central, se describen algunos ([41, 46, 47, 50]) donde llama particularmente la atención la búsqueda de reglas que permitan comprender la dirección que la fractura sigue cuando es forzada a propagar. En este marco es que este trabajo de tesis se desarrolla y pretende ser un aporte al entendimiento del proceso de fractura de las láminas delgadas.

Los experimentos presentados en este trabajo son experimentos hechos en materiales frágiles y en una configuración de carga cuasi-estática. Como resultado de dos configuraciones de carga obtenemos dos familias de espirales logarítmicas sumamente regulares y reproducibles.

El primer experimento consiste en una fractura que crece desde una pequeña incisión inicial. En este caso la fractura es forzada a propagar por medio de empujar un borde de la lámina. Como resultado de este procedimiento una trayectoria en forma de una gran espiral es obtenida rápidamente. A lo largo del capitulo 2 describimos diversos experimentos que nos permiten caracterizar y modelar la trayectoria obtenida. La caracterización de la trayectoria final de la fractura resulta en que la forma final de la espiral obtenida es logarítmica, forma que es explicada a partir de un modelo que se basa en la teoría clásica de fractura y el criterio de “Maximum Energy release rate. De la forma final del crack es posible extraer información respecto al proceso de fractura, y hemos encontrado evidencia a que es posible observar una relación entre la dirección de la fractura en cada instante y la anisotropía del material. A pesar de que no hemos podido validarlo, presentamos un modelo que permitiría extender el criterio de “Maximum Energy Release Rate a situaciones en que el material es anisotrópico.

En un segundo experimento presentamos otra forma de generar una espiral logarítmica, en el capítulo 3 se presenta un procedimiento que se inicia desde una simple con-

figuración que consiste en cortar, lejos de los bordes, un pequeño sector circular de la lámina y através del perímetro de este zona circular hacer un corte. Como resultado al interior de la lámina y lejos de los bordes se genera una lengüeta que se puede tirar perpendicularmente al plano que contiene a la lámina. En este caso la deformación que guía la fractura es mas complicada de caracterizar y por lo tanto no ha sido posible establecer un modelo desde primeros principios, sin embargo una relación geométrica nos ha permitido estimar como se comporta la fuerza requerida para tirar la lámina en relación a la energía requerida para propagar el crack. Este experimento muestra un sistema de gran complejidad, al ser tirada la lámina esta se deforma fuera del plano produciendo estructuras sumamente interesantes, puesto que este trabajo se enfoca al estudio de fracturas estas estructuras fuera del plano son solamente analizadas cualitativamente y se deja abierto el estudio cuantitativo de este fenómeno.

B.2 Capitulo 2

En el capitulo 2 se describe las condiciones en las que son llevados a cabo los experimentos que producen fracturas en forma de espirales logarítmicas de gran tamaño. Por medio del seguimiento de la herramienta usada para empujar el borde de la lámina y la comparación de las espirales resultantes hemos logrado demostrar que este las espirales generadas son independientes de la velocidad y el movimiento de la herramienta, esto siempre y cuando se respete una única regla en el procedimiento, siempre empujar el mismo borde.

Para lograr entender esta regularidad hemos aislado la forma en que se alimenta de energía la fractura. Un simple experimento en que un borde es empujado al centro, nos ha permitido demostrar que la energía en el sistema es de la forma:

$$U_E = 0.0076EtL^2\alpha^{3.5} \tag{B.1}$$

Donde E es el módulo de Young, t es el espesor y α es el ángulo de indentación descrito en la Fig. 2.7. Un segundo experimento nos ha permitido extender este resultado para el caso en que la herramienta no empuja en el centro, esto nos da pie para escribir la energía elástica del sistema de la forma:

$$U_E = aEtL^2\alpha^{3.5} \tag{B.2}$$

Es importante destacar que esta expresión, al ser lineal con E y con t, da cuenta de que el proceso de fractura esta siendo llevado por energía de “stretching, este resultado es importante dado que nos permite tener una idea de cual es la deformación que esta sufriendo la lámina.

Una vez encontrada esta expresión para la energía en el sistema hemos desarrollado un modelo que nos entrega a partir de las características geométricas

del sistema, los parámetros de la fractura, umbral de fractura y dirección de la fractura. Para esto hemos usado el criterio de Griffith y el criterio de "Maximum Energy Release Rate. Como resultado nuestro modelo predice que la fractura esta caracterizada por:

$$\alpha_c = \left(\frac{\gamma}{3.5aEL}\right)^{0.4} \tag{B.3}$$

$$\beta = \frac{\pi}{2} + 0.4\alpha_c \tag{B.4}$$

donde $alpha_c$ es el valor crítico del ángulo de indentación y β define la dirección de propagación del crack.

Haciendo mediciones del ángulo α_c en un sistema en que se empuja el borde a distintas distancia L (ver Fig .2.13(a)) hemos encontrado es compatible con nuestra ley de potencia $\alpha^{3.5}$ para la energía elástica en el sistema.

Habiendo encontrado estas expresiones para los parámetros del proceso de fractura, volcamos nuestro esfuerzo en entender como a partir de aquí podemos explicar la trayectoria final de la fractura en forma de espiral.

Se observan tres etapas para la evolución de la espiral. Las dos primeras etapas corresponden a espirales centradas en puntos fijos que coinciden con los dos extremos de la incisión inicial. Una tercera etapa se caracteriza por una espiral que crece de forma auto-similar. Puesto que es la que controla la mayor parte de la propagación de la trayectoria de la fractura, esta tercera etapa es sumamente importante, es por esto que hemos calculado como se comporta la espiral resultante respecto del parámetro de propagación β. Hemos obtenido una relación que nos dice que nos muestra que este proceso auto similar en efecto genera una espiral logarítmica.

Para garantizar estas afirmaciones hemos generado un simple algoritmo que

recrea el crecimiento de la espiral y comparar con la trayectoria de la fractura obtenida en nuestro experimento. Se muestra, a partir de mediciones hechas sobre las espirales experimentales y la simulación, una completa compatibilidad en términos de las características geométricas de la forma final de la fractura. Para realizar estas mediciones se usaron dos métodos diferentes entre las espirales experimentales y la obtenida por medio de la simulación, ambos métodos son detallados y se explica la razón de usar cada uno en cada caso.

Un resultado sumamente interesante es que a pesar de que en promedio el comportamiento de la forma final es el de una espiral logarítmica, existen oscilaciones locales en el valor del ángulo de fractura β. Estas oscilaciones han sido caracterizadas y en particular su periodicidad π nos indica que se relacionan con la anisotropía del material.

Para corroborar esta suposición presentamos un experimento hecho con un material mucho mas anisotrópico que el usado a lo largo de los experimentos anteriores. Como resultado de reproducir en este material el mismo procedimiento, se obtiene una forma semejante a una espiral pero donde se puede notar claramente la incidencia de la orientación en la dirección de la fractura. A pesar de que la forma de la espiral no es suave, es posible repetir las mediciones geométricas sobre esta forma final, y sorprendentemente hemos encontrado que también en promedio se comporta como una espiral logarítmica. Mas aún al medir el ángulo de propagación de la fractura hemos encontrado nuevamente una oscilación con la misma periodicidad π pero ahora con una amplitud dos veces mas grande que en el caso menos anisotrópico.

Usando argumentos que nos parecen naturales presentamos una relación que da cuenta de cómo se debería comportar el ángulo β cuando el material es

anisotrópico. Esta relación simplemente argumenta que existe una competencia entre liberar tanta energía elástica como sea posible por medio de propagar la fractura y cuanto cuesta romper el material en una dirección dada. Como resultado una simple expresión es presentada.

A pesar de que estamos sumamente confiados de que esta relación es congruente con el proceso de fractura, los experimentos que hemos realizado para demostrarla no han sido concluyentes, más aún los resultados obtenidos son contradictorios con la física detrás de la relación propuesta. Es por esto que no podemos concluir nada al respecto de una relación cuantitativa entre la oscilación del ángulo β y la anisotropía del material. Sin embargo estamos confiados de que con experimentos mas detallados con mejor muestreo y precisión podremos comprobar la relación propuesta.

B.3 Capítulo 3

Inspirados en la espiral obtenida en el capítulo 2 y en resultados obtenidos en el trabajo de Hamm et al. [50], hemos desarrollado un experimento en que al tirar una lengüeta formada en la lámina delgada se genera una espiral logarítmica. Para poder llevar a cabo este experimento es necesario crear una configuración inicial conveniente en el sentido de que al producirse el tirado solamente un crack pueda propagar. La mas simple configuración consiste en una en remover una pequeña zona circular de material y hacer un corte através de su perímetro, con esto se consigue que el stress, producido al tirar la lengüeta resultante, se focalice solamente en el extremo del corte inicial.

Al tirar esta lengüeta al rápidamente se forma una fractura en forma de espiral. Esta espiral crece de manera muy similar a la forma auto-similar en que crece la espiral del capítulo refchap:spiral1 en la tercera etapa. Nuevamente como es de esperarse vemos que la caracterización geométrica de la forma final de la espiral es la de una espiral logarítmica pero ahora crece un poco mas lento. El ángulo de propagación de la fractura es en promedio menor que el de la espiral obtenida en el capítulo refchap:spiral1. Al comparar ambos resultados vemos que existe una clara similitud, sin embargo un extraño Peak secundario se observa sin que tengamos una explicación clara para esto.

Para poder entender el proceso de fractura hemos construido un montaje que nos permite acceder a la información de la fuerza de tirado requerida para propagar la fractura. Hemos encontrado que a pesar de no ser estrictamente constante, se mantiene acotada a pesar del crecimiento del sistema.

Por medio de simples aproximaciones, hemos podido encontrar una expresión

que nos permite ver que la fuerza requerida para propagar la fractura necesariamente es mas grande que la cantidad γt que caracteriza la propagación de la fractura. Esto esta expresado en la relación:

$$F = 3.29\gamma t \tag{B.5}$$

Donde F es la fuerza de tirado, γ es la energía de fractura y t es el espesor de la lámina. Esta expresión nos da a entender que el sistema no es eficiente puesto que se requiere mas fuerza para romper de esta manera que la que simplemente se requeriría por ejemplo propagando el crack de la forma presentada en el trabajo de Hamm et al. [50]. Sin embargo, a pesar de que es una trayectoria divergente que crece exponencialmente, el hecho de que la fuerza se mantenga acotada le da un potencial importante para su uso en la industria de empaquetamiento de productos. Es por esto que hemos decidido patentar las condiciones iniciales que generan una trayectoria de estas características. La correspondiente patente se presenta en el apéndice D.

En la parte final del capítulo 3 presentamos una discusión sobre las condiciones geométricas iniciales que se deben satisfacer para que la trayectoria final de la fractura se desenvuelva exitosamente como una espiral divergente y no se generen fracturas secundarias que hagan que la trayectoria converja como sucede en el trabajo de Hamm et al. [50].

Finalmente mostramos el tipo de estructuras, similares a las observadas en crumpling, que se prooducen durante el proceso de tiraje.

Appendix C

Basics Notions in Fracture and Elasticity Theories of Thin Sheets

C.1 Elasticity

C.1.1 Elemental Relations in Elasticity

When self equilibrating forces act on an object, it deforms, producing a change in the coordinates, x_i, of each material point. This deformation is characterized by a relative displacement, u_i, which establishes how much the coordinates change from their original positions. Of course, if the points of the object move, there is associated change in the distances between different points, which is described by the strain, ϵ_{ij}. Consider a deformed body, because of the deformation a distribution of forces, T_i is produced through the object. This distribution of forces are a consequence of a stress field, σij, and connected by the relation $T_i = \sigma_{ij} n_j$, where n_j is the normal to the j-face of the infinitesimal volume (i and j are subindexes representing the respective spatial components, so $i, j = 1, 2, 3$)

The derivation of the relation that connects displacement and strain is straightforward, and can be found in many elasticity textbooks [2]. This is:

$$\epsilon_{ij} = \frac{1}{2}\left(\frac{\partial u_i}{\partial x_j} + \frac{\partial u_j}{\partial x_i} + \frac{\partial u_i}{\partial x_i}\frac{\partial u_j}{\partial x_j}\right) \tag{C.1}$$

In linear elasticity the last term in Eq. C.1 is neglected, so the equation becomes:

$$\epsilon_{ij} = \frac{1}{2}\left(\frac{\partial u_i}{\partial x_j} + \frac{\partial u_j}{\partial x_i}\right) \tag{C.2}$$

The relation between strain and stress is constitutive and depends on the kind of system being described. In linear elasticity Hookes law is used to describe elastics bodies, Which in tensorial shape has the form:

$$\sigma_{ij} = C_{ijkl}\epsilon_{kl} \tag{C.3}$$

Where C_{ijkl} is the elastic tensor. This is a tensor of fourth order with 81 elements. However not all the elements are independent. For example this matrix has the properties $C_{ijkl} = C_{klij} = C_{jikl} = C_{ijlk}$. which reduce the number of independent elements considerably. Depending on material symmetries, the elastic tensor can be reduced even more, but at some point it is necessary to do experiments to find the irreducible elements.

Finally, since the external forces are at equilibrium, the internal stress must be balanced for every volume element in the object, this is expressed by:

$$\frac{\partial \sigma_{ij}}{\partial x_j} = 0 \tag{C.4}$$

This set of equations is the foundation of the theory of elasticity. With this tool it is possible to understand many problems where bodies are been deformed by balanced external loads.

C.1.2 Energy Storage in Thin Sheets

We assume the internal energy in a system is a function of the strain, ϵ_{ij}, this is, $U = U(\epsilon_{ij})$, we can expand this quantity around the minimum of energy, which occurs when $\epsilon_{ij} = 0$. This is:

$$U = U_o + \frac{\partial U}{\partial \epsilon_{ij}} + \frac{1}{2}\frac{\partial^2 U}{\partial \epsilon_{ij}\partial \epsilon_{lk}}\epsilon_{ij}\epsilon_{lk} \tag{C.5}$$

At the minimum $\partial U/\partial \epsilon_{ij} = 0$. Thus we have:

$$U = U_o + \frac{1}{2}\frac{\partial^2 U}{\partial \epsilon_{ij}\partial \epsilon_{lk}}\epsilon_{ij}\epsilon_{lk} \tag{C.6}$$

We know that the work done by the external forces to the body is transformed in strain energy, this implies that $\sigma_{ij} = \partial U/\partial \epsilon_{ij}$, comparing this to Eq. C.3 we obtain:

$$U = U_o + C_{ijkl}\epsilon_{ij}\epsilon_{lk} \tag{C.7}$$

Depending on the symmetries of the material, the number of independent components in the elastic matrix C_{ijkl} could be reduced considerably. Their values are obtained by comparing the stress-strain relation with experiments. In particular for isotropic materials, it is possible to simplify the stress-strain expression in:

$$\sigma_{ij} = \frac{E}{(1+\nu^2)}((1-\nu)\epsilon_{ij} + \nu\delta_{ij}Tr\,(\epsilon) \tag{C.8}$$

Where E is the Young's modulus, and ν is the coefficient of Poison.

Finally the energy is given by multiplying Eq. C.10 by ϵ_{ij}. This results in:

$$U = \frac{E}{2(1+\nu^2)}((1-\nu)\epsilon_{ij}^2 + \nu\delta_{ij}Tr^2\,(\epsilon)) \tag{C.9}$$

This equation can be expressed in the form:

$$U = \frac{E}{2(1+\nu^2)}\left\{\frac{(1-\nu)}{2}[Tr^2(\epsilon) - 4\mathsf{det}(\epsilon)] + \frac{(1-\nu)}{2}Tr^2(\epsilon)\right\} \tag{C.10}$$

If we want the energy stored in the system it is necessary to integrate this volume density of energy over the volume. In particular, if the body is a thin plate, meaning small thickness (t), for an in-plane deformation, the integration through the thickness is trivial and it is:

$$U_{\mathcal{S}} = \frac{Et}{2(1+\nu^2)} \int_{\mathcal{A}} \left\{ \frac{(1-\nu)}{2} [Tr^2(\epsilon_{\mathcal{S}}) - 4\text{det}(\epsilon_{\mathcal{S}}] + \frac{(1-\nu)}{2} Tr^2(\epsilon_{\mathcal{S}}) \right\} dxdy \quad \text{(C.11)}$$

Another possible deformation is related to pure bending. In this case, the integration of the volume density energy trough the thickness results:

$$U_{\mathcal{B}} = \frac{Et^3}{2(1+\nu^2)} \int_{\mathcal{S}} \left\{ (\kappa_1 + \kappa_2)^2 - 2(1-\nu)\kappa_1\kappa_2 \right\} d\mathcal{S} \quad \text{(C.12)}$$

Where κ_1 and κ_2 are the gaussian curvatures describing the out of plane deformation of the body.

The difference between both integration process is in the dependency in the thickness coordinate, for in-plne deformation the energy does not depend on it, in contrast with the bending deformation where the energy does depends in the thickness.

For any given configuration, it is possible to write the strain as the sum of a strain producing bending ($\epsilon_{\mathcal{B}}$) and a strain producing stretching ($\epsilon_{\mathcal{S}}$), the term $Tr^2(\epsilon)$ is now $(Tr(\epsilon_{\mathcal{S}}) + Tr(\epsilon_{\mathcal{B}}))^2$. The cross term resulting from this, $2Tr(\epsilon_{\mathcal{S}})Tr(\epsilon_{\mathcal{B}})$, depends in the thickness direction in an even power, this implies $\int_{-t/2}^{t/2} 2Tr(\epsilon_{\mathcal{S}})Tr(\epsilon_{\mathcal{B}}) = 0$. The same analysis with the term $4\text{det}(\epsilon)$ yields the condition where the total energy in the system can be written as the sum of the bending and stretching contributions:

$$U = U_{\mathcal{S}}(t) + U_{\mathcal{B}}(t^3) \quad \text{(C.13)}$$

C.2 Fracture Mechanics

C.2.1 Fracture Modes

Consider a body with a crack on it, the stress at the crack tip can be separated as the combination of the three modes illustrated in Fig. C.1.

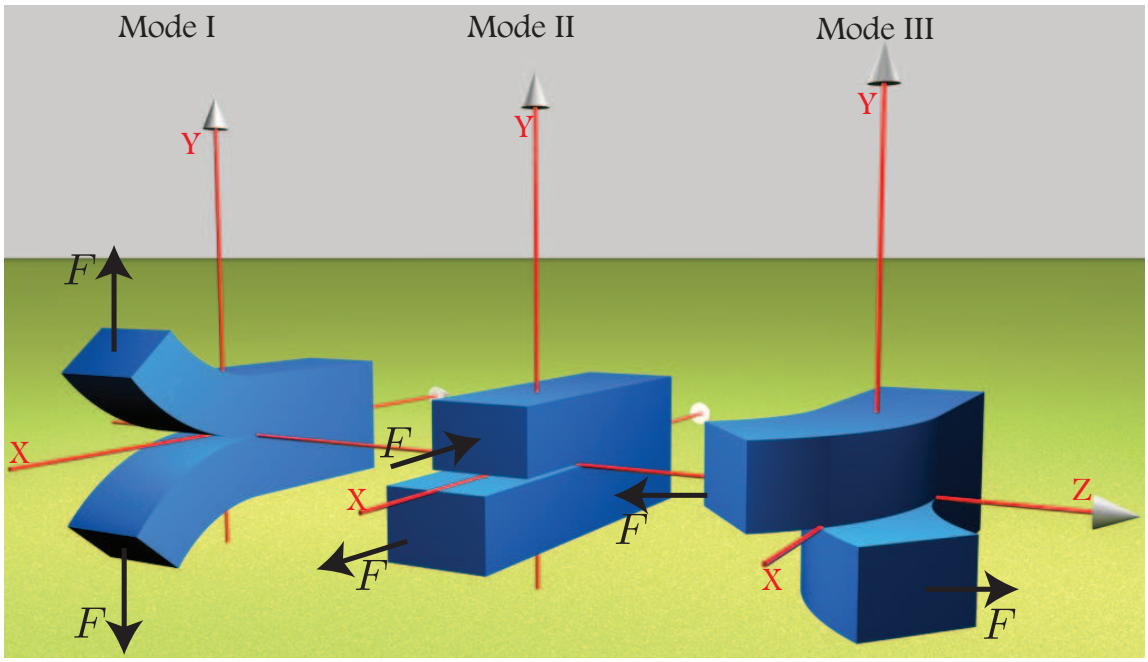

Figure C.1: *Possible modes for fracture propagation.*

1. Mode I: the surfaces of the crack are separated symmetrically with respect to the planes xy and xz.

2. Mode II: the surfaces of the crack slide in opposite direction with respect to each other, without losing their symmetry with respect to the plane xy.

3. Mode III: the surfaces of the crack slide in opposite directions, breaking the symmetry with respect to the planes xy and xz.

It is possible to demonstrate that at the crack tip, the stress diverges as $1/\sqrt{r}$, where r is the radial coordinate of a polar system with origin in the crack tip.

The form of the stress for each of the modes is given by the expressions:

Mode I

$$\lim_{r\to 0}\sigma_{ij}^{I} = \frac{K_I}{\sqrt{2\pi r}} f_{ij}^{I}(\theta) \tag{C.14}$$

Model II

$$\lim_{r\to 0}\sigma_{ij}^{II} = \frac{K_I}{\sqrt{2\pi r}} f_{ij}^{II}(\theta) \tag{C.15}$$

Model III

$$\lim_{r\to 0}\sigma_{ij}^{III} = \frac{K_I}{\sqrt{2\pi r}} f_{ij}^{III}(\theta) \tag{C.16}$$

Where the functions $f_{ij}^{I}(\theta)$,$f_{ij}^{II}(\theta)$ and $f_{ij}^{III}(\theta)$ are related to the geometrical configuration of the system, and the three quantities K_I, K_{II}, and K_{III} are the intensity factors and their physical meaning is how much the stress applied to the body is been amplified because of the presence of the crack. For example, for a plate with a crack of size $2a$ with a load at infinity with uniform tension σ_y, the intensity factor is given by $K_I = \sigma\sqrt{(a\pi)}$.

In a mixed mode problem, it is possible that individual contributions are additive, so the total stress is $\sigma_{ij}^{total} = \sigma_{ij}^{I} + \sigma_{ij}^{II} + \sigma_{ij}^{III}$.

In this framework, a critical stress intensity is defined, K_{Ic} or K_{IIc} or K_{IIIc}, so when the intensity factor reaches this value, the crack propagates.

This approach is very useful in engineering applications, where it is possible to distinguish the corresponding modes of deformation. However, in thin sheets it is very complicated to apply this methodology since the fracture process occurs with a large complex deformation.

C.2.2 Griffith Criteria

The approach made by Griffith is in terms of the balance of the participating energies in the system. If we do not include plasticity, the energies involved are related to the work performed by an external load W,the elastic energy stored as strain in the system U_E, and the surface energy related to the crack surface, U_s. Hence, the total energy is:

$$U = \Pi + U_s \tag{C.17}$$

Where $\Pi = U_s - W$.

By considering the moment of fracture as a position of equilibrium, when the crack increases its surface in dA, the energy in the system must be minimal:

$$\frac{dU}{dA} = \frac{d\Pi}{dA} + \frac{dU_s}{dA} = 0 \tag{C.18}$$

The quantity $-d\Pi/dA$ is called the energy release rate and corresponds to the amount of energy transformed into the new surface. The surface energy is proportional to the change of the area of the crack. The factor of proportionality is defined as fracture energy.

C.2.3 Brittle, Quasi-static Crack Propagation, Stable

Depending on the material properties, we can classify two kinds of fracture. Ductile fracture is associated with large permanent deformation. In this case the high stress near the crack tip induces plastic deformation of a wide zone of the material. Thus, it requires a high level of energy because of plastic deformation and the crack must be fed. This kind of crack usually occurs at low velocity. A second

kind is brittle fracture, the concentration of stress at the crack tip produces a very small zone of plastic deformation, the amount of work given to the system is stored or converted into crack surface, and a very low amount of energy is dissipated. Hence, this kind of fracture occurs with a low amount of energy. With unstable configurations of loading, the crack propagates at high velocities.

Fracture classification not only depends on material properties, but also on the way in which stress is distributed in the system. If the loading driving the fracture process varies abruptly or the crack grows rapidly, stress waves propagate through the material. In this case, the fracture process is in a dynamic phase and a portion of work applied to the system is converted into kinetic energy. The formalism used to model dynamic fracture is based on elastodynamics and includes inertial effects, rate-dependent material behavior and reflected stress waves. In the present work we do no include dynamic effects and focus on experiments in a quasi-static phase where the kinetic energy due to inertial effects in the system is negligible.

One final idea is needed to understand the systems presented in this work, namely the stability of the fracture process. We present here a simplified explanation for the condition of stability. As we showed in the previous section, the condition for crack propagation is given by the minimization energy in the system, which leads to $d\Pi/dA = -dU_s/dA$, where $\Pi = U_E - W$, and U_E is the strain energy, and W is the work of the external load configuration). If we set a configuration with a controlled load, meaning that external loading is constant, for some critical values of the load, the crack propagates and consequently the load works. The work performed by the external load feeds the system with more energy, and the crack keeps propagating, and if the work is greater than the amount of released

energy, the crack becomes unstable and propagates dynamically. On other hand, if we perform the same experiment with controlled displacement, the movement instantly is transformed in strain energy and the work is null. When the critical condition to fracture is achieved, the system decreases its energy, and displacement, if it is small, does not increase the energy over the critical point immediately, the crack is stable and does no propagate dynamically. In order to fully determine the conditions of crack propagation, an explicit expression of the release rate and the work performed by the external load as a function of the crack length are necessary. What we have presented here is a brief description of the physics behind the stability analysis for fracture propagation; a more detailed discussion on this matter is made by Gurney and Mai [66].

In conclusion, the experiments presented in this experiment are made with brittle materials, with settings so the crack is stable and propagates in a quasi-static way.

C.2.4 Path Selection Criterion

In fracture mechanics there still are many open questions. In particular, one very important and fundamental question that remains unsolved is how to predict the crack path. Until now there are several criteria, however there is no fundamental answer to this problem.

A recompilation of the most common criteria for isotropic material is made by Leblond [67]. In his book he presents these three:

Criterion of maximum opening stress: This criterion, proposed by Ergodan and Sih [59], dictates that the direction of cracking is perpendicular to the direction of maximum opening stress, $\sigma_{\theta\theta}$, at the crack tip.

Criterion of the local symmetry: This idea, introduced in the work of Goldstein and Salganik [68], states that the crack will follow the path for which the shear mode of fracture (Mode II) is canceled at the growing crack tip.

Criterion of the maximum energy release rate: Palaniswamy and Knauss [69] suggested this criterion, whereby the direction of crack propagation can be obtained by maximizing the energy release rate as a function of the crack propagation angle. It was also postulated by Erdogan et al in [59] they argue that the greatest release of elastic energy is in the direction of the crack, perpendicular to the maximal tension.

We remark the fact that all the presented criteria are based on the assumption of isotropic material.

The experiments studied in this work are characterized by large deformation inducing a mixed mode configuration for the fracture process. An approach based on intensity factors will result very complex. Thus, we base our discussion on Griffiths approach and the criterion of the maximum energy release rate.

From the results obtained in the geometrical characterization of the final path of the crack, we realize that it is necessary to include material anisotropy in the description of the fracture process at least in terms of the crack energy. In section 2.6.2 we present a possible modification of the maximum energy release rate criterion that includes the dependence in the orientation of the fracture work, similar to what is suggested in [64, 65, 70].

Appendix D

Patent

TITRE de L'INVENTION

Film mince d’emballage à amorce de déchirure

TEXTE de L'ABREGE

Un film mince d’emballage 1 comporte une zone de référence 2 ayant un contour fermé et qui est entourée sur toute sa périphérie par une zone déchirable, une amorce de déchirure 3 étant prédécoupée dans ce film en sorte d’intercepter ce contour en débouchant à l’intérieur de celui-ci tout en formant une portion de préhension 4 apte à être tirée à l’écart du plan de ce film mince, la zone de référence étant conçue en sorte de piéger une extrémité de cette amorce de déchirure à l’intérieur dudit contour pendant que l’autre extrémité se propage par déchirure en spirale de la zone déchirable sur au moins 180° autour de cette zone de référence lorsque la portion de préhension commence à subir une traction.

Ce contour fermé est de préférence circulaire.

La zone à contour fermé peut être notamment une ouverture, ou une portion de film entourée par une boucle en un matériau de renforcement.

(Figure 1)

L’invention concerne l’ouverture d’emballages minces, typiquement en matière plastique.

De manière classique, divers produits de consommation (paquets de biscuits, de cigarettes, de CD, de DVD, etc.) sont recouverts d’un emballage formé d’un film (ou feuille) mince fragile, c'est-à-dire capable d’être déchiré. Un tel emballage permet une protection efficace du produit pendant la période de temps séparant la fin de la fabrication de ce produit et sa mise en service ; cela signifie que, avant de mettre le produit en service, il faut enlever cet emballage. Lorsqu’un tel enlèvement est réalisé à la main, c'est-à-dire sans outil, il se produit en pratique par déchirures aléatoires jusqu’à pouvoir dégager les portions d’emballage ainsi séparées.

Il est bien connu que de telles déchirures aléatoires ne permettent pas un enlèvement fiable et rapide de l’emballage. En effet, il est rare d’arriver avec les doigts à provoquer une déchirure qui se propage correctement au point de séparer deux parties d’emballage aisées à enlever ; au contraire, il est souvent nécessaire de procéder à plusieurs déchirures dont chacune tend à s’interrompre rapidement ; le nombre de déchirures successives qu’il faut provoquer est particulièrement important lorsqu’il faut entamer soi-même une déchirure à partir d’un bord du film d’emballage.

Pour remédier à cette situation, il a déjà été proposé de former dans le film d’emballage une amorce de déchirure, typiquement sous la forme d’une languette prédécoupée. Mais il est apparu que, lorsqu’on déchire un film fragile en tirant sur une telle languette prédécoupée, les côtés de celle-ci tendent à

converger l'un vers l'autre au cours de la déchirure, ce qui se traduit par un détachement d'un simple lambeau effilé, de sorte qu'il faut rechercher une nouvelle amorce de déchirure, ce qui se traduit par l'arrachage d'un nouveau lambeau, et ainsi de suite.

Il a également été proposé d'associer à une languette prédécoupée une bande d'un matériau sous-jacent destinée à guider la déchirure d'une manière appropriée ; toutefois, à moins de solidariser cette bande au film d'emballage sur toute sa longueur (ce qui se révèle complexe en pratique et risque de fragiliser l'emballage tant qu'il sert de protection), il n'est pas rare que cette bande ne permette pas un guidage jusqu'au bout de la ligne de déchirure prévue. Et, à supposer que cette bande permette un guidage de la déchirure tout au long de cette bande, il peut y avoir ensuite des difficultés à dégager le produit hors du réceptacle formé par le reste de l'emballage, compte tenu des frottements entre ce produit et la paroi interne de cet emballage (il peut être nécessaire de générer une ligne supplémentaire de déchirure, avec les difficultés précitées).

Il n'existe donc pas, à ce jour, de film d'emballage permettant, sans préparation complexe de celui-ci, d'assurer une ouverture facile de ce film en sorte d'en permettre un enlèvement en un très petit nombre de morceaux.

L'invention vise à répondre à cet objectif et propose à cet effet un film mince d'emballage comportant une zone de référence ayant un contour fermé et qui est entourée sur toute sa périphérie par une zone déchirable, une amorce de déchirure étant prédécoupée dans ce film en sorte d'intercepter ce contour en débouchant à l'intérieur de celui-ci tout en formant une portion de préhension apte à être tirée à l'écart du plan de ce film mince, ladite zone de référence étant conçue en sorte de piéger une extrémité de cette amorce de déchirure à l'intérieur dudit contour pendant que l'autre extrémité se propage par déchirure en spirale de la zone déchirable sur au moins 180° autour de cette zone de référence lorsque la portion de préhension commence à subir une traction.

Il apparaît en effet que, par application à la portion de préhension d'une traction à l'écart du film mince, en pratique perpendiculaire à celui-ci, on

provoque une propagation en spirale divergente de la déchirure, à partir de l'extrémité externe de l'amorce de déchirure, alors que, du fait de son piégeage dans la zone de référence, l'extrémité interne de la portion de préhension ne risque pas de converger vers cette déchirure en spirale ; cette fonction de piégeage de l'extrémité interne par la zone de référence n'est utile que pendant environ un demi-tour de la spirale car il apparaît qu'ensuite, l'extrémité (voire le bord) interne de la portion de film en train de s'écarter du plan du film d'emballage tend à rester à l'intérieur du début de ladite spirale (voir ci-dessous). En pratique, la spirale ainsi parcourue par la déchirure du film dans sa partie fragile est de forme exponentielle et se poursuit jusqu'aux bords de la face formée par le film d'emballage (et non plus une ligne comme dans les solutions connues) ; pourtant la force à appliquer pour la propagation de la déchirure reste sensiblement constante tout en étant modérée.

De manière avantageuse, la portion de préhension a la forme d'une languette, ce qui facilite le soulèvement puis la prise sur cette portion de préhension ; en variante, cette portion de préhension peut être munie d'une tirette rapportée.

Selon une première forme de réalisation de l'invention, le contour fermé de la zone de référence est longé intérieurement par un matériau ayant une résistance au déchirement plus faible que celle de la zone déchirable entourant ce contour fermé. De manière préférée, cette zone de référence est une ouverture dont le bord constitue le contour fermé ; ce contour fermé est avantageusement arrondi, voire circulaire, ce qui permet un comportement régulier du film lors de la déchirure.

Selon une seconde forme de réalisation de l'invention, le contour fermé de la zone de référence est longé intérieurement par un matériau de renforcement ayant une résistance au déchirement plus élevée que celle de la zone déchirable. Selon une première option, le contour fermé de la zone de référence est longé intérieurement par une boucle dudit matériau de renforcement qui est traversée par l'amorce de déchirure ; à titre d'exemple, la zone de référence comporte une ouverture bordée extérieurement par ladite boucle ; en variante, la zone de référence comporte une zone médiane

entourée par ladite boucle, cette zone médiane ayant de préférence une même résistance au déchirement que la zone déchirable entourant le contour fermé (cela revient à dire que la boucle peut être une boucle rapportée au film d'emballage, en séparant ainsi des zones interne et externe du même film). Selon une autre option, la zone de référence est formée en totalité de ce matériau de renforcement.

On peut noter que l'amorce de déchirure traverse le contour jusque dans la zone de référence, lorsque celle-ci est matérialisée.

Ce matériau de renforcement est avantageusement choisi comme étant plastique (donc peu déchirable).

De manière avantageuse, pour minimiser les risques d'apparition de déchirure intempestive au moment où la ligne de déchirure se propage après un premier tour de spirale, l'amorce de déchirure a une extrémité externe (destinée à se propager à l'extérieur du contour) qui est située en sorte que la tangente en ce point à ladite amorce de déchirure est sensiblement perpendiculaire à une tangente au contour fermé passant par ce point.

Il mérite d'être noté que le contour n'a pas besoin de représenter une fraction importante de la surface de film d'emballage à enlever ; ainsi, la surface interne du contour peut être inférieure à 10%, voire inférieure à 5% (ou même 1%) de la surface d'emballage dudit film.

A titre d'exemple dimensionnel, notamment efficace pour l'enlèvement de films d'emballage pour des produits tels que des boitiers de cassette Hi-Fi ou de CD ou DVD, l'amorce de déchirure a une longueur comprise entre 0.5 cm et 3 cm et/ou le contour fermé a une dimension transversale moyenne comprise entre 1 et 3 centimètres.

De manière préférée, le contour fermé arrondi a une forme globalement circulaire, ce qui garantit un comportement régulier du film lors de la déchirure.

Il est apparu que la géométrie et l'orientation de l'amorce de déchirure, notamment son inclinaison par rapport au contour, n'ont pas une importance significative sur le bon détachement du film par déchirure en spirale.

Des objets, caractéristiques et avantages de l'invention ressortent de la description qui suit, donnée à titre d'exemple illustratif non limitatif, donnée en regard des dessins annexés sur lesquels :

- la figure 1 est une vue en perspective d'un détail d'un film d'emballage conforme à l'invention, en cours de déchirement,
- la figure 2 est une vue de dessus de ce détail, en une phase initiale de déchirement, antérieure à celle de la figure 1,
- la figure 3 en est une vue de dessus en une phase de déchirement postérieure à celle de la figure 1,
- la figure 4 est une vue en perspective d'un détail d'un film d'emballage identique à celui des figures 1 à 3, mais comportant une autre forme d'amorce de déchirure,
- la figure 5 en est une vue de dessus en une phase initiale de déchirement, antérieure à celle de la figure 4,
- la figure 6 en est une vue de dessus en une phase de déchirement postérieure à celle de la figure 4,
- la figure 7 est une vue en perspective d'un détail d'un autre film d'emballage conforme à l'invention, en cours de déchirement,
- la figure 8 est une vue de dessus de ce détail en une phase initiale de déchirement, antérieure à celle de la figure 7,
- la figure 9 en est une vue de dessus en une phase de déchirement postérieure à celle de la figure 7,
- la figure 10 est une vue en perspective d'un détail d'un film d'emballage identique à celui des figures 7 à 9, mais présentant une autre géométrie d'amorce de déchirure,
- la figure 11 en est une vue de dessus en une phase initiale de déchirement, antérieure à celle de la figure 10, et
- la figure 12 en est une vue de dessus en une phase de déchirement postérieure à celle de la figure 10.

Les figures 1 à 3 représentent conjointement un premier exemple de film mince d'emballage conforme à l'invention, avec une première forme d'amorce de déchirure.

Ce film mince, dont une portion est représentée sous la référence 1, comporte une ouverture 2 dont le contour fermé est arrondi. Dans l'exemple représenté, cette ouverture a un contour circulaire, mais il peut, en variante non représentée, être ovale, ou comporter trois (voire plus) sommets arrondis. Toutefois, ainsi que cela sera aisément compris ci-dessous, il est préférable que ce contour soit aussi proche que possible d'une forme circulaire, c'est-à-dire qu'il ait un rayon de courbure aussi constant que possible (à part, au plus, en un point noté A_0 – voir ci-dessous).

Ce film mince est de tout type connu approprié, tant du point de vue matériau constitutif que du point de vue épaisseur ; à titre d'exemple, il s'agit d'un film mince de polypropylène par exemple biorienté (notamment de type BOPP) ayant une épaisseur de quelques centièmes de millimètres, éventuellement métallisé.

Le film mince 1 comporte, à partir d'un point A_0 du contour, une amorce de rupture 3 constituée par une découpe de longueur limitée, notée A_0B_0, partant du contour selon une orientation quelconque.

La fonction de cette découpe 3 est de délimiter, conjointement avec le contour de l'ouverture 2, une portion de préhension 4 apte à être saisie entre des doigts d'un utilisateur.

Dans l'exemple considéré, l'amorce de déchirure 3 est sensiblement tangente au contour de l'ouverture, en A_0, de sorte que la portion de préhension constitue une languette, avant même que l'on commence à lui appliquer une traction transversalement au plan du film.

Cette portion de préhension est délimitée d'un côté par l'amorce de déchirure 3 (qui va pouvoir se propager) et de l'autre côté par le contour 2 (qui va, en un premier temps, piéger le déplacement de l'extrémité interne de l'amorce - voir ci-dessous).

La figure 2 représente le film d'emballage dans une configuration de départ dans laquelle la languette, initialement située dans le plan du film 1, a

été relevée, par les doigts d'un utilisateur, dans une direction sensiblement perpendiculaire à ce plan. Ce redressement de la languette se traduit spontanément par la formation d'un pli 5 (c'est-à-dire d'une zone de très faible rayon de courbure) partant sensiblement de l'extrémité externe de l'amorce de déchirure A_0B_0, c'est-à-dire du point B_0, jusqu'au contour 2 en étant tangent à celui-ci (le point de tangence en cette configuration de départ est noté C_0).

Cette configuration prise spontanément par la languette a pour avantage que, si on exerce sur la languette une traction en sorte de l'écarter du plan du film, une déchirure 3A se produit dans le prolongement de l'amorce de déchirure initiale A_0B_0 tandis que la zone 5 de faible rayon de courbure (qui s'apparente ici à un pli) se déplace dans le film, en s'étendant depuis la nouvelle extrémité B de la ligne de déchirure jusqu'au contour tout en tendant à être tangent à celui-ci en un point C (B et C désignent les positions courantes des extrémités du pli).

On a constaté que cette relation géométrique tend à se conserver, c'est-à-dire que, à fur et à mesure que progresse la déchirure, le pli tourne autour de l'ouverture en restant tangent au contour de celle-ci. C'est ainsi que la figure 3 représente une configuration où le pli 5 a tourné dans le sens trigonométrique autour de l'ouverture, tout en restant tangent en C au contour de cette dernière, tandis que l'extrémité B de la déchirure 3A, donc cette déchirure elle-même, décrit une courbe assimilable à une spirale, de sorte que la languette 4 s'élargit progressivement. La spirale diverge d'autant plus vite que les dimensions de l'ouverture sont importantes.

On comprend que, plus la direction de traction est proche d'une direction perpendiculaire au plan du film, plus l'angle du pli 5 (c'est-à-dire l'angle entre le plan du film et la zone de languette située auprès de ce pli) est constant. Il est de ce fait préférable que la direction de traction soit aussi exactement perpendiculaire que possible au plan du film, mais la pratique a montré que cela n'est pas critique (à titre d'exemple, un écart d'une dizaine de degrés est tout à fait acceptable (une traction par les doigts d'un opérateur n'est généralement pas exactement perpendiculaire au plan du film)).

Il a été observé que ce phénomène continue à apparaître, même lorsque le pli atteint et dépasse le point A_0, c'est-à-dire que, au-delà de ce point A_0, le pli tend à rester tangent au bord de l'ouverture, désormais formé par le début de la ligne de déchirure (l'amorce A_0B_0 puis la suite 3A de la déchirure).

La poursuite de la traction de la languette se traduit dans les faits par la propagation de la déchirure 3 selon une courbe en spirale jusqu'à atteindre un bord du film. Le film d'emballage peut alors être enlevé en une seule partie.

Il a été indiqué ci-dessus que, lorsque l'on tend à déchirer une languette à partir d'un film, les lignes latérales de déchirure tendent à converger. Tout se passe ici comme si la déchirure 3A (bord externe) tendait à se rapprocher de l'autre bord (bord interne) de la languette, c'est-à-dire du contour de l'ouverture 2, puis la déchirure elle-même, mais avec une courbure qui est moindre que la courbure de ce bord interne, de sorte que, contrairement aux languettes de l'état de la technique, cette tendance à la convergence ne suffit pas pour permettre au bord externe 3A de se rapprocher de son bord interne, d'où une progression continue de la déchirure jusqu'à un bord du film (ou au moins jusqu'au bord de la partie plane du film lorsque celui-ci enveloppe un produit).

Il a été précisé que le contour de l'ouverture 2 est arrondi, au moins en dehors du point A_0. En effet, un point anguleux de ce contour, dont la pointe serait orientée vers l'extérieur de l'ouverture, serait susceptible de constituer, du fait des contraintes appliquées à la languette, une amorce de rupture qui ferait apparaître une seconde ligne de déchirure, intempestive, qui pourrait converger, jusqu'à l'intercepter, vers la ligne 3. Bien entendu, ce commentaire ne s'applique pas au point A_0 puisque l'amorce de déchirure passe par ce point, de sorte qu'il importe peu, pour le début de la propagation de la déchirure, que l'ouverture présente ou non un point anguleux au point A_0 ; après que la déchirure a fait un tour de spirale, il importe peu également que le point A_0 forme ou non un point anguleux, puisqu'un tel point anguleux n'a pas sa pointe dirigée vers l'extérieur de l'ouverture.

On comprend qu'il est également avantageux qu'il n'y ait pas, dans l'amorce de déchirure 3, de point anguleux présentant sa pointe dirigée vers

l'extérieur puisque, après avoir franchi le point A_0, le pli 5 tend à rester tangent au nouveau bord constitué par l'amorce de déchirure 3 puis la déchirure 3A. Le plus simple est de donner à l'amorce de déchirure une forme dépourvue de tout point anguleux.

Dans l'exemple représenté, la ligne de déchirure 3A se propage au-delà de B_0 dans le prolongement de l'amorce de déchirure 3, de sorte que, lorsque le pli 5 atteint le point B_0, après la propagation de la déchirure sur un tour en étant tangent au bord constitué par l'amorce de déchirure 3A, il le franchit tout en restant tangent à la déchirure 3A qui a démarré à partir de B_0.

Toutefois, on comprend que (voir ci-dessus à propos du caractère arrondi du bord de l'ouverture 2), si le point B_0 constitue un point anguleux dont la pointe est dirigée vers l'extérieur, il peut provoquer le démarrage d'une ligne de déchirure intempestive lorsqu'il est atteint par le pli. Il est donc avantageux d'éviter cette configuration. Puisque la propagation de la déchirure à partir du point B_0, au moment où commence la traction sur la languette, tend à se faire pratiquement perpendiculairement au pli 5 (donc perpendiculairement à B_0C_0), on comprend qu'il est avantageux que la tangente en B_0 à l'amorce de déchirure 3 soit perpendiculaire à la ligne tangente à l'ouverture 2 en passant par B_0 (voir l'angle droit représenté en B_0 à la figure 2). On comprend toutefois que, si la déchirure 3A part du point B_0 en formant un angle supérieur à 90°, il en découlera que ce point B_0 constitue un point anguleux entre l'amorce 3 et la ligne de déchirure 3A, mais puisque la pointe de ce point anguleux n'est pas dirigée vers l'extérieur de l'ouverture, il n'y aura pas de risque de déchirure secondaire lorsque le pli franchira ce point B, après un tour de déchirure. En d'autres termes, il est préférable que l'amorce de déchirure 3 soit découpée d'une manière telle que l'angle formé en B_0 par la tangente à cette amorce de déchirure et la tangente à l'ouverture 2 passant par ce point B_0 (c'est-à-dire B_0C_0) soit supérieur ou égal à 90°.

En pratique une autre manière de minimiser les risques de déchirure intempestive lors du franchissement du point B_0 est de donner à l'amorce de déchirure une forme courbe dont la concavité est tournée vers l'ouverture ;

cette amorce de déchirure peut en particulier avoir la forme d'un début de spirale.

Il est rappelé que le risque de départ intempestif d'une ligne de déchirure dépend aussi des propriétés mécaniques du matériau constitutif du film, de sorte qu'on peut aussi minimiser le risque de déchirure intempestif par le choix d'un matériau ayant une fragilité limitée.

Par contre, après le franchissement de ce point B_0, il n'y a plus de point anguleux le long du contour auquel le pli tend à être tangent, puisque ce contour est alors la ligne 3A, dont il a été dit qu'elle avait la forme d'une spirale.

Il a été indiqué que l'angle que forme l'amorce de déchirure avec le contour 2 est quelconque. En fait, si l'on conforme cette amorce 3 suivant une tangente au contour 2 (s'il est arrondi, de préférence circulaire), la languette ainsi formée est étroite, de sorte qu'il est avantageux que cette languette ait une longueur suffisante pour minimiser le risque que, au début de la propagation de la déchirure à partir du point B_0, cette déchirure converge vers le contour 2 dans le cas d'un défaut de maîtrise de l'orientation de la traction appliquée à cette languette. Il peut donc paraître préférable de conformer l'amorce de déchirure en sorte qu'elle présente un angle non nul avec la tangente locale au contour, c'est-à-dire qu'elle ne soit pas tangente à ce contour ; par contre, si cet angle augmente, la largeur de la languette augmente, mais il est préférable (voir ci-dessus) de courber cette amorce de déchirure en sorte de tourner sa concavité vers l'intérieur de l'ouverture.

Les figures 4 à 6 représentent ainsi une variante des figures 1 à 3 ; les éléments similaires à ceux de ces figures sont désignés par des signes de référence qui se déduisent de ceux des figures 1 à 3 par l'ajout de l'indice « prime ». Le film 1' s'y distingue par le fait que l'amorce de déchirure 3' s'étend à partir du bord du point A_0', sur le contour de l'ouverture 2', suivant un angle sensiblement égal à 90°, c'est-à-dire que l'amorce 3' est, auprès de ce point A_0', sensiblement perpendiculaire à la tangente locale. Toutefois, cette amorce 3' est courbe, avec une courbure telle que, au point B_0', sa tangente est sensiblement perpendiculaire à la direction du pli 5' (entre les points B_0' et C_0') qui se forme dès que l'on applique une traction sur la languette

perpendiculairement au plan du film. Comme indiqué ci-dessus, cette traction se traduit par une propagation de la déchirure, au-delà de B_0', dans le prolongement de cette amorce, de sorte qu'il n'apparaît pas de point anguleux en ce point B_0'. Après un tour de ce pli, celui-ci franchit donc sans difficulté ce point B_0'.

La longueur de ce tronçon A_0B_0 (ou $A_0'B_0'$) est en pratique choisie en sorte de permettre une saisie aisée, par les doigts d'un utilisateur, de la languette délimitée par cette découpe et le contour de l'ouverture ; une longueur de l'ordre de 0.5 cm à 1cm (voire 1.5 cm ou même 3 cm) est une plage qui semble tout à fait appropriée pour des ouvertures 2 ou 2' ayant une dimension transversale moyenne (il s'agit d'un diamètre si ces ouvertures sont effectivement circulaires) de quelques centimètres (typiquement comprise entre 1 et 3 cm). Les dimensions de la spirale alors obtenue par traction sur cette languette sont suffisamment importantes pour assurer un dégagement raisonnablement rapide (en un nombre raisonnable de tours) du film vis-à-vis du produit qu'il sert à emballer. Bien entendu, des dimensions supérieures sont possibles.

Il apparaît ainsi que le fait de prévoir une ouverture 2 (ou 2') dans le film, avec une amorce 3 (ou 3') prédécoupée qui part du contour de cette ouverture, a pour effet d'imposer un chemin prédéterminé au bord interne (en particulier à l'extrémité interne) de la languette, au fur et à mesure qu'on tire cette languette à l'écart du plan du film tandis que son bord externe se déchire, ce bord interne imposé étant tout d'abord le contour de l'ouverture, puis le contour de la déchirure 3A (ou 3A'), après un tour de la languette autour de l'ouverture. Il y en effet un piégeage du bord interne de la languette, et donc de son extrémité interne, à l'intérieur de l'ouverture initiale (pendant environ le premier demi-tour) puis de l'ouverture définie par la progression de la spirale.

En fait, l'ouverture 2 (ou 2') est susceptible de constituer localement un défaut dans la protection du produit assurée par le film d'emballage ; en effet, des poussières, notamment, peuvent pénétrer jusqu'au produit en traversant le film via cette ouverture. Toutefois, cet inconvénient peut aisément

être supprimé en prévoyant, sous le film, ou au dessus de celui-ci, une protection localisée à la zone comportant cette ouverture.

Lorsque la zone prédécoupée du fait de la présence de l'amorce de déchirure est petite, on peut améliorer la facilité de préhension en engageant une bande additionnelle en tout matériau approprié formant une tirette.

Les figures 7 à 9 représentent un autre exemple de réalisation d'un film mince d'emballage conforme à l'invention, qui ne présente pas l'inconvénient d'un tel défaut potentiel de protection.

Les éléments similaires à ceux des figures 1 à 3 sont désignés par des chiffres de référence qui se déduisent de ceux de ces figures 1 à 3 par addition du nombre 10 ; quant aux lettres, elles sont différentes.

Ainsi, ces figures représentent un film mince d'emballage 11 comportant une zone de référence 12 dont le contour fermé 12A est arrondi et dans lequel une languette 14 est prédécoupée. Un bord de cette languette est une amorce de déchirure 13 constituée par une découpe de longueur limitée, notée E_0F_0 ; cette languette forme, lorsqu'elle est tirée à l'écart du plan du film mince d'emballage, un pli 15.

Le film mince 11 se distingue de celui des figures 1 à 3 par le fait que, au lieu de s'interrompre le long du contour de l'ouverture 2, il se prolonge dans la zone 12, celle-ci étant bordée par une boucle en matériau de renforcement 16, qui longe intérieurement le contour 12A. L'amorce de déchirure 13 s'étend depuis le contour interne de la boucle 16 (à partir du point marqué E_0), au travers de cette boucle jusqu'au point G_0 situé sur le contour 12A, et à l'extérieur de celle-ci jusqu'au point F_0.

En outre, une seconde amorce de déchirure 17 est avantageusement prévue le long du contour intérieur de la boucle 16 à partir du point E_0, jusqu'à un point noté H_0. La languette 14 peut ainsi être redressée par rapport au plan du film mince sans le moindre effort.

Toutefois, en variante, cette amorce de déchirure 17 peut être omise, le passage d'un ongle (ou tout autre outil) au travers de la prédécoupe E_0F_0 étant suffisant pour provoquer un début de déchirure le long du contour interne de la boucle 16.

On comprend qu'un tel film ne comporte pas de défaut de protection à l'emplacement de la zone 12.

On comprend en outre que, par traction sur la languette dans un sens propre à l'éloigner du plan du film, on tend à provoquer une propagation de la déchirure, notée 13A, de manière tout à fait analogue à ce qui a été expliqué à propos de la propagation de la déchirure 3 dans le film mince des figures 1 à 3 : cette déchirure se propage selon une ligne en spirale (la lettre F désigne la position courante de l'extrémité externe de la déchirure tandis que la lettre H désigne la position courante de l'extrémité interne de la déchirure interne).

En effet, le contour interne de la boucle 16 se comporte, lors de la traction sur la languette, comme le bord de l'ouverture 2. Ainsi, que la déchirure 17 ait été prédécoupée ou qu'elle soit apparue lors du passage d'un ongle au travers de l'amorce E_0F_0 de déchirure, cette déchirure 17 ne peut se propager que le long du bord interne de la boucle 16, puisqu'elle ne peut traverser cette boucle (puisque celle-ci est en matériau de renforcement, il est plus facile pour la déchirure 17 de se propager dans le film, à l'intérieur de la boucle 16, que de traverser cette boucle). En d'autres termes, l'extrémité interne de la languette est, au moins au début de la propagation de la déchirure, piégée à l'intérieur du contour 12A, le long du contour interne de la boucle 16.

Ainsi, à la figure 8, la languette 14 est juste redressée, avant de provoquer la propagation des extrémités des déchirures 13 et 17 au-delà des points F_0 et H_0, respectivement (voir les traits en tirets 13A et 17A). Par contre, on voit à la figure 9 une configuration dans laquelle la trace instantanée du pli 15 est sensiblement tangente au contour interne de la boucle 16, tandis que la déchirure 13A se propage selon une courbe en spirale.

On comprend que, après une fraction de tour du pli autour de la boucle (approximativement après un demi-tour), la propagation de la déchirure 17A s'interrompt (il devient plus facile pour la portion 12 du film de se plier avec la languette plutôt que de se déchirer le long du bord interne de la boucle). A partir de ce moment, la traction exercée sur la languette ne provoque plus, comme dans l'exemple des figures 1 à 3, que la propagation de la déchirure

13A, tandis que le pli continue de se déplacer le long du contour interne jusqu'à traverser la boucle, en franchissant le point E_0, puis le point G_0 ; l'extrémité interne de la languette n'est alors plus piégée à l'intérieur du contour 12A. La suite de la propagation de la déchirure se produit alors, le long du contour défini par la déchirure 13, ainsi que cela a été décrit à propos des figures 1 à 3.

La plupart des commentaires exprimés à propos de cet exemple des figures 1 à 3 s'appliquent aussi à ce second exemple, y compris en ce qui concerne la géométrie de l'amorce de déchirure auprès de son extrémité F_0 ; en particulier, cette amorce est avantageusement courbée de telle manière que la déchirure qui se produit du fait de la traction est dans le prolongement de l'amorce.

Toutefois, on peut noter que les risques mentionnés en cas de languette très étroite au tout début de la propagation sont bien moindres ici, car le risque que la déchirure 13A traverse la boucle à partir du point F jusqu'à rejoindre la déchirure 17 est infime compte tenu de la résistance du matériau constitutif de cette boucle.

C'est pourquoi ce second exemple se prête particulièrement bien à des amorces faiblement inclinées par rapport à la tangente locale au contour (de préférence inférieure à 15°).

Toutefois, comme indiqué précédemment, l'invention n'est pas limitée à une quelconque valeur d'angle entre l'amorce de déchirure et le contour extérieur de la zone renforcée.

Cette boucle 16 est par exemple constituée d'une surépaisseur constituée du même matériau que le film mince. Il peut aussi s'agir de polyéthylène, de polypropylène (éventuellement biorienté), voire de métal, notamment.

Cette boucle est avantageusement rapportée au film mince sous celui-ci, de manière à ne pas risquer de s'accrocher avant le moment où le film doit être enlevé. Il a été constaté que cette disposition ne nuit pas à la solidité de la liaison entre cette boucle et le film mince, lors de l'application de la traction sur la languette.

Cette boucle est avantageusement annulaire auquel cas sa dimension transversale moyenne est un diamètre ; cette dimension transversale moyenne est avantageusement de l'ordre du centimètre, par exemple comprise entre 1 cm et 3 cm, comme précédemment. On comprend que, compte tenu de cette petite taille, il est bien plus facile de mettre en place une telle boucle que de mettre en place une bande tout au long d'une ligne de déchirure souhaitée, comme dans des solutions connues.

La largeur de la boucle (c'est-à-dire la largeur de la bande de renforcement constituant cette boucle) est avantageusement de l'ordre de quelques millimètres, par exemple comprise entre 1 et 5 mm (cela peut dépendre du matériau constitutif ; plus le matériau est résistant, moins sa largeur a besoin d'être importante).

Comme précédemment, les dimensions peuvent être bien plus grandes ; il appartient à l'homme de métier de choisir des dimensions appropriées en fonction de l'application envisagée (notamment des dimensions du produit emballé).

Les figures 10 à 12 représentent une variante des figures 7 à 9. Les éléments similaires à ceux de ces figures sont désignés par des signes de référence qui se déduisent de ceux des figures 7 à 9 par l'addition de l'indice « prime ».

La principale différence entre le film 11' de ces figures 10 à 12 par rapport au film 11 des figures 7 à 9 réside dans le fait que l'amorce de déchirure 13', non seulement traverse la boucle 16' de renforcement, mais pénètre en outre à l'intérieur de la zone médiane 12, jusqu'à un point noté J'_0. Lors de l'application d'une traction à la portion de préhension $J'_0F'_0$ ainsi formée, une déchirure se produit à partir du point F'_0, comme dans l'exemple des figures 7 à 9, tandis qu'une autre déchirure se produit à partir du point J'_0, à l'opposé de l'amorce elle-même ; cette autre déchirure 17' se propage spontanément d'une manière quelconque, mais dès qu'elle rencontre le contour interne de la boucle 16', elle est contrainte de suivre, comme dans l'exemple des figures précitées, le contour interne de cette boucle. Comme précédemment, il y a donc un piégeage de l'extrémité interne de l'amorce de déchirure 13' à l'intérieur du

contour externe 12A' de cette boucle (ce piégeage a même lieu à l'intérieur du contour interne de cette boucle).

Selon une variante non représentée, le matériau de renforcement n'est pas limité à une boucle à l'intérieur du contour 12A, mais se prolonge sur toute la zone 12 ; en d'autres termes ce matériau de renforcement a la forme d'un disque, à contour circulaire ou non (il peut s'agir d'une zone massive de contour quelconque). Dès lors que ce matériau de renforcement est suffisamment peu déchirable, le fait d'appliquer une traction à la portion de préhension définie par l'amorce provoque une propagation de la seule extrémité qui peut se propager, à savoir l'extrémité externe située à l'extérieur de cette zone de renforcement tandis que l'extrémité interne est piégée dans cette zone de renforcement ; cet effet de piégeage cesse dès que, comme dans le cas des figures 7 à 12, cette zone de renforcement commence à se plier, auquel cas la déchirure continue, tandis que le pli de la languette tourne en restant tangent à la déchirure 13A, en continuant la spirale qui a commencé à se former.

Ainsi on constate qu'il y a plusieurs configurations selon l'invention ; dans un premier exemple, le film mince a une plus grande résistance que le vide situé à l'intérieur du contour 2 (le bord de l'ouverture constituée par ce vide confine la propagation de l'extrémité interne de l'amorce de déchirure), tandis que, dans un second exemple, le contour est longé intérieurement par un matériau de renforcement qui confine également l'extrémité interne de l'amorce de déchirure. On comprend que d'autres configurations sont possibles ; c'est ainsi que, selon encore un autre exemple, lorsque le contour est bordé intérieurement par un matériau de renforcement, lequel a la forme d'une boucle, la partie résiduelle, à l'intérieur de cette boucle peut être une ouverture sans matériau, être formée d'un film de propriétés différentes de celles du film à l'extérieur du contour ou au contraire être formée du même film déchirable qu'à l'extérieur.

REVENDICATIONS

1. Film mince d'emballage (1, 1', 11, 11') comportant une zone de référence (2, 2', 12, 12') ayant un contour fermé et qui est entourée sur toute sa périphérie par une zone déchirable, une amorce de déchirure (3, 3', 13, 13') étant prédécoupée dans ce film en sorte d'intercepter ce contour en débouchant à l'intérieur de celui-ci tout en formant une portion de préhension (4, 4', 14, 14') apte à être tirée à l'écart du plan de ce film mince, ladite zone de référence étant conçue en sorte de piéger une extrémité de cette amorce de déchirure à l'intérieur dudit contour pendant que l'autre extrémité se propage (3A, 3A', 13A, 13A') par déchirure en spirale de la zone déchirable sur au moins 180° autour de cette zone de référence lorsque la portion de préhension commence à subir une telle traction.

2. Film mince selon la revendication 1, caractérisé en ce que la portion de préhension a la forme d'une languette.

3. Film mince selon la revendication 1 ou la revendication 2, caractérisé en ce que le contour fermé de la zone de référence est longé intérieurement par un matériau ayant une résistance au déchirement sensiblement plus faible que celle de la zone déchirable entourant ce contour fermé.

4. Film mince selon la revendication 3, caractérisé en ce que ladite zone de référence est une ouverture (2, 2') dont le bord constitue le contour fermé.

5. Film mince selon la revendication 1 ou la revendication 2, caractérisé en ce que le contour fermé de la zone de référence est longé intérieurement par un matériau de renforcement (16, 16') ayant une résistance au déchirement sensiblement plus élevée que celle de la zone déchirable.

6. Film mince selon la revendication 5, caractérisé en ce que le contour fermé de la zone de référence est longé intérieurement par une boucle dudit matériau de renforcement qui est traversée par l'amorce de déchirure.

7. Film mince selon la revendication 6, caractérisé en ce que la zone de référence comporte une ouverture bordée extérieurement par ladite boucle.

8. Film mince selon la revendication 6, caractérisé en ce que la zone de référence comporte une zone médiane (12, 12') entourée par ladite boucle, cette zone médiane ayant une même résistance au déchirement que la zone déchirable entourant le contour fermé.

9. Film mince selon l'une quelconque des revendications 1 à 8, caractérisé en ce que l'amorce de déchirure a une extrémité (B, B', F, F'), destinée à se propager à l'extérieur du contour, qui est située en sorte que la tangente en ce point à ladite amorce de déchirure (3, 3', 13, 13') est sensiblement perpendiculaire à une tangente au contour fermé passant par ce point.

10. Film mince selon l'une quelconque des revendications 1 à 9, caractérisé en ce que la surface interne du contour fermé est inférieure à 5% de la surface d'emballage dudit film.

DESSIN D'ABREGE

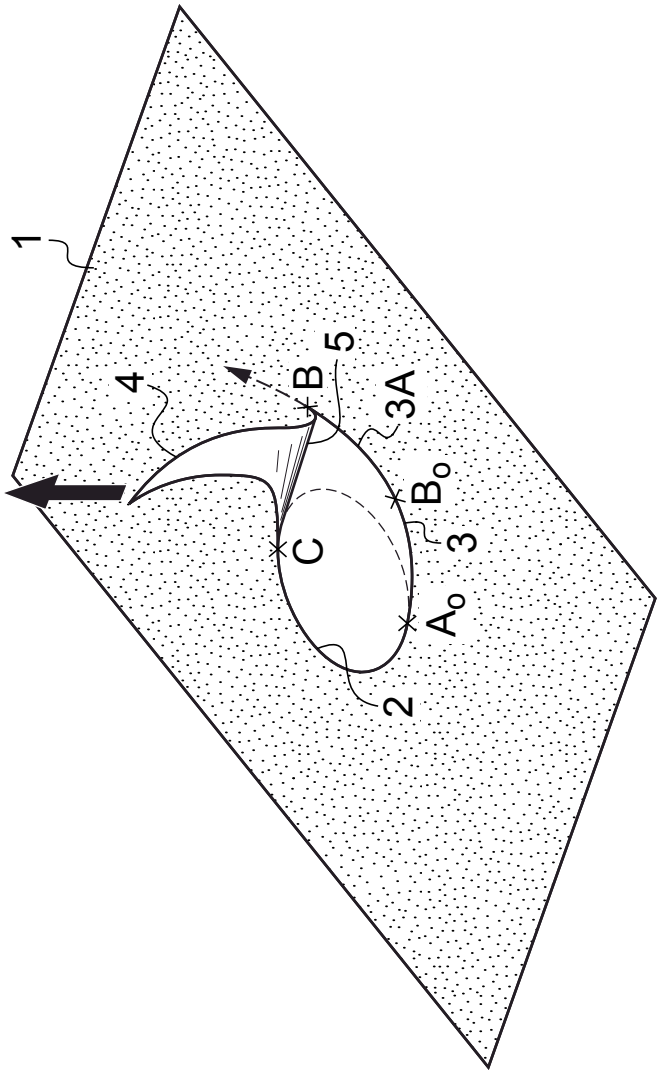

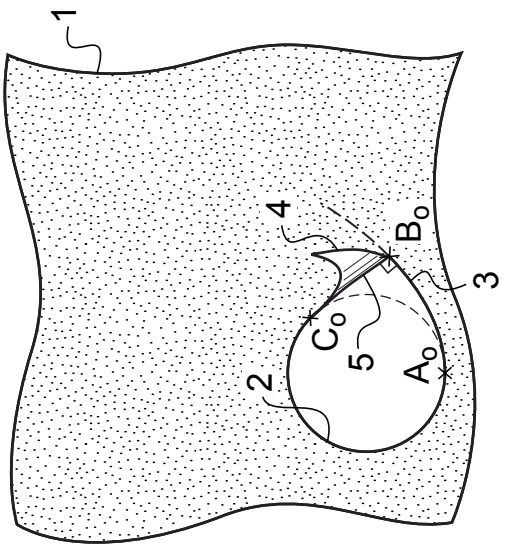

Fig. 2

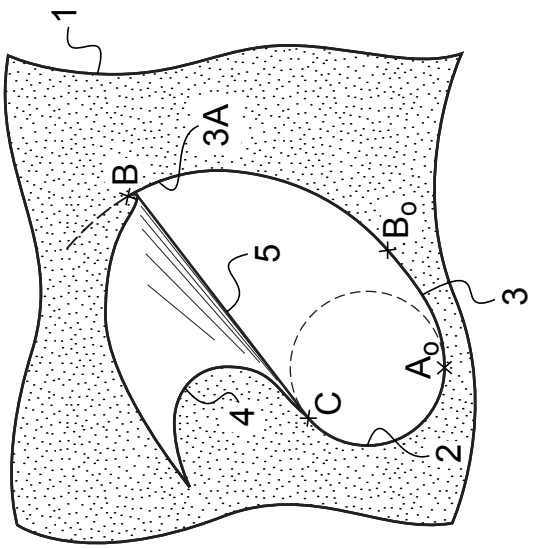

Fig. 3

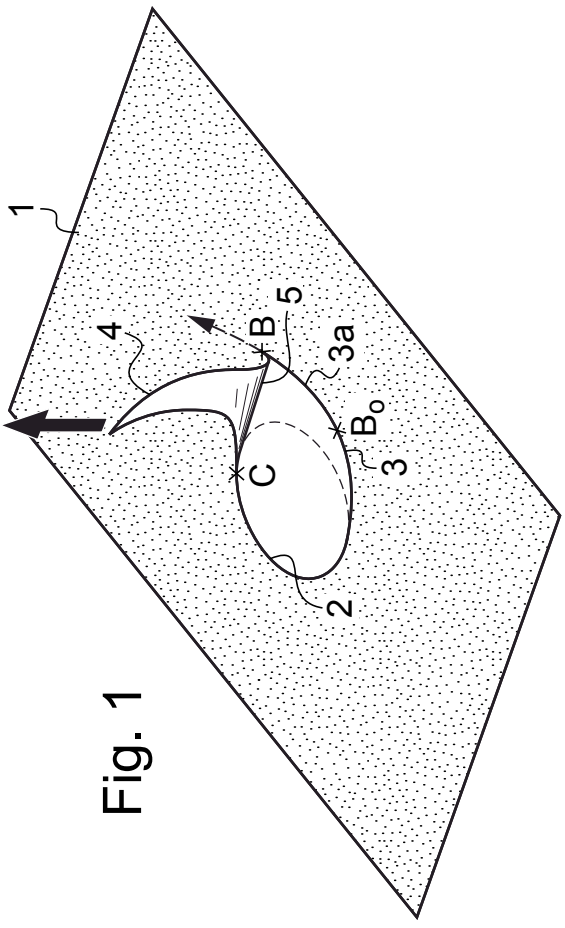

Fig. 1

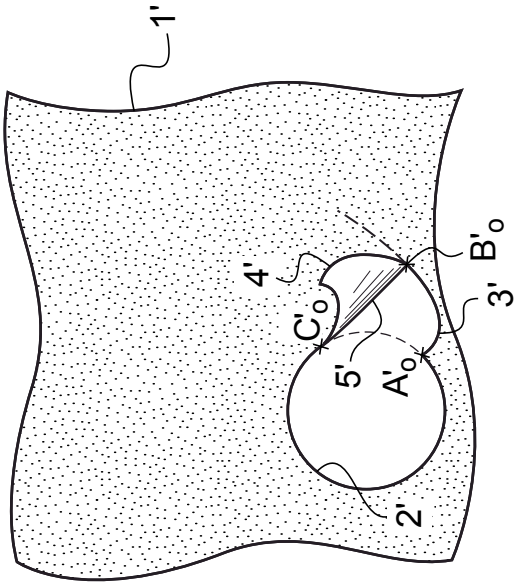

Fig. 5

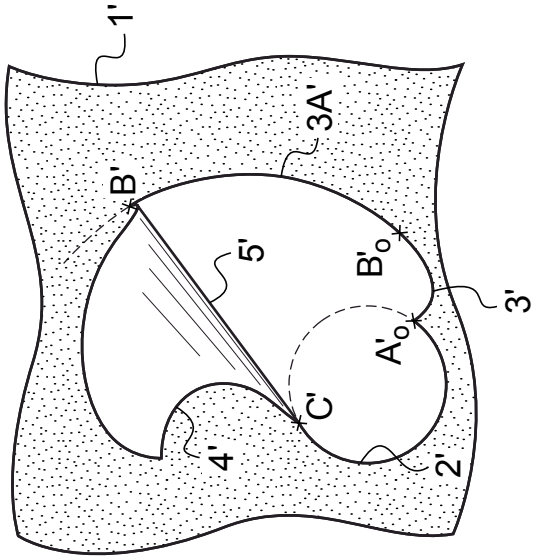

Fig. 6

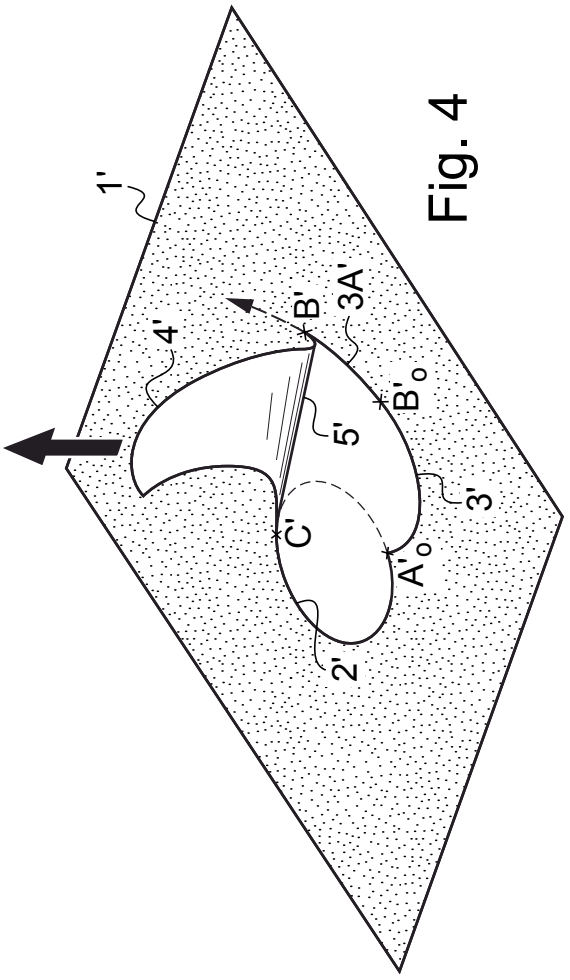

Fig. 4

Fig. 7

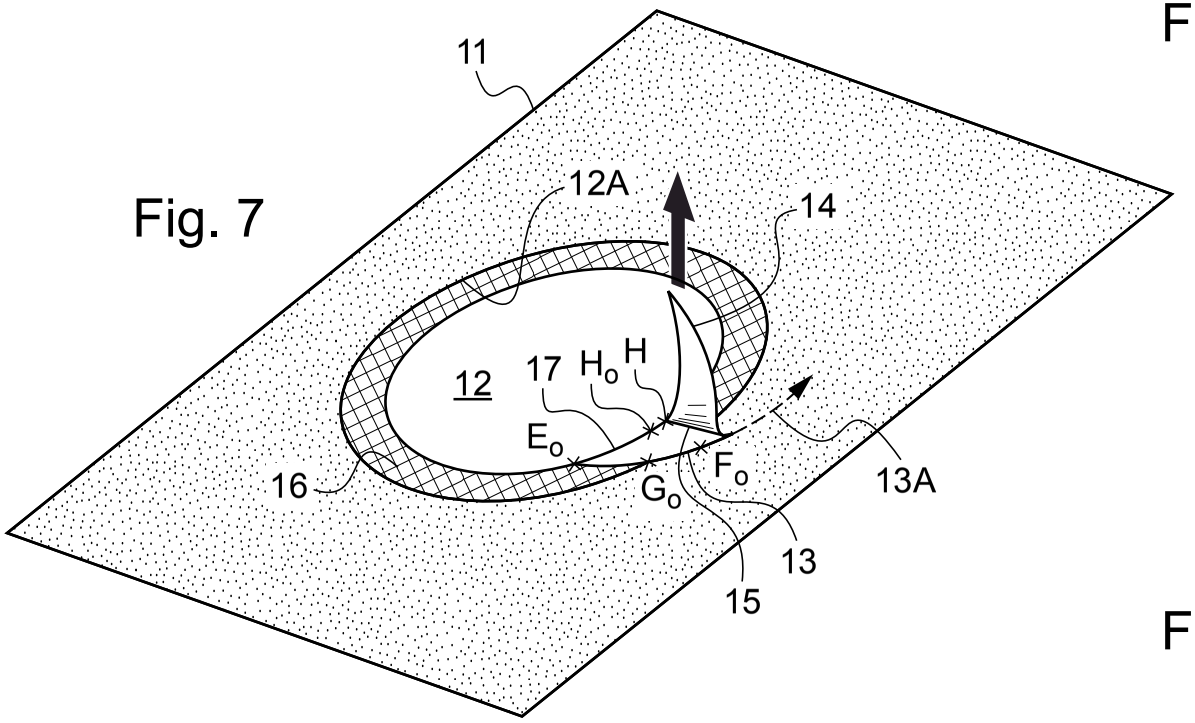

Fig. 8

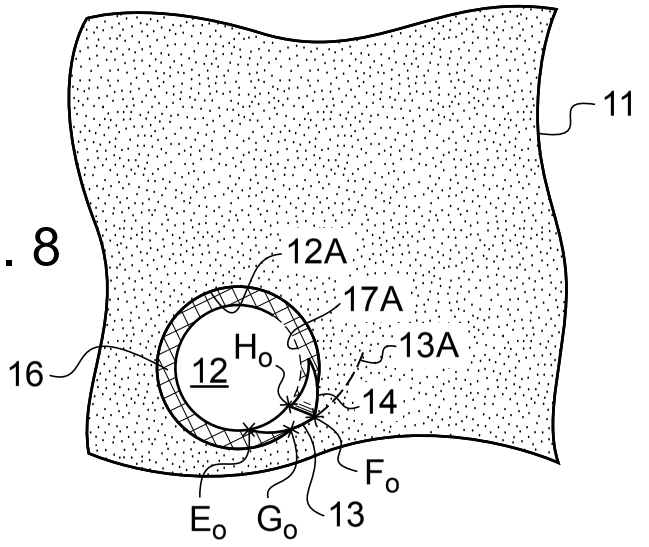

Fig. 9

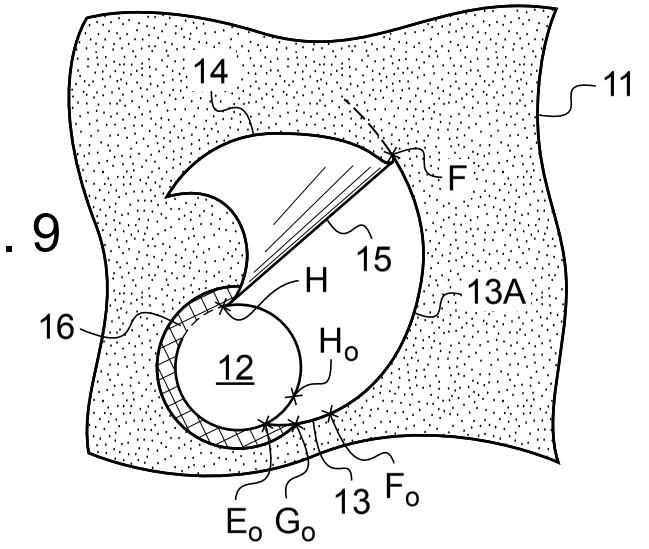

Fig. 10

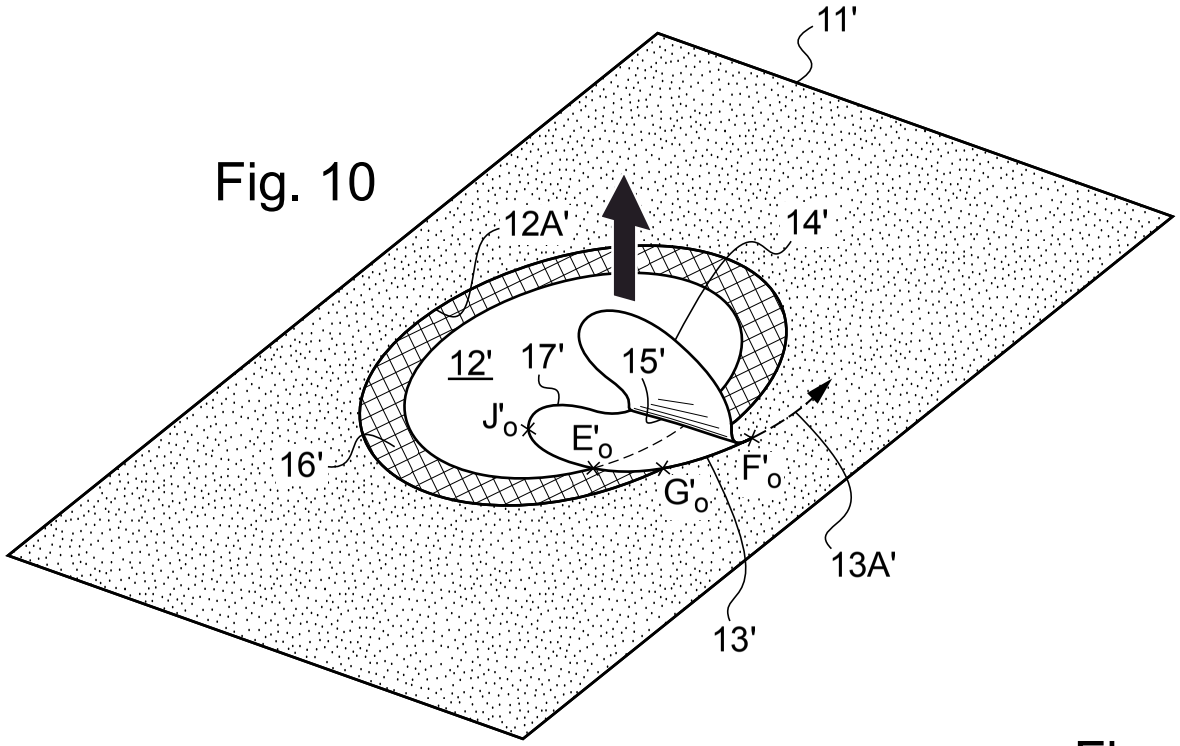

Fig. 11

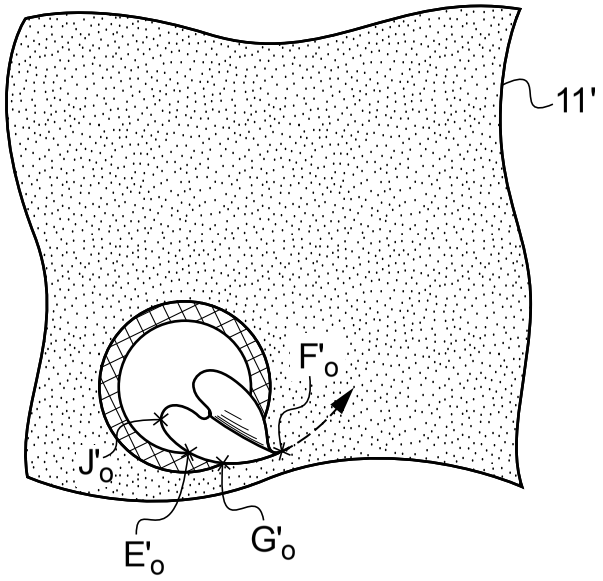

Fig. 12